Delft3D Flexible Mesh modelling of the Guayas River and Estuary system in Ecuador

Pedro D. Barrera Crespo

Faculty of Civil Engineering & Geosciences

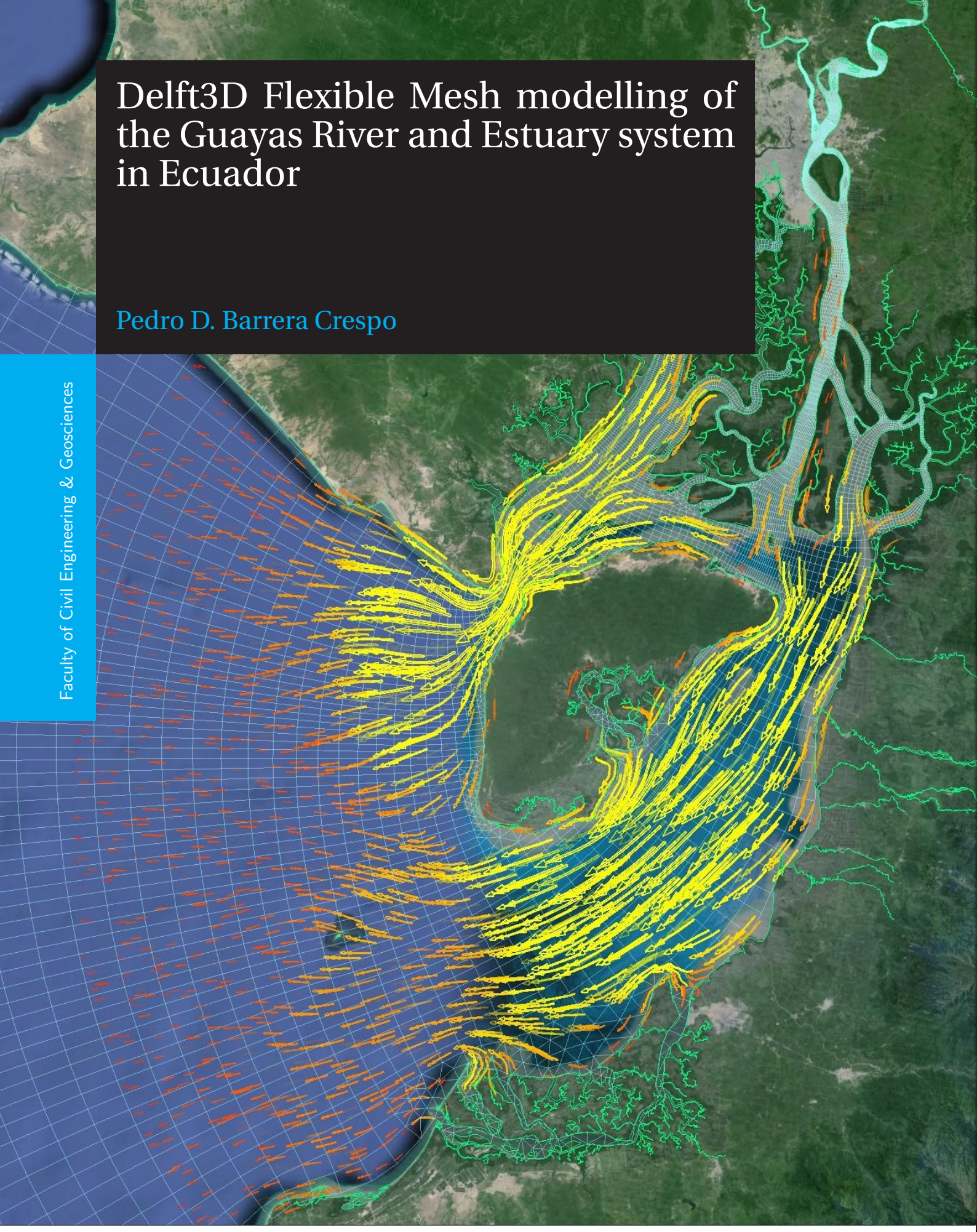

NUS National University of Singapore
TU Delft
Deltares Enabling Delta Life

Delft3D Flexible Mesh modelling of the Guayas River and Estuary system in Ecuador

by

Pedro D. Barrera Crespo

in partial fulfillment of the requirements for the degree of

Master of Science
in Civil Engineering, Hydraulic Engineering track
at the Delft University of Technology,

and the degree of

Master of Science
in Hydraulic Engineering and Water Resources Management
at the National University of Singapore,

to be defended publicly on Tuesday May 10, 2016 at 09:00 AM.

TUD student number:	4341147	
NUS student number:	A0118976	
Author's contact:	pdbc_1985@hotmail.com	
Supervisor:	Dr. ir. E. Mosselman,	Deltares / TU Delft
Thesis committee:	Prof. dr. ir. W. S. J. Uijttewaal,	TU Delft
	Prof. dr. ir. Z. B. Wang,	TU Delft
	Dr. V. P. Chua,	National University of Singapore

An electronic version of this thesis is available at http://repository.tudelft.nl/.

NUS National University of Singapore

TU Delft Delft University of Technology

Deltares Enabling Delta Life

A mi Abuela

María Alejandrina

PREFACE

This thesis marks the culmination of my Master of Science studies at the National University of Singapore and at the Delft University of Technology. It has been an amazing ride, I got to know very interesting people and places over these years. The memories will be everlasting and my horizon has widely expanded through the unique projects, techniques and applications of hydraulic engineering that have boosted my interest and inspiration in the field. During this period I was able to learn valuable lessons and live unique experiences that make me realize how fortunate I am. None of this could have been done without the help and support of my professors, colleagues, family and friends. I would like to take this opportunity to express my appreciation and gratitude.

First of all I would like to thank all the members of my thesis committee, your valuable input and comments during the meetings are greatly appreciated. Especially to my supervisor Dr. ir. Erik Mosselman, thank you very much for helping me find a suitable research topic and for arranging a work place at Deltares. But most of all, thank you for your guidance and advice. Your tutelage and expertise not only guided me throughout this research but were also a major source of inspiration.

I would like to thank the professionals working at Deltares whose valuable talks, comments and remarks help me with the tweaks and tricks about morphodynamic modelling with Delft3D-FM. In particular thanks to Dr. ir. Willem Ottevanger and Dr. ir. Mohamed Nabi whom were always available to share their knowledge and kept me up to date with the latest implementations in the software.

I would also like to acknowledge Dr. ir. Alessio Giardino. Thanks for the discussions and debates about long term morphodynamic modelling and for the overall interest that you freely and willingly demonstrated for my work.

To all my colleague interns at Deltares, it is amazing how diverse our group became. I made friends, literally, with people from all over the world. You will always have a friend and will always be welcome in Ecuador as well.

To my family, friends and of course Andrea, you always have been there for me, and your unconditional support encouraged me to finish my studies. Thanks, you are what drives my motivation.

Y finalmente a mis padres Nancy y Oswaldo, gracias a Ustedes he podido realizar mis sueños y a pesar de la distancia están siempre conmigo. Esto es de Ustedes, esto es por Ustedes, esto es para Ustedes. Muchas gracias.

Pedro D. Barrera Crespo
Delft, May 2016

ABSTRACT

The Guayas River estuary supports extensive socio-economic processes. It is formed at the confluence of the Babahoyo and Daule Rivers and runs for around 65 km before discharging into the Pacific Ocean. Its relevance within the national context is linked to the city of Guayaquil, the most populated city and commercial capital of Ecuador. Recently it was considered the main seaborne trading route for the country. Nowadays the estuary experiences a number of sedimentation related issues which hinder its navigability and increase the potential risk of flooding in the northern low lying areas of Guayaquil. Although these problems have been accentuating over the years, little is known about the estuary's morphological evolution. Therefore, the main focus of this study is to provide a comprehensive explanation of the estuary's morphological development and the processes behind its evolution. In this regard, a morphodynamic numerical model was implemented using the software Delft3D Flexible Mesh.

The estuary itself has not been the subject of many studies related to morphology. The lack of information was one of the major challenges for this research, especially in relation to bed topography. In order to cope with this, state of the art techniques were applied to derive the missing data. This is the basis to set up the model for the different scenarios that simulate natural events and anthropic interventions carried out within the estuary and that have been identified as some of the potential causes of sedimentation. A total of five events or so called 'interventions' were defined, namely: the reduction of intertidal areas due to mangrove deforestation and shrimp farms, El Niño phenomenon, the construction of the Daule-Peripa dam at the headwaters of the Daule River, the construction of the 'Puente de la Unidad Nacional' bridge over the Daule and Babahoyo Rivers near their confluence and finally the sediment overload due to deforestation of the upstream basin.

The final analysis of the different cases determined that the changes in tidal asymmetry are the main causes of sedimentation and the overall estuary morphological evolution. Amongst others, the leading contributors to this tidal variability can be attributed to the discharge of the Daule and Babahoyo Rives and the decimation of intertidal areas.

Depending on the magnitude of the discharges, the predominant flood dominant character of the estuary is either reduced or even shifted towards ebb dominance. This is verified when the hydrographs peak during the wet season particularly in the higher regions near the confluence of the rivers.

The intertidal flats, on the other hand, have been severely reduced due to increased shrimp farming practices and the sequential loss of mangrove forests along the estuary banks. This has principally reduced hydraulic friction and natural wave damping effects which has ultimately enhanced flood dominance.

It was also concluded that events such as the bridge construction over the Daule and Babahoyo Rivers as well as the sediment overload related to deforestation of the upstream basin are of minor importance.

In view of the above, in order to control the sedimentation in the estuary and especially around Guayaquil, three alternatives are proposed (or a combination of them) as potential mitigating measures. The first is to control the discharge of the Daule River through the operation of the Daule-Peripa dam. The second is to recover some of the intertidal flats which have been decimated by aquaculture practices. The third is to dredge the area of the estuary close to Guayaquil. The final solution requires a more detailed study. However it will involve a compromise between the cost of dredging and the decreased profit from hydro power generation and aquaculture.

SUMMARY

The Guayas River is formed at the confluence of the Babahoyo and Daule Rivers and is part of a larger estuarine system known as the Gulf of Guayaquil. Nowadays the estuary experiences a number of sedimentation related issues that are related to natural events and anthropic interventions carried out within the estuary. Potential causes of sedimentation have been identified, namely: shrimp farming and aquaculture practices, "El Niño" events, the construction of a dam at the headwaters of the Daule River, the construction of the "Puente de la Unidad Nacional" bridge and the sediment overload due to deforestation of the upper basin.

Therefore, the central topic of this research is to understand the estuarine system from the hydrodynamic and morphology perspectives.

As a first assessment of the situation, an analytical model according to what has been proposed by Savenije (2006) is implemented. In equilibrium conditions, alluvial estuaries shared common features ,i.e., the mean depth, the tidal velocity amplitude and the tidal range remain constant. The actual situation of the Guayas River estuary, reveals that the tidal wave is amplified as it travels upstream. This is due to an imbalance between convergence and friction, being the latter grater in this case. In order to reach equilibrium, the estuary will then tend to reduce the effects of convergence and increase those related to friction. By comparing the actual and equilibrium states, the natural development of the estuary would then lead to the relative reduction of the cross sectional convergence length in relation to the width convergence length. This means that, in order to increase friction, the estuary's mean depth needs to be reduced. Hence the natural tendency is to deposit sediment on the bed.

The considered interventions carried out within the estuary fundamentally make reference to two aspects in particular: changes in the shape due to the decimation of the intertidal flats and changes in the river discharges. The effects of these aspects can also be assessed based on this equilibrium perspective:

- The reduction of the tidal flats translates into a reduction of friction since the average mean cross sectional depth would then increase. This is against the equilibrium condition, consequently the estuary will deposit more sediment.

- A reduction of the river discharges leads to a reduction of the convergence length which would further enhance sedimentation.

A more detailed analysis of the estuary is done with the aid of a morphodynamic numerical model. In that regard, the new software Delft3D Flexible Mesh is used. This is a new unstructured-grid approach that is based on the finite-volumes method. The unstructured character eliminates the restriction imposed by structured grids, since it is possible to construct networks with shapes other than rectangular. The model is then more versatile in the sense that the grid can better be constructed to mimic complex geometries with optimal network resolution.

One of the major challenges faced during the implementation of the model was the lack of information about the estuary. Scarce data are available at the area of interest, in particular that concerning with boundary conditions and the initial bed topography. In view of this, the domain layout covers the whole Gulf of Guayaquil and extends about 65 km inland. The boundary conditions then are derived from world tidal models at the seaward side and from available river gauging stations at the landward side. Once the domain and boundary conditions are defined, the the initial bed

topography of the Guayas River estuary can be derived. This is achieved by means of a long-term morphological simulation in the order of centuries. The idea behind this approach assumes that under steady forcing the estuary develops towards an equilibrium conditions for which changes in the shape is the response to the hydrodynamic forcing. The thus derived topography seems to correlate well with observations from satellite images. Moreover, the model is further validated based on information from tidal stations and measurements of the tidal propagation carried out by Murray et al. (1976).

To explain the evolution of the estuary as a consequence of the interventions, 5 scenarios are defined. From the consequent analysis it was found that the effects on the sediment balance is a direct consequence of the changes in the residual sediment transport caused by the interventions, which in turn are related to the changes in the tidal asymmetry. The two sources of asymmetry that are directly linked to sediment transport stem from the influence of residual currents and the distortion of the tidal wave.

It was shown that changes in the river hydrographs affect principally the first source of asymmetry. The second source of asymmetry is significantly influenced when the shape of the estuary is modified. In that regard, the addition of the intertidal areas causes the most prominent effect on this source of asymmetry. It was also found that sediment overload at the river boundaries does not induce any changes on the sediment balance.

Finally, the sedimentation problem around Guayaquil is also related to the tidal asymmetry. The mitigation measures to be undertaken must be directed towards increasing the effect of the residual currents and minimizing the effect of the distortion of the wave.

Three alternatives are proposed as mitigating measures. The first is related to managing the operation of the Daule-Peripa dam in a fashion that more water is delivered especially during the wet season. The second is to reforest and recover some the intertidal flats that have been decimated by the aquaculture practices. The third is to dredge the area of the estuary close to Guayaquil. However, further research must be done to define and evaluate the extent, viability, socio-economic and environmental impacts related to each of them.

CONTENTS

LIST OF FIGURES

LIST OF TABLES

NOMENCLATURE

α	Tidal Froude number [-]
α_s	Shape factor [-]
α_{bn}	Transverse bed gradient factor for bed-load transport [-]
$\Delta\lambda$	Length of a flow link in the numerical grid [m]
Δ	Realtive mass density of sediment under water [-]
$\Delta\rho$	Density difference of ocean and river water [kg/m^3]
δ_U	Damping rate of the tidal velocity amplitude [1/m]
δ_η	Damping rate of tidal amplitude [1/m]
η	Tidal amplitude [m]
$\hat{u}_{M2}$	Velocity amplitude of the M_2 tidal constituent [m/s]
$\hat{u}_{M4}$	Velocity amplitude of the M_4 tidal constituent [m/s]
$\hat{u}_{M6}$	Velocity amplitude of the M_6 tidal constituent [m/s]
κ	Correction factor [-]
ν	Kinematic viscosity [m^2/s]
ω	Angular velocity [1/s]
ρ	Density of water [kg/m^3]
θ_{SD}	Fraction of erosion to assign to adjacent dry cells [-]
v	Tidal velocity amplitude [m/s]
v_0	Tidal velocity amplitude at the estuary's mouth [m/s]
v_{back}	Background eddy viscosity [m^2/s]
ε	Phase lag between HW and HWS, or LW and LWS [-]
φ	Phase angle [-]
$\vec{T}$	Force vector due to subgrid stresses in the momentum equation [m/s^2]
$\vec{u}$	depth-averaged velocity vector [m/s]
ζ	Instantaneous free surface position [m]
A	Cross sectional area [m^2]
a	Cross-sectional convergence length [m]
A_0	Cross sectional area at the estuary mouth [m^2]
B	Stream width [m]
b	Convergence length of the stream width [m]
B_0	Width at the estuary mouth [m]
B_s	Storage width [m]
C	Chézy coefficient [m$^{0.5}$/s]

c	Wave celerity [m/s]
c_0	Celerity of a progressive wave [m/s]
c_f	Bed friction coefficient [-]
d	External forcing term in the momentum equation [m/s^2]
d_s	Sediment transport factor [m$^{(2-n)}$s$^{(n-1)}$]
D_{50}	Median sediment grain size [m]
E_0	Tidal excursion [m]
E_m	Potential energy per tidal cycle [kg.m^2/s^2]
E_t	Kinetic energy per tidal cycle [kg.m^2/s^2]
f	Friction factor [-]
f'	Adjusted friction factor [-]
f_2	Scaling factor for the amplitude of the M_2 component [-]
g	Acceleration due to gravity [m/s^2]
H	Tidal range [m]
h	Stream depth [m]
h_0	Constant tidal average stream depth [m]
L	Estuary length [m]
n	Degree of non-linearity for the transport formulation [-]
n	Manning roughness coefficient [s/m$^{1/3}$]
N_R	Estuary Richardson number [-]
p	Porosity [-]
P_t	Tidal prism [m^3]
Q	Discharge [m^3/s]
q	Source forcing term in the momentum equation [m/s^2]
Q_f	Fresh water discharge [m^3/s]
Q_s	Sediment discharge [m^3/s]
R_s	Source term [m^2/s]
r_S	Storage width ratio [-]
S	Bed-load transport [m^3/s/m]
T	Tidal period [s]
t	Time [s]
U	Mean cross-sectional flow velocity [m/s]
u	Flow velocity [m/s]
u_0	Residual flow that stems from a river discharge [m/s]
x	Distance [m]
Z	Water level [m]
Z_b	Bottom elevation [m]

1

INTRODUCTION

1.1. THE GUAYAS RIVER AND THE GUAYAS RIVER ESTUARY

Guayaquil "La Perla del Pacífico" (The Pearl of the Pacific) is the most populated city and the industrial and commercial capital of Ecuador. The economic relevance of the city can be attributed to its particular location at the Guayas River, which in recent years was considered the main seaborne trading route for the country.

The river is formed at the confluence of the Babahoyo and Daule rivers and is part of a larger estuarine system known as the Gulf of Guayaquil, which is considered the largest estuary on the Pacific coast of South America (13711 km^2), (Armijos and Montolío, 2008). The location is shown in Figure 1.1.

The Gulf has been defined as an outer and an inner estuary. The outer estuary extends from the mouth of the Gulf at about 130 km inland up to the 'Puna Island', including the 'Canal del Morro' and 'Canal de Jambelí' channels. The inner estuary is composed of the 'Estero Salado' estuary and the 'Guayas River' estuary. The latter extends from the northern shore of the Puna Island (Canal de Cascajal) up to the tidal signature about 100 km inland through the Babahoyo and Daule rivers, (Armijos and Montolío, 2008). Tides are semidiurnal in the Gulf with an amplitude of 1.8 m, however, due to the funnel shape of the Guayas estuary the tides are amplified up to 3 to 5 m near the city of Guayaquil, (Murray et al., 1976).

The drainage basin area of the Guayas River covers 32130 km^2 and is the most important fluvial system in the country. The discharge records for both tributaries indicate that, on average, the contribution of the Babahoyo River exceeds that of the Daule River. The contribution of the former adds up to 60% during the dry season and 66% during the wet season, (Soledispa, 2002). The available tidal stations located throughout the Gulf and the river gauges scattered throughout the basin are also presented in Figure 1.1.

1.2. PROBLEM STATEMENT AND ANALYSIS

For over four decades the Guayas River estuary has been a subject of study, however, most of the information is yet to be processed, integrated and disseminated, (Armijos and Montolío, 2008). Moreover, little is known about the estuary's morphodynamics and evolution. Currently the problems that stem from the morphological development revolve around the sedimentation in the estuary, especially along the Guayas and the lower part of the Babahoyo and Daule rivers. This has posed a number of concerns that are mainly related to the following aspects:

- Harm to the navigability in the Guayas and the lower Babahoyo and Daule rivers. The commercial and economic development has been severely affected mainly due to the effects of the sedimentation of the estuary in front of Guayaquil. Gradually the river traffic has been

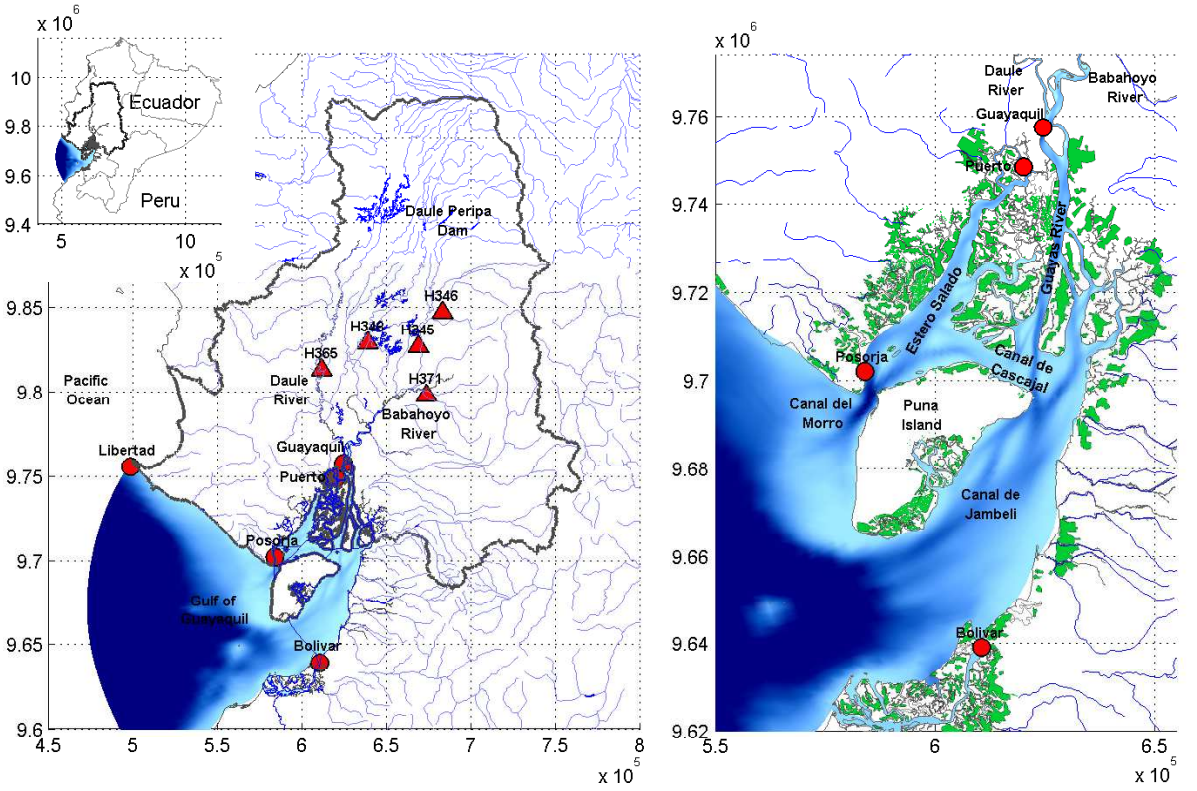

Figure 1.1: Guayas River Basin (left) & Guayas River Estuary (right). River gauging stations (red triangles), tidal gauging stations (red circles), shrimp farms (green)

decreasing. Today navigation is down to canoes or boats and bigger vessels have to wait for high tide conditions. Even then, the maximum draft of the ships has been reduced anyway. According to an article by the Maritime Chamber of Ecuador (CAMAE, 2013), the maximum draft has been reduced from 7.00 m to 6.80 m .

- Increase of the potential risk of flooding in the lower areas around the margins of the rivers especially in the northern part of Guayaquil and the cities of Daule and Babahoyo.

- The "El Palmar" islet: Located at the confluence of the Daule and Babahoyo Rivers, it is deemed as the most prominent and evident feature of the sedimentation of the Guayas River and the Guayas River estuary. However it is not necessarily a sign of the overall sedimentation. It could be a local effect caused by sudden widening of the Daule River near the confluence. The islet occupies the channel of the Daule River, which has been further subdivided in two branches at its mouth. Dumont et al. (2007) describe the evolution of the islet based on the bathymetric surveys carried out by the National Oceanographic Institute of the Navy (INOCAR). The results are summarized in Figure 1.2. The growth is predominantly towards the south and in the current situation it has attained a triangular shape covering a surface of 16 ha approximately.

  The continuous growth of the islet constricts the river and causes a backwater effect that increases the potential risk of flooding of the nearby zones, especially the northern part of Guayaquil. The bathymetric surveys also reveal that, due to the islet, there is a tendency for the river to scour the right bank, which poses a threat to the stability of structures in the proximity. Another factor of concern is the particular location of the islet near Guayaquil international airport. The presence of birds that nest and breed on the islet hinder the takeoff and landing of aircraft.

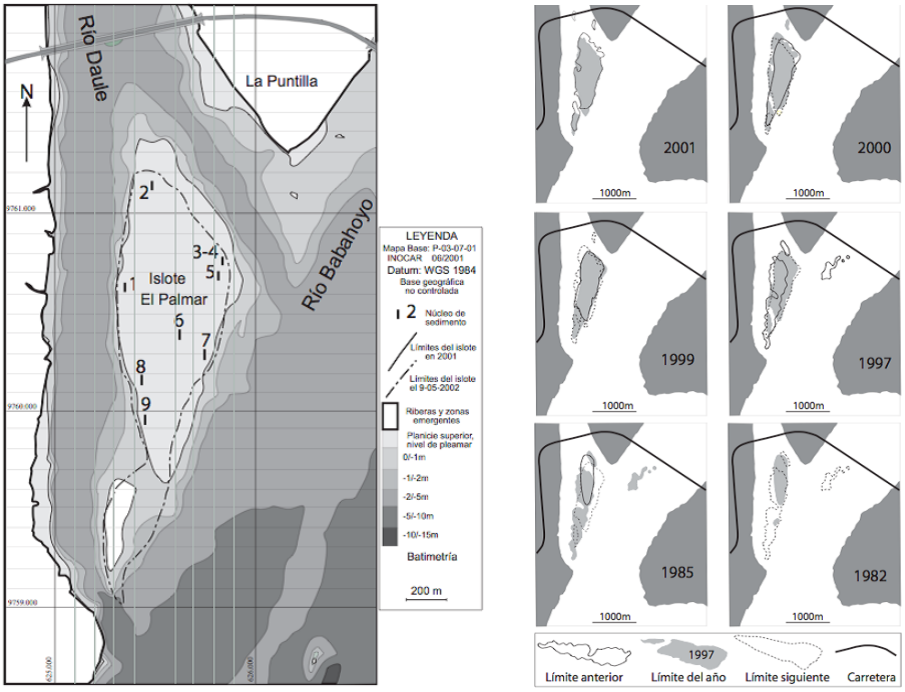

Figure 1.2: Morphology at the confluence of the Daule and Babahoyo Rivers (left), development of the "El Palmar" islet (right). Dumont et al. (2007)

Several studies conducted by the Ecuadorian National Secretary of Water (SENAGUA, former CEDEGE) and INOCAR have suggested that the causes of sedimentation are the consequence of interventions carried out in the upper basin and natural events such as El Niño. However, they have not considered the response of the estuary to interventions carried out within the estuary itself and the potential effects on the tidal dynamics which influences the sediment transport on longer time scales.

1.2.1. CAUSES OF SEDIMENTATION ALONG THE GUAYAS ESTUARY

DEFORESTATION AND CHANGES IN THE LAND USE

Soledispa (2002) underscores the increase of the deforestation in the upper and middle basin of the Guayas River mainly due to changes in the agricultural practices, logging and changes in the land use. Deforestation accelerates the erosion processes, since the soil loses its natural cover, and becomes more exposed to the erosive effects of the surface runoff, which in turn increases the sediment transport to the rivers. CAMAE (2013) makes reference to previous studies by CEDEGE in which it is estimated that on average 15 million tons of sediment are produced annually in the Guayas River basin as a result of logging, changes in the land use and landslides. However there is no evidence that the sediment coming from the upstream basin is actually being deposited within the estuary.

EL NIÑO EVENTS

The ENSO phenomenon (El Niño Southern Oscillation) causes the influx of unusually warm surface water in the southeast Pacific Ocean, which triggers a change in the climate patterns that prompts torrential rainfalls to occur on the coastal areas of Ecuador. A clear example of El Niño is shown

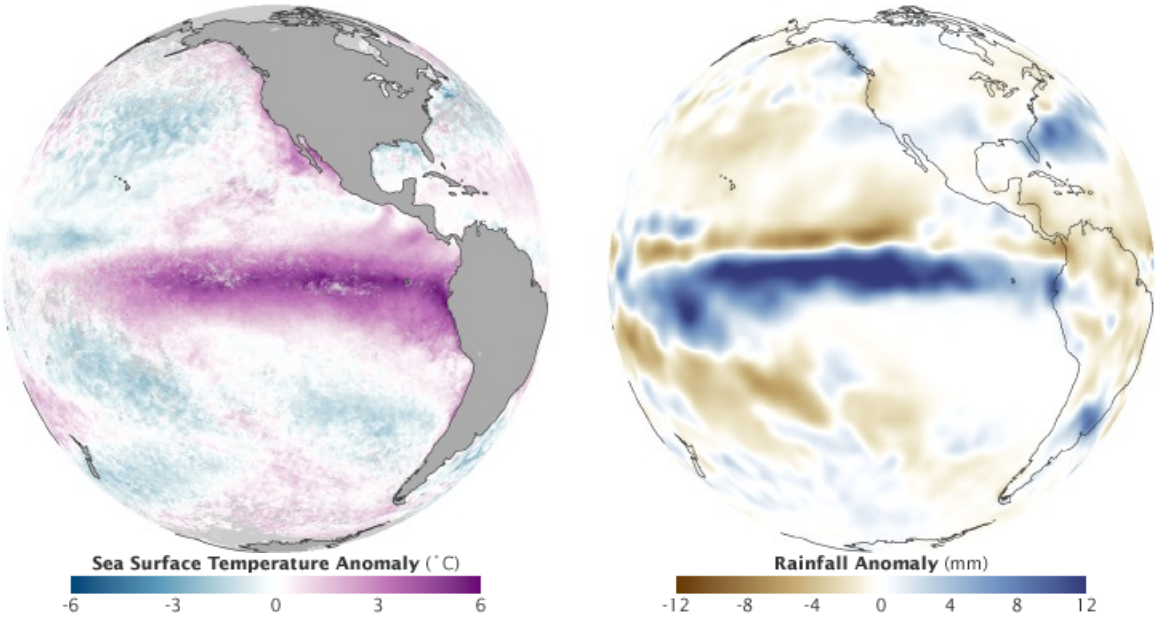

Figure 1.3: Changes in sea surface temperature (right) and rainfall (left) during the 1997 El Nino event, (Riebeek, 1985)

in Figure 1.3 for the 1997 event. Unusually warm waters were as much as 6°C above the average temperature. The atmosphere is warmed as a consequence of the warmer ocean surface, which enhances evaporation and the subsequent development of rainstorms. During the 1997 event as much as 12 millimeters more rain than average were recorded. The event typically peaks around December.

Severe floods are a direct consequence of El Niño. Moreover, in steep areas especially near the coast where clay soils are predominant, landslides are prone to occur during heavy rainfall events. These effects do not only increase the discharge of rivers but also their sediment load.

The occurrence of the phenomenon has been registered 5 times in the last 50 years (1972 – 1973, 1982 – 1983, 1997 – 1998, 2009 – 2010, 2015 – 2016). The most severe one was that of 1982 – 1983 which caused a great socio-economic impact on the coastal region due to a tremendous increase in rainfall, flooding and landslides.

DAULE-PERIPA DAM PROJECT

The Daule-Peripa Dam is a part of the Multi Purpose Jaime Roldós Aguilera Project that was developed towards three main objectives: regulation and control of discharges in the Daule River, hydropower generation, and water supply.

The dam is located in the upper Daule river catchment 186 km north from Guayaquil at the confluence of the Daule and Peripa rivers. The construction was finished in 1988. The dam creates an impoundment (Figure 1.1) that covers 34000 ha and stores over 6.0 km^3, (CELEC, 2013).

Among the specific objectives are:

- Storage of water for irrigation of 50000 ha in the lower valley of the Daule River.
- Water transfer to the Santa Elena Peninsula to comply with the drinking, industrial and agricultural demands.
- Flooding control in the lower valley of the Daule River during the wet season and prevention of salt-water intrusion during the dry season.

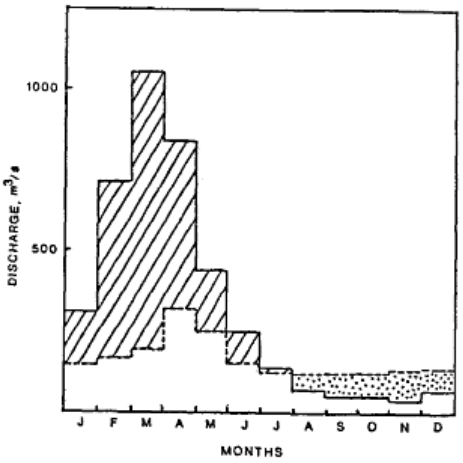

Figure 1.4: Comparison of the monthly averaged discharges at the confluence of the Daule and Peripa Rivers before and after the construction of the dam (Twilley, 1989)

- Water supply for the city of Guayaquil and cities along the Daule River.
- Hydro-power generation

The dam operation is such that the monthly averaged flow rates vary between 321 m^3/s and 124 m^3/s during the wet and dry seasons, respectively, Figure 1.4. A comparison with the situation before the construction of the project shows that during the wet season, the discharge is significantly less than in the normal condition and that during the dry months, the situation is reversed. This has a direct effect on the sediment budget and transport rates of the Daule River, and also a long-term effect on the morphology which also has not been addressed yet by any study.

SHRIMP FARMING AND MANGROVE FOREST RECLAMATION

The shrimp farming activities have intensified since 1970 and are the main drivers for the transformation of the mangrove forest into shrimp-raising lagoons, (Gobierno Autónomo Descentralizado Provincial del Guayas, 2013). The loss of the mangrove forest due to the growth of shrimp ponds (identified as green areas in Figure 1.1) can be seen along the banks of the different branches of the estuary and along the boarders of the Puna island.

Besides the decimation of the intertidal flat areas, the shrimp farming techniques involve a continuous exchange of seawater that is pumped from the estuary to the ponds. During this exchange, less water is returned to the estuary mainly due to evaporation losses in the ponds. Moreover, according to Twilley (1989), this water loss could result in the discharge of hypersaline waters to the estuary. The mangrove forest does not only help to prevent erosion but also enhances the sedimentation along the tidal flats, hence, another possible side effect of the reclamation is the increase of the suspended sediment load within the estuary.

In addition to the aforementioned, perhaps the most important effect of shrimp polders, that has been overlooked by previous studies, is related to the changes in tidal asymmetry which governs the net transport of sediment. Most estuaries have a sand river bed and the tide dissipates along the river by hydraulic friction. When the intertidal areas are reduced considerably, the hydraulic drag is also reduced which causes the tide to have a more flood dominant character which in turn favors the import of sediment. This is addressed later in the report.

THE 'PUENTE DE LA UNIDAD NACIONAL' BRIDGE

The 'Puente de la Unidad Nacional' bridge spans over the Daule and Babahoyo Rivers and consists of a set of bridges that connect Guayaquil with the cities of Samborondón and Durán. Located near the confluence of the rivers the bridge was a necessity to cope with the increasing commercial and touristic development of Guayaquil. At present time the 'Puente de la Unidad Nacional' bridge complex consists of 4 bridges, 2 that run in parallel over the Daule River (bridge Rafael Mendoza Avilés) and 2 placed in parallel over the Babahoyo River (bridge Carlos Pérez Peraso). The construction of the first set of bridges over both Rivers was finished in October 1970. After that the third bridge over the Daule River was constructed between 2002 and 2006, Figure 1.5. Finally the fourth bridge over the Babahoyo River was finished in 2011.

The structure is that of a girder bridge with piers located every 75 m. In total, the foundations block approximately 20% of the width of both rivers. The obstruction of the flow may cause backwater effects that increase the water levels. This is the result of the energy loss in the flow caused by the drag forces acting on the piers. Moreover, in alluvial rivers the scouring of the riverbed takes place at the crossings between abutments. These two processes are linked in the sense that once the scour has developed, the backwater effects will be reduced (Liu et al., 1961). Event though the scouring of the bed and the deposition of sediment caused by the abutments can be easily discerned locally, the net effect on the sediment transport in a larger scale is yet to be analyzed.

TIDAL ASYMMETRY

The distortion of the tidal signal plays a determinant role in the net sediment transport of tide dominated areas. The tidal asymmetry in general refers to the difference between the flood and ebb durations, considering flood as the time when the current velocities are in inland direction and ebb when the current velocities are directed in offshore direction.

The asymmetry arises mainly due to the effects of bottom friction, partial reflections at the landward end and energy convergence within the estuary. The latter is mainly a consequence of the geometry of the basin. In case of a funnel shaped estuary as the Gulf of Guayaquil, the progressive narrowing of the cross section gives rise to a convergence of energy, which, in turn, increases the amplitude as the tide travels up the estuary. On the other hand, bottom friction produces an opposite effect that dampens the amplitude of both the water level and velocity signals. The net effect of all these processes depends on the case. However, a characteristic feature is the introduction of a phase shift between the horizontal and vertical tides that changes the propagating character of the wave. Without the phase shift the flood and ebb duration would be the same and so would the respective flood and ebb velocities.

Whether a basin is flood or ebb dominant is determined by the magnitude of the maximum flood and ebb velocities correspondingly. In general, flood dominance is enhanced when the basin characteristics render long shallow channels and large tidal amplitudes; whereas ebb dominance is enhanced by the presence of large intertidal storage areas or the input of residual currents such as a river discharge, (Bosboom and Stive, 2012).

A clear example of the influence of the tidal distortion is found in the morphology analysis study of the Loire estuary in France carried out by Briére et al. (2011). The estuary serves as the main seaborne trading route for the cities of Saint-Nazaire and Nantes. It also connects some industrial areas such as Montoir and Donges. Due to the combined action of the natural development and human interventions, the tidal asymmetry in the Loire has evolved from an ebb-dominant to a flood-dominant situation. Operations mainly related to dredging and bank protection resulted in the deepening of the main channel and the progressive obstruction of the intertidal flats. Consequently, the damping effect of friction reduced and the tidal amplitude along the estuary increased.

The developments carried out in the Guayas River estuary and the Guayas River basin have

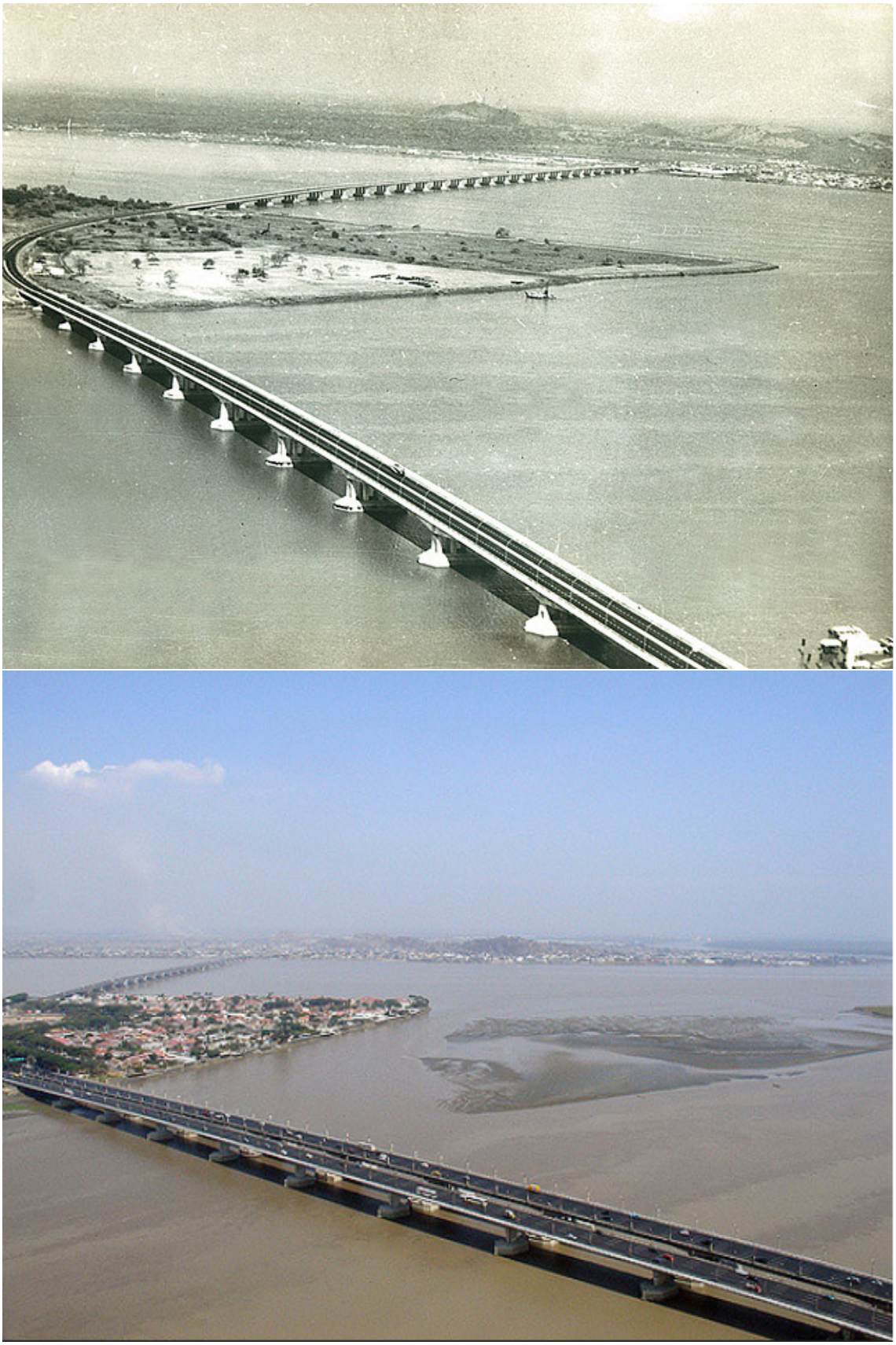

Figure 1.5: 'Puente de la Unidad Nacional' bridge looking downstream from the right bank of the Daule River. After construction in 1970 (top), and the situation in 2006 (bottom).[a]

[a]Photographs courtesy of Pedro Gambarrotti

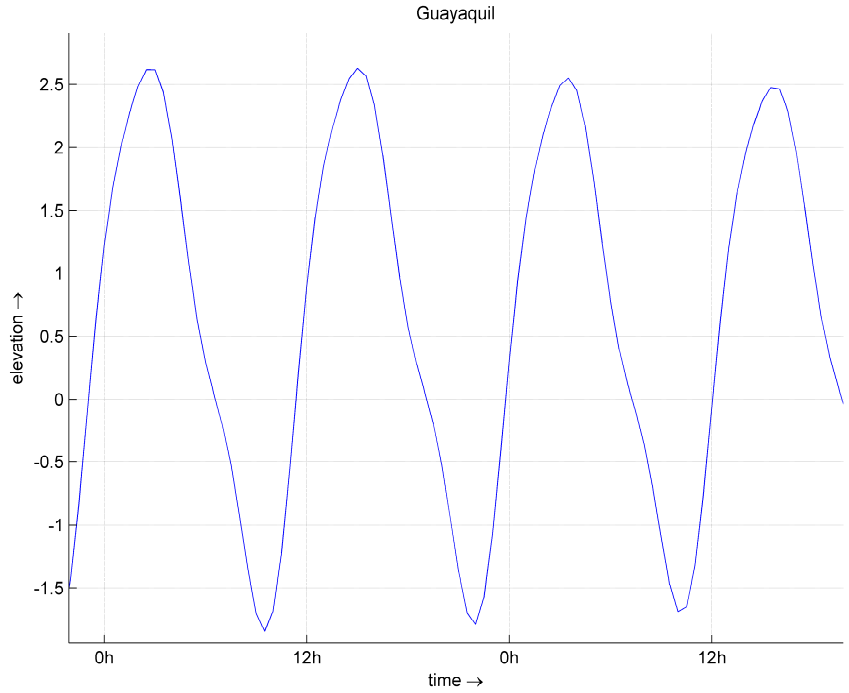

Figure 1.6: Tidal curve at the Guayaquil gauging station (elevations taken relative to Mean Sea Level)

yielded results analogous to those in the Loire. In broad terms, the aquaculture activities with the major increase of shrimp ponds have reduced the intertidal areas, and the construction of the Daule-Peripa dam in the upper basin reduced the discharge in the Daule River. The latter, among others, allows the tide to protrude further inland, thus increasing the total volume of the estuary.

A sample of the tidal curve recorded at the Guayaquil gauging station during September 2015 is presented in Figure 1.6. The records show a longer falling period of approximately 7 hours compared to the rising period duration of 6 hours. This is an indication for the flood-dominant character of the estuary since shorter flood duration means that the maximum flood velocities are higher than the maximum ebb velocities.

1.2.2. NUMERICAL MODELLING

Process-based numerical models pose a very useful tool to analyze and predict the behavior of hydraulic systems. They provide the opportunity to test different scenarios and isolate effects in order to gain insight into the physical phenomena. They are more flexible compared to analytical models and field experiments. The former often involve a great amount of simplifications and are mostly applicable for ideal situations, and the latter are limited by scaling effects. Nevertheless, numerical models constitute a complement rather than a substitute to the other approaches, since they also present shortcomings and limitations on their own, which are mainly related to truncation errors, calibration, data availability and computational power.

A reductionist approach is used in physics-based models, in which all processes are described either by differential equations at the smallest scales or empirical relations. The main assumption is that the overall combination of the processes yields a good representation of reality.

Among the available numerical models, Delft3D has been applied in a variety of scientific projects for rivers, estuarine and coastal systems worldwide, for which it has proven its reliability and accuracy. Delft3D is a morphodynamic model developed by Deltares. It solves the two-dimensional depth-averaged and the full 3D Reynolds-averaged Navier-Stokes equations, and it is also capable

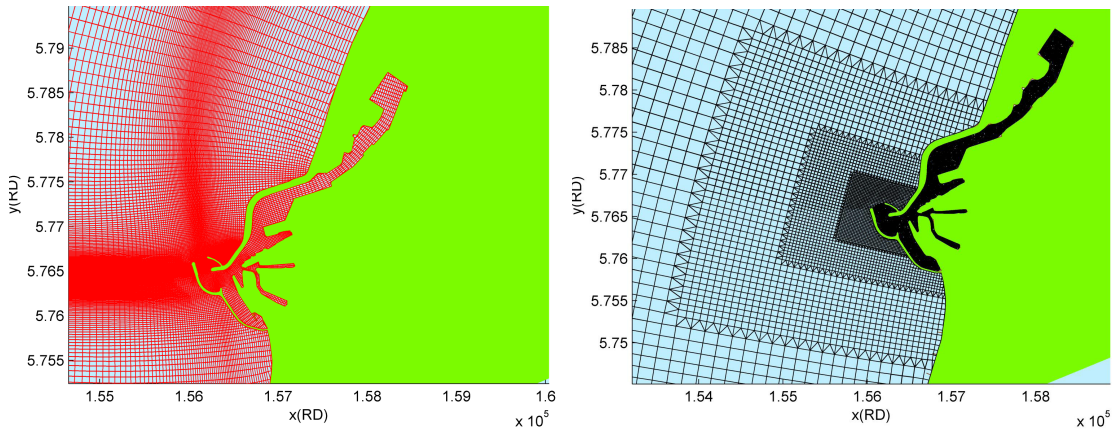

Figure 1.7: Structured grid vs unstructured grid,(Hasselaar et al., 2013)

of computing sediment transport and bed level changes.

Over the last couple of years Deltares has developed a new hydrodynamic engine for the Delft3D suite named Delft3D Flow Flexible Mesh (from here onward referred to as Delft3D-FM). This new unstructured-grid approach is based on the finite-volumes method which allows for polygon-shaped cells and couples 1D, 2D and 3D modelling concepts. In contrast with Delft3D-FLOW, that is based on finite differences on structured grids (by applying conservative discretization, the finite differences of Delft3D-FLOW are equivalent to finite-volumes), the new approach is more versatile and overcomes the drawbacks linked to curvilinear structured grids such as:

- High grid resolution in a particular zone is achieved at the expense that this high resolution extends along the m- and n- lines in the entire domain.
- In inner bends, unwanted grid refinement might lead to a very small cell size which in turn could be translated into a severe time step restriction.
- Curvilinear grids are not always able to mimic all the boundaries accurately in complicated geometries. In some instances, staircase boundaries are unavoidable, which lead to artificial wall friction.

A clear example of the advantages of unstructured grids is presented in Figure 1.7 for the Harlingen harbour in the Netherlands. High grid resolution is limited to the area of interest only.

The performance on hydrodynamic computations of Delft3D-FM for 2D models is proven to be similar to known shallow water codes such as Delft3D-FLOW, WAQUA and TRIWAQ (Kernkamp et al., 2011). By the time of this research most of the features of the morphology module were already coupled with the hydrodynamics and implemented for 2DH models. However, some features were still being under development and testing, in particular those related to:

- Changes in the bed shear stress and sediment transport due to curvature induced secondary flow (or spiral flow).
- Sediment transport over fixed layers.

The spiral flow is determinant to accurately model the flow structure, sediment transport and morphology especially around bends. It stems from the imbalance between the local pressure gradient and the centrifugal forces, hence it is directed perpendicular to the main flow direction. The 3D nature of the spiral flow is lost for the 2D depth-averaged Navier Stokes equations. Therefore, this 3D feature needs to be parametrized in order to include its effects in a 2DH model. This is done

by means of the spiral flow intensity (Deltares, 2015a) , which is then used to compute additional shear stresses to be included in the momentum equations, and to adjust the direction of the bed load transport. The implementation on unstructured grids is described by Nabi et al. (2016), however it has not yet been fully tested and validated.

Struiksma (1999) shows that bed perturbations propagate significantly faster once the non-erodible layer is exposed. This is related to the sediment transport capacity exceeding the sediment supplied by the bed. In that regard, he also proposed a model concept that represents the bedload transport over the non-erodible layer and the effect on the celerity of bed perturbations. The model has been successfully implemented in Delft3D but is currently under development and testing for Delft3D-FM.

1.3. MOTIVATION

Due to the remarkable importance of the Guayas river basin within the national context, in 1965 the commission for study and development of the basin (CEDEGE) was created with the purpose of developing an integrated management of the catchment. However, the lack of political interest and funding resources made it difficult for CEDEGE to achieve its goals and the interest was focused mainly around the major projects involving dam construction and irrigation. Consequently, little emphasis has been put towards an integral development and a control and monitoring plan of the catchment.

There are some studies addressing the temporal development of some areas of interest such as the “El Palmar” islet and the port of Guayaquil. However, a study that covers the morphodynamic evolution of the estuary on larger spatial and temporal scales is yet to be performed. Within this context, numerical models become useful for understanding and predicting the morphodynamics of the estuarine system. Moreover, they serve as a numerical lab where different scenarios can be defined in order to determine the hydrodynamic or morphodynamic effects of interventions and perturbations of different nature.

1.4. OBJECTIVE AND RESEARCH QUESTIONS

Based on the problems and the need to develop an integral approach to manage the Guayas River basin and estuary, the main objective of this study is to:

Understand the estuarine system and the processes behind its morphological development

In order to achieve the proposed objective the following research questions need to be addressed:

- What are the sedimentation and erosion patterns due to fluvial and tidal processes?
- What is the relative impact on the sediment balance and the morphology of the estuary caused by the different interventions carried out in the Guayas River basin and the estuary itself?
- Besides the identified causes of sedimentation by previous studies, is the estuary importing sediment from the adjacent coast?
- How sensitive is the system to the different events and interventions?
- What are the possible measures to be taken in order to control the sedimentation in the Guayas River, specially around the city of Guayaquil?

This is done with the aid of the mophodynamic model Delft3D-FM. As mentioned before the model has been validated for hydrodynamics, but the coupling with the morphology module is still under development. In that regard, a secondary objective of this study is to test and diagnose problems related to the morphology module. The following research question addresses this secondary objective:

- Is Delft3D-FM able to reproduce similar results for sediment transport and morphology as the structured grid version of Delft3D, in relation to the effects caused by spiral flow and sediment transport over fixed-layers?

1.5. METHODOLOGY

The approach to meet the objectives is described as follows:

- Review the literature in order to understand the relevant physical processes influencing sediment dynamics in similar estuarine areas. This step also involves gathering all the relevant hydrodynamic and morphological data available for the Guayas River estuary. This refers to information about river hydrographs, water levels records, bathymetric surveys, salinity concentrations and sediment properties.
- Schematize the situation by setting up a model using Delft3D-FM. First the extent of the model needs to be defined based on the size of the area of interest and the available data needed to describe initial and boundary condtions.
- Analyze the morphological evolution of the estuary, taking into account all the factors previously described. This step involves the calibration of the model parameters based on the historical data.
- Assess the effects of the events and interventions by determining different scenarios in which the morphological evolution is modelled.

Due to the lack of information in some cases, a number of assumptions and simplifications are made throughout this study, which will be appropriately discussed and justified .

2

LITERATURE REVIEW

2.1. ALLUVIAL ESTUARIES

An estuary is the transition between a river and the sea. The river discharges fresh water and the sea fills the estuary with salty water. They have particular hydraulic and morphologic conditions and often act as a sink for sediment from both river and the sea. Among their most prominent features, the topography is a crucial one since it provides the most important boundary conditions for tidal hydraulics, mixing and salt water intrusion.

2.1.1. SHAPE OF ALLUVIAL ESTUARIES

Alluvial estuaries are characterized by movable beds, indeed, there is an interdependence between topography and hydraulics that shapes the estuary itself. Their mere existence can be explained by a dynamic equilibrium between erosion and sedimentation that takes place on different time scales, namely: the inter-tidal time scales that range from diurnal (semi-diurnal) cycles to spring-neap cycles, and the residual current time scale as a result of the river discharge.

The shape of alluvial estuaries is similar all around the world, (Savenije, 2006). Converging banks in the upstream direction and small or even horizontal bottom slopes are characteristic of this type of estuaries. According to the shape the estuaries are classified as:

- Funnel shaped: The longitudinal variation of the cross section A and width B can be described by exponential functions.

$$\begin{aligned} A &= A_0 e^{-x/a} \\ B &= B_0 e^{-x/b} \end{aligned} \tag{2.1}$$

  Where x is the distance taken from the mouth in the upstream direction, a and b are length scales, however, b is the width rate of convergence named convergence length. The combination of both equations gives an expression for the mean estuary's depth.

$$h = h_0 e^{\frac{x(a-b)}{ab}} \tag{2.2}$$

  Depending on the values of a and b the depth either increases, decreases or remains constant.

- Prismatic: An estuary with an infinite convergence length

The main factors that determine the estuary's shape are the tidal range and the upland discharge. Funnel and prismatic shaped estuaries are characterized by large values of the former and the latter, respectively.

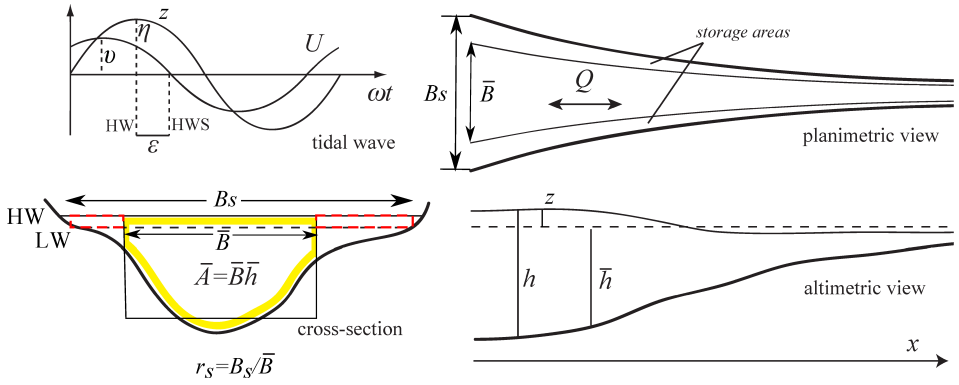

Figure 2.1: Notation of tidal and estuary parameters, (Savenije, 2006)

2.1.2. TIDAL HYDRAULIC PARAMETERS AND BASIC EQUATIONS

The interaction between water and sediment in its simplest form is described by a set of equations in 1 dimension namely: the Saint-Venant equations that state the conservation of mass and momentum for water, the conservation of mass for sediment and a transport formulation that relates flow and transport quantities. The equations read:

$$\frac{\partial Q}{\partial t} + \alpha_s \frac{\partial (Q^2/A)}{\partial x} + gA\frac{\partial h}{\partial x} + gA\frac{\partial Z_b}{\partial x} + gA\frac{h}{2\rho}\frac{\partial \rho}{\partial x} + gA\frac{U\,|\,U\,|}{C^2 h} = 0 \tag{2.3}$$

$$r_S \frac{\partial A}{\partial t} + \frac{\partial Q}{\partial x} = R_s \tag{2.4}$$

$$B\frac{\partial Z_b}{\partial t} + \frac{\partial Q_s}{\partial x} = 0 \tag{2.5}$$

$$Q_s = B d_s U^n \tag{2.6}$$

where Q is the discharge, α_s is a shape factor to account for the spatial variations of the velocity in a cross section, A is the cross section area, h is the mean cross sectional depth, Z_b is the mean cross sectional bottom elevation, ρ the fluid density, U the mean cross sectional velocity, C is the Chézy coefficient, B the stream channel width, B_s the storage width, $r_S = B_s/B$ the cross sectional storage ratio, R_s is a source term, Q_s is the sediment discharge including pores, d_s is a parameter linked to the sediment transport formulation that depends on the sediment characteristics and channel roughness, g is the acceleration due to gravity, finally x and t refer to the distance and time variables, respectively.

Savenije (2006) proposed a solution to the above equations applied to alluvial estuaries of the well mixed type. He assumes beforehand that the tidal wave can be described by sinusoidal functions. This is an implicit solution of the coupled set of equations once they have been linearised. However, the non-linear terms in the equations are retained throughout the derivation. Therefore, the approach to solve the equations is deemed as quasi-linear. The key to the solution is to include the characteristics of alluvial estuaries, i.e., the effect of density differences, the tidal motions and the shape which is described by the exponential variations of width and cross-sectional area.

Before addressing the solution to the Saint-Venant equations, some of the tidal characteristics must be defined:

- Tidal excursion is the distance a water particle travels between low water slack (LWS) and high

water slack (HWS).

$$E_0 = \int_{LWS}^{HWS} U(0,t)\,dt \tag{2.7}$$

- Tidal prism is the volume of water entering the estuary between low water slack (LWS) and high water slack (HWS). The tidal excursion E_0 times the cross sectional area at the mouth A_0 is a good approximation for the tidal prism.

$$P_t = \int_{LWS}^{HWS} Q(0,t)\,dt \approx A_0 E_0 \tag{2.8}$$

- The Estuary Richardson number is a good indicator for the degree of mixing or stratification within the estuary. It is defined as the ratio between the potential energy provided to the estuary by the river through buoyancy and the kinetic energy supplied by the tide in order to realize the mixing during a tidal period.

$$N_R = \frac{E_m}{E_t} = \frac{\Delta\rho}{\rho}\frac{ghQ_fT}{A_0E_0v_0^2} = \frac{\Delta\rho}{\rho}\frac{ghQ_fT}{P_tv_0^2} \tag{2.9}$$

  where E_m and E_t are the potential and kinetic energy per tidal cycle respectively, Q_f is the fresh water discharge, v_0 is the tidal velocity amplitude at the estuary's mouth and T is tidal period.

  Based on observation it can be said that stratification occurs if $N_R \geq 0.8$, and well mixed conditions occur if $N_R \leq 0.08$.

2.1.3. THE EFFECT OF DENSITY

In well mixed estuaries the salinity decreases gradually from the mouth in the upstream direction. The effect of the density gradient in the momentum equation is then taken into account by a residual water level slope over the salt intrusion length. After some simplifications regarding the advection term and with the introduction of the gradual density variation, the Saint-Venant equations can be expressed as a function of the mean cross sectional velocity U, and the water level $Z = Z_b + h$ as:

$$\frac{\partial U}{\partial t} + U\frac{\partial U}{\partial x} + g\frac{\partial h}{\partial x} + \frac{gh}{2\rho}\frac{\partial \rho}{\partial x} + g\frac{\partial Z_b}{\partial x} + g\frac{U\,|\,U\,|}{C^2h} = 0 \tag{2.10}$$

$$r_S\frac{\partial h}{\partial t} + U\frac{\partial h}{\partial x} + h\frac{\partial U}{\partial x} + \frac{hU}{B}\frac{\partial B}{\partial x} = 0 \tag{2.11}$$

The density gradient effect is reflected in the fourth term of Equation 2.10. It always exerts a pressure in the upstream direction. This pressure is counteracted by a residual water level slope as illustrated in Figure 2.2. The resulting forces are equal in magnitude and act in opposite direction in different vertical positions. The momentum generated by the forces is then responsible for the vertical mixing process in well mixed estuaries which is called gravitational circulation. This process is also responsible for the continuous supply of marine sediment that moves in the upstream direction near the bottom.

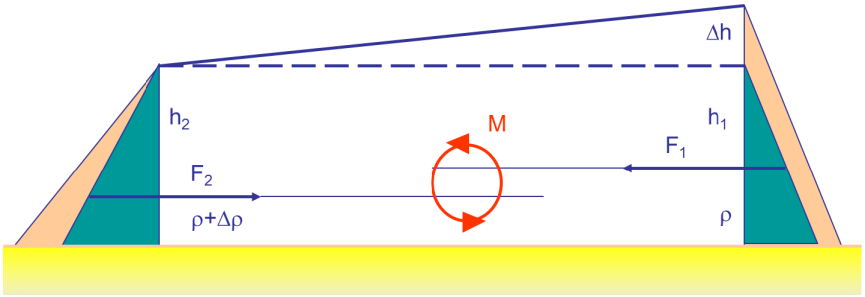

Figure 2.2: Forces driving vertical net circulation, (Savenije, 2006)

2.1.4. THE EFFECT OF THE TIDE

The effect of the tide is taken into account by considering that the water levels and velocities vary according to periodic functions, i.e., a tidal wave. The water movement related to the tidal wave is predominantly horizontal and parallel to the banks and is the main reason why the analysis can be done from a 1-dimensional perspective.

The tidal wave can be deemed to have a standing, progressive or mixed character according to its propagation speed (also known as wave celerity or phase speed). For a standing wave high water and low water are reached at the same time within the estuary , hence the wave speed is infinite, $c = \infty$. The water level signal is 90 degrees out of phase with the velocity signal ($\phi = \pi/2$), which means that high water and low water slacks coincide with high water and low water instants correspondingly. In contrast, the occurrence of a progressive wave is only possible on a prismatic frictionless channel with infinite length. The water level and velocity signals are in phase ($\phi = 0$), and the wave celerity is computed as $c = \sqrt{gh}$.

In reality the tidal wave in alluvial estuaries has a mixed character. It propagates as a wave that has features of both progressive and standing waves, i.e., the phase lag between the vertical tide (water level) and horizontal tide (velocity) is between 0 and $\pi/2$. As the wave travels up the estuary, the tidal amplitude is either amplified or damped. Whether one of the other occurs, it all depends on the imbalance between topographic convergence and friction. If friction dominates, the wave is damped; if convergence is predominant the wave is amplified; if both are equal the amplitude remains constant. Savenije (2006) states that the most important factor determining the phase lag is the shape of the estuary, i.e., the bank convergence. Especially when the tide is amplified or remains constant the effect of friction is mild. This is generally the case in the lower part of the estuaries where the amplitude to depth ratio is small ($\eta/h \ll 1$) and the tidal fluxes dominate over the influence of the river discharge.

IDEAL ESTUARY

The idea of an ideal estuary stems from the equilibrium between convergence and friction. This idea is further confirmed by observations in estuaries around the world which seem to share common geometric features as:

- The mean depth remains somewhat constant along the estuary.
- The amplitude of the velocity signal also remains constant along the estuary, this implies that the tidal excursion is also constant.
- The tidal range also remains more or less constant despite the presence of some degree of amplification or damping.

These characteristic features of an ideal estuary also indicate a state of morphodynamic equilibrium conditions which implies that no residual currents and transports occur. This is further confirmed by Van der Wegen et al. (2008).

Based on the aforementioned the definition of an ideal estuary reads:

"A funnel shaped estuary with the width obeying an exponential function, that preserves a constant tidal range and hence maintains a constant amount of wave energy per unit volume of water"

This definition is key for an analytical solution of the Saint-Venant equations.

TIDAL ASYMMETRY AND MORPHOLOGY

The term tidal asymmetry refers to both the vertical and horizontal tide. It stems from the distortion of the semi-diurnal tide due non-linear processes that occur through interaction with bottom friction and the morphology. These secondary effects are mathematically modelled as overtides. Wang et al. (1999) make an analysis of the non-linear terms in Equation 2.10 and Equation 2.11, and found that overtides are generated by the interaction of the M_2 tidal component with itself and other fundamental constituents. They also determine that the degree and nature of the asymmetry depend on the ratio between the amplitudes of the semi-diurnal tide and the overtides, and on the phase difference of the tidal constituents respectively.

The asymmetry of the vertical tide is linked to the difference between flood and ebb periods. The tide is said to be flood-dominant when the rising period is shorter than the falling period, and vice versa the tide is ebb-dominant when the rising period is larger that the falling period. On the other hand, the asymmetry of the horizontal tide makes reference to two aspects: the difference between ebb and flood velocities, and the duration of the slacks. Regarding the first aspect, flood-dominance occurs when the maximum flood velocity is larger than the maximum ebb velocity. For the second one, flood-dominance is portrayed when the duration of high water slack (HWS) is longer than that of the low water slack (LWS).

There is a feedback mechanism between tidal asymmetry and morphology. On the one hand, morphology influences tidal asymmetry in the sense that the tidal wave is distorted as it propagates; it can be concluded that flood-dominance is enhanced by shallow estuaries, and ebb-dominance is enhanced by deeper estuaries with large intertidal storage areas. On the other hand, tidal asymmetry also influences morphological development through the residual sediment transport. Indeed, Van de Kreeke and Robaczewska (1993) determine that the asymmetry of the horizontal tide and the tide averaged residual currents are mechanisms that contribute to a residual sediment transport:

- Residual currents originate from several sources. Among the most relevant are an upstream river discharge and tide induced horizontal circulation. In river dominated situations the effect of the tidal asymmetry is of secondary importance and the residual sediment transport merely depends on the river discharge. In funnel shaped estuaries the main effect of the river discharge is related to the influence over the tidal currents. The ebb currents become larger until the point where is no longer change in flow direction, hence, the timing of both high (HWS) and low water slack (LWS) is directly influenced too, as depicted in Figure 2.3.

  Tidally induced circulations are mainly governed by geometry, bathymetry and the effects of inertia. In general terms, it can be said that the residual flow in deeper channels is in the ebb direction whereas in the shallower part it is in the flood direction.

- Asymmetry of the horizontal tide has an impact on the bed-load and suspended load transport. The bed-load is assumed to react instantly to the changes of flow velocity, Van de Kreeke

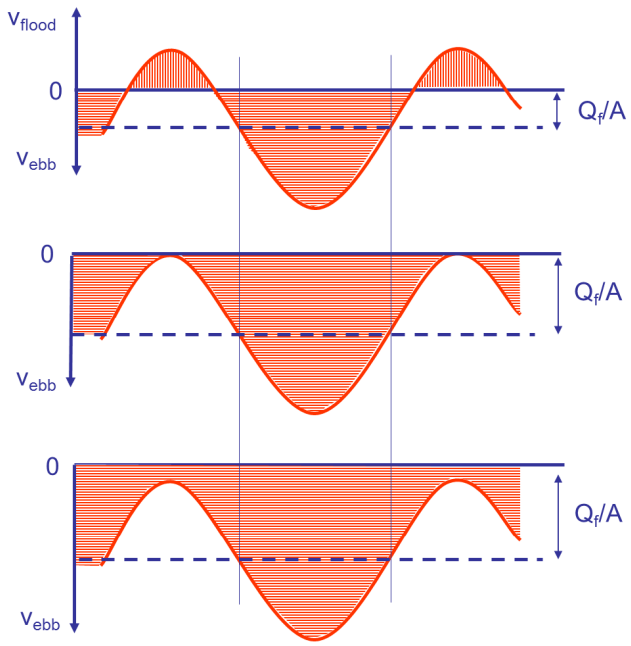

Figure 2.3: Influence of the river discharge, (Savenije, 2006)

and Robaczewska (1993) analyzed the influence of the asymmetry on the long-term mean bed-load transport assuming that the M_2 constituent dominates the flow velocity and the transport rate is proportional to a power of the current velocity. They found that the most important contributions to the net tide-induced bed-load transport are given by the residual flow velocity, the amplitude of the M_2 tidal current and the amplitude and phases of the M_2 overtides (M_4 and M_6). These conclusions imply that for morphodynamic modelling it is not necessary to prescribe the complete set of tidal constituents since in the long-term their effect would be averaged out; it is rather enough to prescribe the M_2 tide and its overtides.

In contrast with the bed-load transport, suspended load transport depends not only on the instantaneous flow velocity but also on the flow conditions upstream and in the past. The erosion and sedimentation timescales are of similar order of magnitude as the tidal period, therefore the assumption of an instantaneous response is no longer valid. This adaptation effect is responsible for the transport of suspended sediment even when the residual bed-load transport is zero. The flood or ebb dominance is then determined merely by the duration of the slack water periods, i.e., there is a residual import of sediment if the HWS is longer than the LWS and vice versa (Bosboom and Stive, 2012).

The horizontal tide is related to the vertical tide through the continuity equation. This relation is also non-linear since the cross sectional area depends on the water level. This non-linear relationship suggests that flood or ebb dominance of the vertical tide does not automatically translate into flood or ebb dominance of the horizontal tide. Therefore, the morphological evolution of an estuary is a non-linear process in space and time (Bolle et al., 2010).

In summary, as the tide propagates into the estuary, non-linear processes triggered by the morphology become more and more important which causes the tide to become asymmetric. In case of the vertical tide, flood or ebb dominance is determined by the relative duration of the water level rise and fall. A shorter water level rise describes a flood dominant character. Asymmetry of the vertical tide causes asymmetry in the horizontal. However, the relation between the tides is non-linear, hence, a flood dominant behavior of the vertical does not necessarily implies flood dominance of

the horizontal tide.

On the other hand, asymmetry of the horizontal tide refers to two aspects, i.e., the difference of ebb and flood velocities, and the duration of the high and low water slacks. For the former, if the flood velocities are larger, then the residual bed-load transport is also in the flood direction. The latter is related to residual transport of suspended sediment, if HWS is longer than LWS the residual transport of fine material is in the flood direction and vice versa. The horizontal tide is directly related to the sediment transport S since it is thought that coarse sediment responds instantaneously to flow velocity u as follows:

$$S \approx d_s \mid u^{n-1} \mid u \tag{2.12}$$

Where d_s is a proportionality constant. Considering that the velocity signal can be written in terms of tidal constituents and assuming $n = 3$, Van de Kreeke and Robaczewska (1993) derived an expression for the long-term averaged bed-load transport $\langle S \rangle$ that describes which are the most important contributions:

$$\frac{\langle S \rangle}{d_s \hat{u}_{M2}^3} = \underbrace{\frac{3}{2}\frac{u_0}{\hat{u}_{M2}}}_{(1)} + \underbrace{\frac{3}{4}\frac{\hat{u}_{M4}}{\hat{u}_{M2}}\cos\varphi_{M4-2}}_{(2)} + \underbrace{\frac{3}{2}\frac{\hat{u}_{M4}}{\hat{u}_{M2}}\frac{\hat{u}_{M6}}{\hat{u}_{M2}}\cos(\varphi_{M4-2} - \varphi_{M6-2})}_{(3)} \tag{2.13}$$

wherein u_0 is the residual flow that stems from a river discharge for example. $\hat{u}_{M2}$, $\hat{u}_{M4}$ and $\hat{u}_{M6}$ are the amplitudes of the M_2, M_4 and M_6 tidal constituents, respectively. φ_{M4-2} is the phase lag $\varphi_{M4} - 2\varphi_{M2}$ and φ_{M6-2} is the phase lag $\varphi_{M6} - 3\varphi_{M2}$. The terms on the right hand side represent the net transport as a result of:

1. Asymmetry introduced by the residual flow

2. Asymmetry of the tide introduced by the interaction between the M_2 and M_4 components. This type of asymmetry is characterized by two parameters: the amplitude ratio η_{M_4}/η_{M_2} which determines the strength of the asymmetry, and the phase difference φ_{M4-2} that determines flood or ebb dominance.

3. The interaction between M_2, M_4 and M_6 which is relatively small compared to the previous terms.

2.1.5. RELATION BETWEEN TIDE AND ESTUARY SHAPE

By analyzing the conservation of mass together with the exponential shape of the alluvial estuaries, Savenije (2006) derived three equations: the phase lag Equation 2.14, the geometry-tide Equation 2.15, and the scaling Equation 2.16 which is only a combination of the other two. These link typical geometry aspects with tidal hydraulic parameters, and result very useful since they offer a first estimate of parameters that are very difficult to measure, such as the tidal excursion E and the tidal prism P_t, based on parameters that can be directly determined from aerial photographs or maps, such as the width at the mouth B_0 and the convergence length b.

$$\tan(\varepsilon) = \frac{\omega b}{c(1 - \delta_U b)} \tag{2.14}$$

$$\frac{H}{E} = \frac{\eta\omega}{v} = \kappa\frac{h}{r_S b}\frac{(1 - \delta_U b)}{\cos(\varepsilon)} \tag{2.15}$$

$$\frac{\eta}{h} = \kappa \frac{v}{c} \frac{1}{r_S \sin(\varepsilon)} \tag{2.16}$$

Where δ_U is the longitudinal damping rate of the velocity amplitude, κ is a correction factor between 1 and 1.1 for amplitude to depth ratios $\eta/h < 0.5$. The remaining unknowns, velocity amplitude v, water level amplitude η, wave celerity c and the phase lag between HW and HWS ε, are addressed with two more equations derived from the momentum balance.

The tidal damping Equation 2.17 is derived under the assumptions that $\eta/h \ll 1$ and the velocity of the river discharge is small compared to the tidal velocity. The wave celerity Equation 2.18 is derived under the same assumptions as the latter plus considering the phase lag ε and celerity c to be constant along the estuary.

$$\frac{1}{\eta}\frac{d\eta}{dx}\left(1 + \frac{g\eta}{cv\sin(\varepsilon)}\right) = \frac{1}{a} - f'\frac{v\sin(\varepsilon)}{hc} \tag{2.17}$$

$$c^2 = \frac{c_0^2}{1 - \frac{\sin(2\varepsilon)}{2(1+\alpha)}\left(\frac{c}{\omega a} - \frac{f' v \sin\varepsilon}{\omega h}\right)} \tag{2.18}$$

$f' \approx f = g/C^2$ for small amplitude to depth ratio is a friction factor. $\alpha = \dfrac{cv\sin\varepsilon}{g\eta}$ is the tidal Froude number and $c_0 = \sqrt{gh}$ is the celerity of a progressive wave.

This set of 4 equations (without considering Equation 2.16) is then enough to solve the Saint-Venant equations analytically for idealized alluvial estuaries.

2.2. SIMILAR CASE STUDIES

2.2.1. LOIRE ESTUARY IN FRANCE

The Loire estuary is the maritime trading route between main ports and industrial areas in France such as Saint-Nazaire, Nantes and Montoir, to name a few. To promote navigation a number of interventions has been carried out over the twentieth century, which have caused changes in the geometry and morphology of the estuary. The interventions are related mainly to intense dredging and dumping activities especially around the port of Nantes. The changes involve the deepening and regularization of the main channel and variation of the banks and tidal flats due to the dumping activities. The situations in 1945 and 2002 are presented in Figure 2.4. It can be seen that as a result of the interventions, the width in the central part is reduced, tidal channels and tidal flats are also reduced, the meanders are less pronounced in the outer estuary and the number of main channels decreased from 2 to 1.

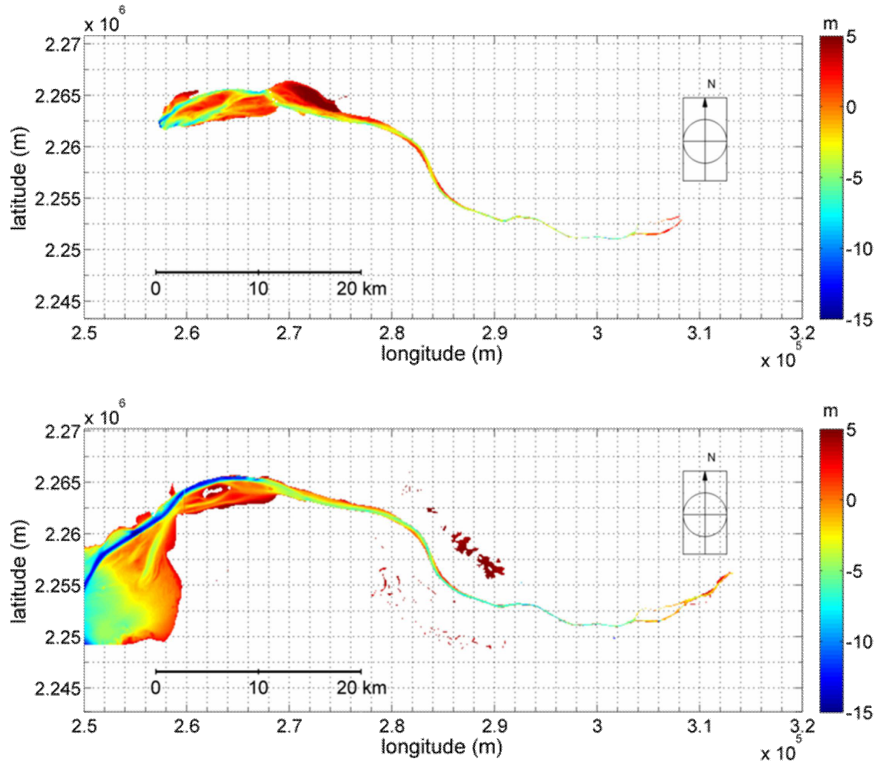

Figure 2.4: Loire estuary bathymetric surveys 1945 (top) & 2002 (bottom) , relative to MSL, (Briére et al., 2011)

Briére et al. (2011) analyze the morphological development of the estuary in the stretch between the cities of Nantes and Paimboeuf. They framed the study towards explaining the factors that influence the morphology and its evolution.

The geometric and topographical changes due to the numerous interventions have caused changes in the behavior of the tide. The top plot of Figure 2.5 shows the lines representing the envelopes of the high an low water during spring tide along the estuary for different years. Prior to 1903 the damping of the tidal amplitude is fairly regular along the estuary. Due to the changes in depth and storage in subsequent years, the damping effect of friction is reduced, hence the amplitude increases significantly and the tide is able to protrude further into the upstream direction.

Besides the implications for the tidal amplitude, the tidal asymmetry is also affected by the changes within the estuary. The middle plot of Figure 2.5 shows the phase difference between the vertical and horizontal tide along the estuary. The tide evolves towards a more progressive character since the phase differences are less in 2002 than in 1947 in most part of the estuary.

A further look into the evolution of the tidal asymmetry is done by an analysis of the harmonic components of the water level signal. A quick reconstruction of the tidal signal is based on the M_2 and M_4 constituents is:

$$\eta = \cos(\omega_2 t) + \frac{M_4}{M_2}\cos[2\omega_2 t + (2\varphi_2 - \varphi_4)]$$

where ω_2 is the frequency of the M_2 component, M_2 and M_4 are the amplitudes, and φ_2 and φ_4 are the phases. The ratio between the amplitudes and phases is presented in the bottom plot of Figure 2.5. Both the amplitude and phase difference ratios increase between 1947 and 2002. By examining the equation above this means that the tide evolves towards a more flood dominant character which intensifies the import of sediment.

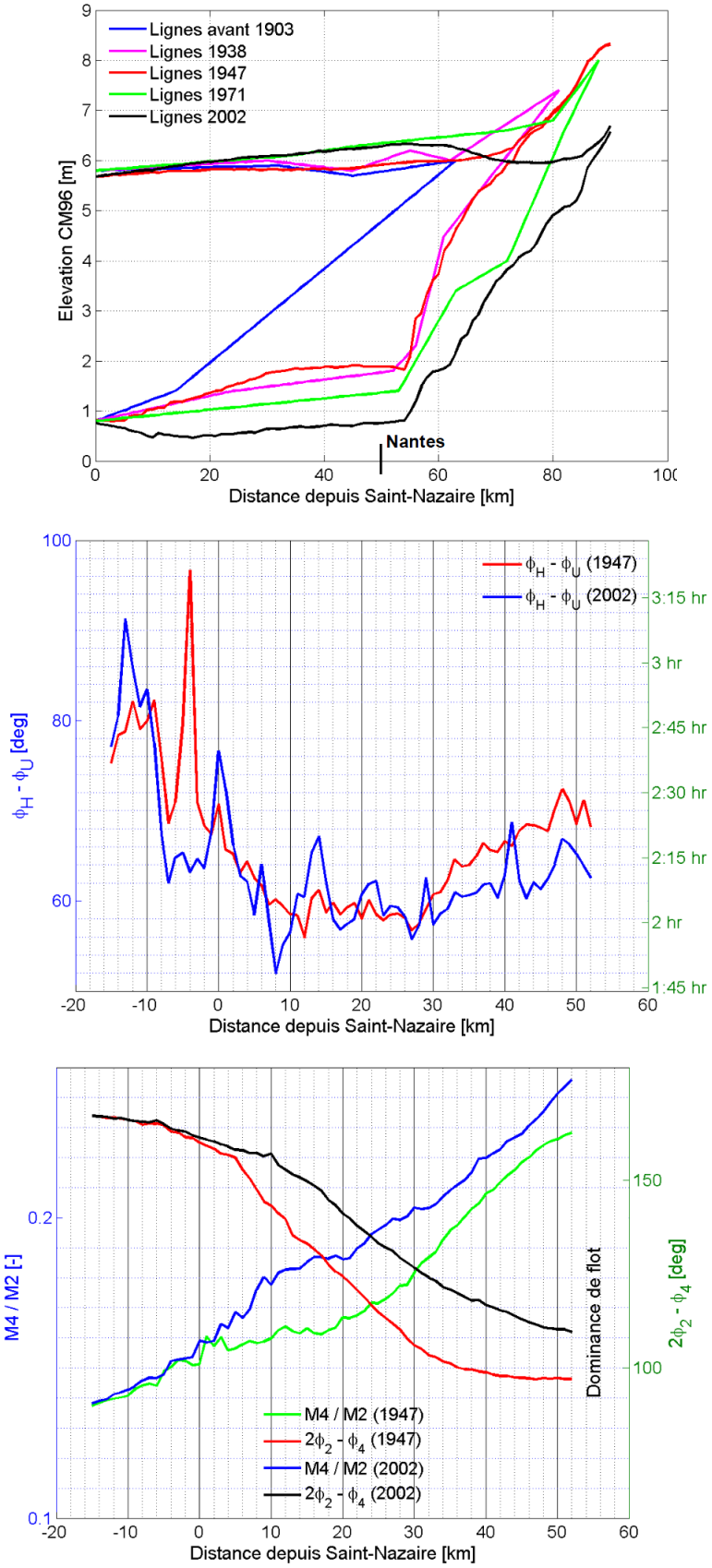

Figure 2.5: Spring tide HW and LW envelopes along the estuary (top), phase difference between horizontal and vertical tide (middle), amplitude ratio and phase difference between the M2 and M4 tidal components (bottom), (Briére et al., 2011)

2.3. AVAILABLE DATA

One of the challenges of this research has to do with the lack of information. The Ecuadorian National Oceanographic Institute of the Navy (INOCAR) is identified as the main data source. However, by the time of this research, the arrangements for collaboration and transfer of information were still pending and the information could not be retrieved in time. In view of the above, an extensive search for studies involving any type of development or infrastructure (such as bridges, docks or ports) around the Guayas River was carried out. Most of these studies refer to INOCAR as their main source. Among the most relevant are Benites (1975), Gobierno Autónomo Descentralizado Provincial del Guayas (2013) and Soledispa (2002).

2.3.1. BATHYMETRY

The bathymetry is obtained from the General Bathymetric Chart of the Oceans, (GEBCO, 2015). The data set is provided in a 30 arc-second resolution grid. This resolution is suitable for the outer part of the Gulf of Guayaquil, however for the Guayas River estuary itself the resolution is too coarse. The bathymetry for the inner estuary is then generated by making a long-term morphological computation with the model starting with a flat bottom. The basis of this approach is that the morphological features ought their development to the interaction between tidal forcing and the basin geometry which can be assessed by a process based model. The approach is further discussed on section 5.2.

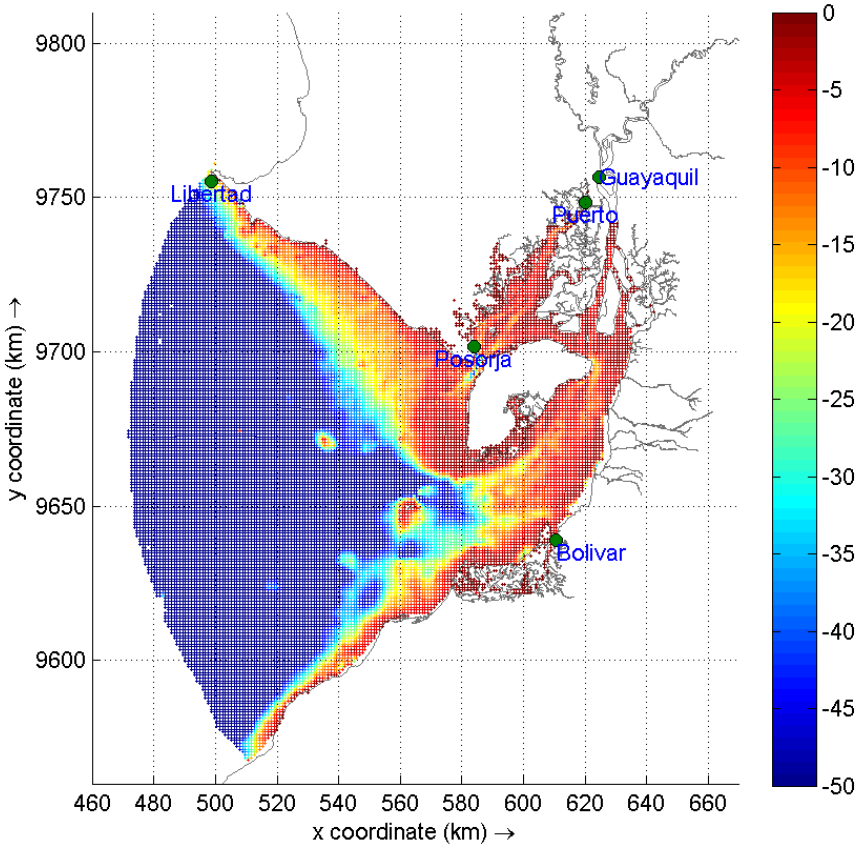

Figure 2.6: Bathymetry of the Gulf of Guyaquil referenced to mean sea level & tidal stations

2.3.2. WATER LEVELS

Water level information is obtained at 5 tidal gauging stations namely: La Libertad, Posorja, Puerto Bolivar, Puerto Maritimo and Guayaquil. The locations are shown in Figure 2.6. The information at each station is given as tidal components, so the data can be derived at any date and time.

Table 2.1: Tidal components at the different stations

	Guayaquil		*Puerto Maritimo*		*Puerto Bolivar*		*Posorja*		*La Libertad*	
Comp	*Ampl.* [m]	*Phase* [deg]	*Ampl.* [m]	*Phase* [deg]	*Ampl.* [m]	*Phase* [deg]	*Ampl.* [m]	*Phase* [deg]	*Ampl.* [m]	*Phase* [deg]
M2	1.504	20.90	1.483	324.20	1.022	298.60	0.914	288.20	0.786	251.70
S2	0.348	67.50	0.420	27.10	0.301	326.00	0.193	341.90	0.231	299.20
N2	0.250	21.10	0.282	292.20	0.206	278.50	0.186	260.40	0.175	223.20
M4	0.146	313.40	0.073	92.20	0.047	359.50	0.012	9.60		
MU2	0.139	119.80	0.166	39.10	0.044	324.60	0.030	44.50	0.026	224.70
L2	0.112	17.50	0.178	319.80	0.031	303.60	0.076	295.00	0.018	270.90
K2	0.095	67.90	0.114	27.50	0.082	326.40	0.052	342.30	0.063	296.90
K1	0.088	92.10	0.119	47.00	0.169	47.60	0.121	48.90	0.114	42.10
MS4	0.081	3.00	0.046	152.60	0.036	30.00	0.011	125.90		
MSF	0.079	10.30	0.037	34.20	0.026	244.70	0.027	38.10	0.070	277.70
M6	0.069	143.60	0.096	379.70	0.016	348.20	0.039	170.50		
2MS6	0.049	202.80	0.078	434.70	0.014	363.30	0.031	239.70		
MN4	0.049	314.10	0.025	59.80	0.018	342.10	0.003	229.50		
NU2	0.049	21.50	0.055	292.60	0.040	278.90	0.036	260.80	0.032	227.50
2SM2	0.045	188.20	0.037	205.70	0.036	178.00	0.007	277.30		
MM	0.043	63.60	0.068	65.40	0.012	341.90	0.009	115.60	0.015	349.60
SN4	0.043	310.30	0.019	165.40	0.015	25.50	0.008	108.90		
MSN6	0.042	162.10	0.024	129.20	0.006	350.30	0.011	227.70		
O1	0.037	95.10	0.033	12.60	0.015	74.60	0.035	3.10	0.029	8.80
2MN6	0.035	168.00	0.047	325.70	0.005	278.90	0.023	119.50		
2N2	0.033	21.30	0.038	260.10	0.027	258.40	0.025	232.70	0.023	191.20
P1	0.029	91.70	0.039	46.60	0.056	47.20	0.040	48.50	0.033	39.60
MO3	0.024	110.80	0.018	58.30	0.008	32.40	0.010	55.10		
2SM6	0.022	289.70	0.017	156.50	0.004	434.60	0.010	328.10		
T2	0.021	67.30	0.025	26.90	0.018	325.80	0.011	341.70	0.015	300.70
OO1	0.020	122.90	0.017	237.20	0.025	162.30	0.002	163.50	0.006	87.90
MK3	0.014	43.10	0.017	69.50	0.022	241.20	0.008	131.10		
M1	0.011	166.30	0.006	303.50	0.011	78.70	0.002	325.10		
M3	0.006	73.70	0.007	203.80	0.001	88.70	0.006	100.20	0.009	22.30
Q1	0.006	292.80	0.011	80.40	0.017	177.30	0.002	236.50		
J1	0.002	308.00	0.005	173.10	0.009	64.70	0.014	39.20	0.008	63.80
PI1	0.002	91.50	0.002	46.40	0.003	47.00	0.002	48.30		
2Q1	0.001	130.40	0.001	148.20			0.001	109.90		
FI1	0.001	92.50	0.002	47.40	0.002	48.00	0.002	49.30		
PSI1	0.001	92.30	0.001	47.20	0.001	47.80	0.001	49.10		
SIGMA1	0.001	130.70	0.001	148.50			0.001	110.20		
SA									0.048	17.70
SSA									0.026	332.10
MNS2									0.008	188.30
S1									0.007	152.10
LABDA2									0.005	266.10

2.3.3. RIVER DISCHARGE

The river discharge data are obtained from the hydrological yearbooks published between 1984 and 2012 by the Ecuadorian National Institute of Meteorology and Hydrology (INAMHI). The discharges

are prescribed as monthly averaged values. In case of the Babahoyo River there is not a unique gauging station from which the information can be derived. Instead the existing gauges are located at the 4 main tributaries (H345, H348, H371, H390). These tributaries connect at different points along the Babahoyo. However, for practical reasons only the total contribution is considered as the prescribed discharge. In case of the Daule River the information is directly obtained from a single gauge (H365). The location of these gauging stations is shown in Figure 4.3 and Figure 1.1.

The information is not continuous. For some years there are several months with missing data. Moreover, some of the gauging stations lack more information than others. The strategy to cope with this lack of information is to define typical years for each river by averaging for each month the available data over the years. A total of 3 scenarios has been defined for the Daule and 2 for the Babahoyo according to the following:

- For the Daule River a distinction is made between the situation before and after the construction of the Daule Peripa Dam, that is, before and after 1988.
- A distinction is made between the normal conditions and the "El Niño" event of 1997-1998 for both rivers.

Figure 2.7 presents the hydrographs for each case, the trend for the Daule River is comparable with Figure 1.4. The seasonality is evident, wet and dry seasons can be clearly identified. Maximum discharges are expected between February and April and the minimum between August and October. The significantly larger discharges (compared with a typical year) in the November-February period is characteristic of the "El Niño".

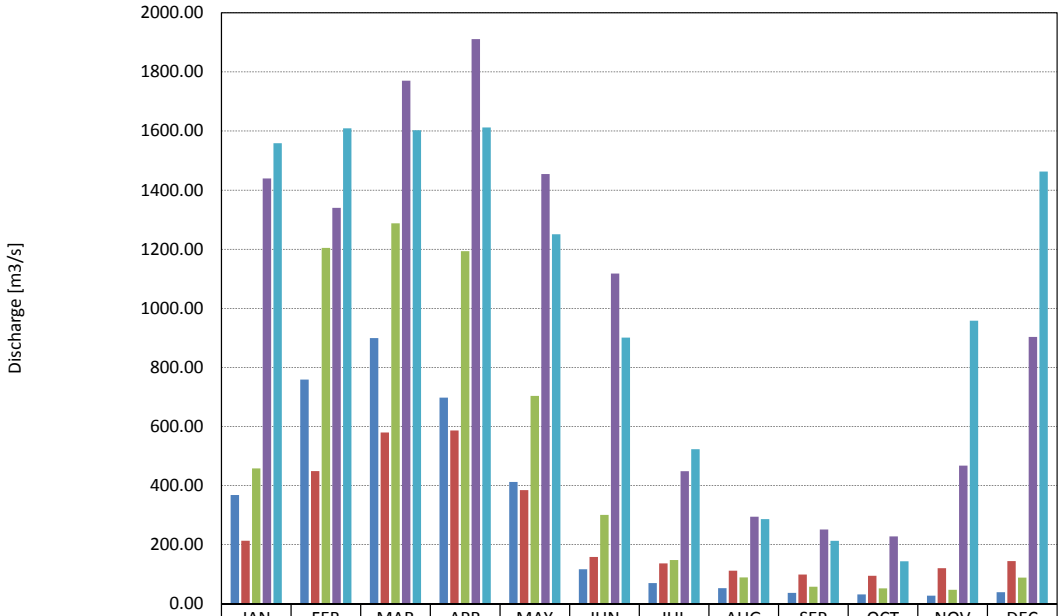

	JAN	FEB	MAR	APR	MAY	JUN	JUL	AUG	SEP	OCT	NOV	DEC
DAULE NO DAM	367.86	758.52	899.10	697.60	412.22	116.69	69.94	52.63	36.92	31.70	27.25	38.90
DAULE DAM	213.12	448.99	579.57	586.28	384.49	158.44	136.66	111.91	98.98	94.72	120.43	144.20
BABAHOYO	458.09	1204.12	1287.45	1193.11	703.47	300.80	148.01	89.22	57.49	52.14	47.17	88.54
DAULE NIÑO 97-98	1439.11	1339.73	1769.99	1910.76	1454.06	1117.29	448.72	294.40	251.23	227.75	467.47	902.91
BABAHOYO NIÑO 97-98	1558.32	1608.79	1602.48	1611.84	1250.29	900.69	523.05	286.48	212.87	143.56	957.88	1462.45

Figure 2.7: Monthly averaged discharge for the Babahoyo and Daule Rivers

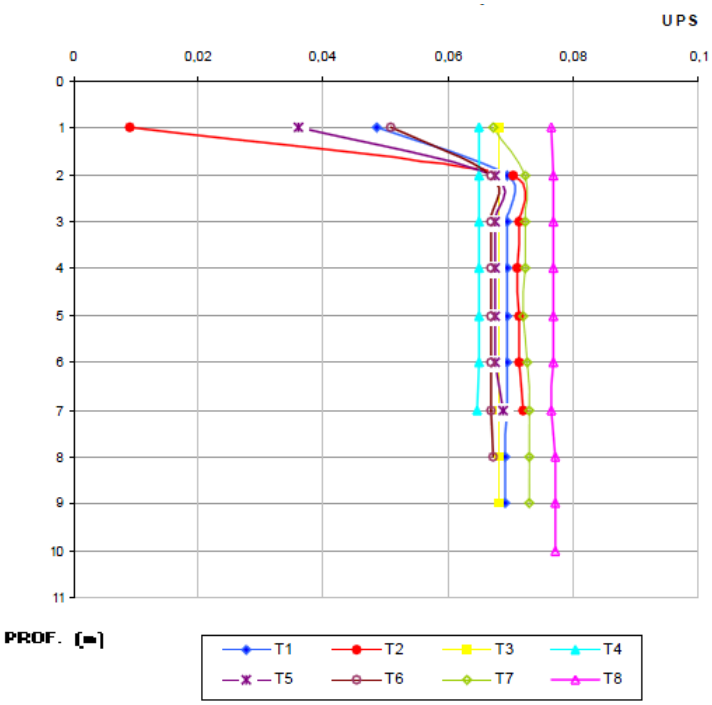

Figure 2.8: Salinity profiles over a tidal cycle (measured every 2 hours) at the confluence of the Babahoyo and Daule Rivers. PROF = Depth, UPS = Practical Salinity Units, (Laraque et al., 2002)

2.3.4. SALINITY

Twilley et al. (2000) deem the Guayas River estuary as partially mixed, nevertheless a more recent study by Laraque et al. (2002) proves that the estuary is actually well mixed. During the study a measurement campaign was conducted at the beginning of May 2002, which can roughly be deemed as the peak of the wet season. Salinity profiles are determined at the confluence of the Daule and Babahoyo Rivers over the period of a tidal cycle. The profiles show a slight variation in the salinity in the first couple of meters of the water column below which the profiles remain constant.

2.3.5. SEDIMENT CHARACTERISTICS

The distribution of the sediment size is shown in Figure 2.9. Apparently the sediment is quite coarse along the Guayas River, and the importance of finer sediment fractions is bounded to the North-West branch of the Gulf (Estero Salado) which is outside the area of interest of this study. Since the information provided in Figure 2.9 is the only one available to characterize the sediment, it does not make much sense to define multiple sediment fractions for the model. However, it does provide the means to make a good estimate. For practical purposes, a mean grain size of 0.30 mm is adopted for the whole Gulf of Guayaquil as a characteristic sediment size.

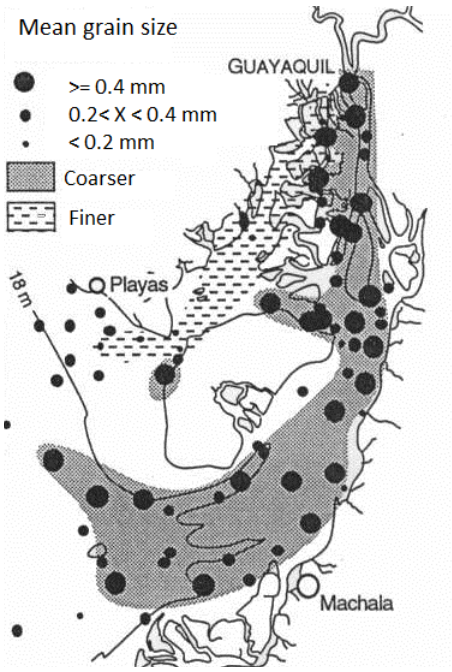

Figure 2.9: Mean sediment size distribution within the Gulf of Guayaquil, (Benites, 1975)

3

ANALYTICAL MODEL

In this part the concepts discussed in the previous chapter will be applied to the Guayas River estuary. The objective is to assess the main geometric and tidal parameters along the estuary, determine what is the relative importance of the river discharge and compare the actual with the equilibrium situation in which convergence and friction are balanced.

3.1. APPLICATION TO THE GUAYAS RIVER ESTUARY

The theory by Savenije (2006) about alluvial estuaries is applicable as long as the main assumptions regarding the shape and hydraulics are fulfilled, i.e., the width obeys an exponential function with a mild or zero bottom slope, the tidal amplitude to depth ratio is small and the river discharge is small compared to the tidal discharge. The latter is to be verified once some of the tidal parameters are computed.

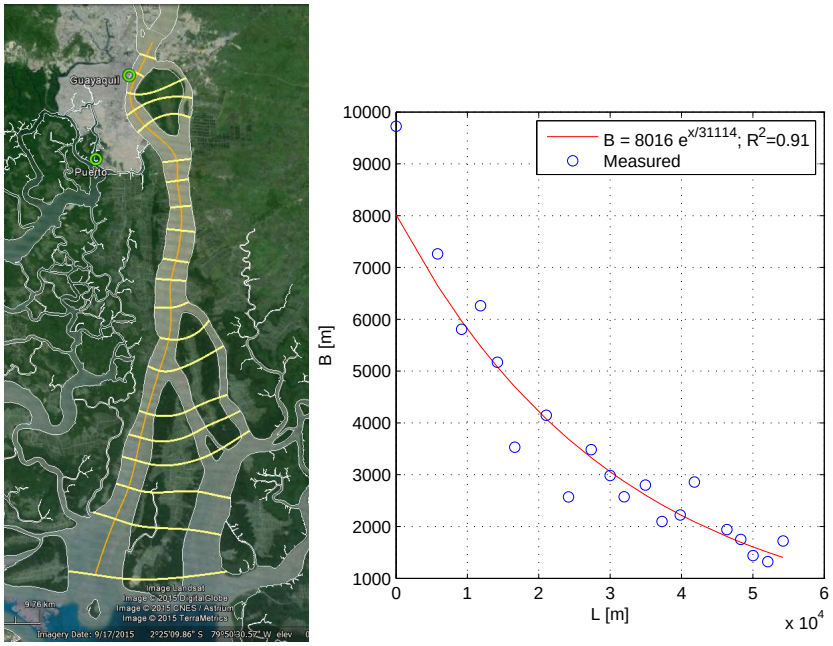

Figure 3.1: Estimation of the estuary width function

Figure 3.1 shows a plan view of the Guayas River estuary, from the confluence of the Babahoyo and Daule Rivers up to the mouth near the Puna island. The width is measured at 20 locations along the estuary. The right plot shows that there is a good agreement between the measurements and the assumption of an exponentially varying width. Since there is no bathymetric information available,

it is assumed that the cross sectional area also obeys an exponential function. The cross sectional convergence length is the result of calibration. The depth along the estuary is computed then with Equation 2.2. The analysis is carried out for spring tide whereby the amplitudes are determined based on the main components M_2 and S_2 given in Table 2.1. Due to the lack of information about the tidal signal at the mouth, it is assumed that the amplitude is the same as that corresponding to the "Bolívar" tidal station shown in Figure 1.1.

3.1.1. CALIBRATION AND SENSITIVITY ANALYSIS

Table 3.1 summarizes the values of the parameters adopted for the analysis. The estuary's length is directly measured, the width convergence length and the width at the mouth are obtained through the measurements by curve fitting, the width storage ratio r_S is assumed as 1 for simplicity. Since the Chézy friction coefficient is depth dependent, the Manning formula is considered more suitable to describe the friction term. The conversion is $C = \frac{h^{1/6}}{n}$, where n is the Manning roughness coefficient. The rest are deemed as calibration parameters. The target is to reproduce the measurements of the tidal amplitude at the Guayaquil gauging station presented by Murray et al. (1976) which are also included in Table 3.1.

Table 3.1: Parameters of the analytical model

Parameter		*Unit*	*Measured*	*Calibrated*
Width convergence length	b	[m]	31114.000	
Width at the mouth	B_0	[m]	8016.000	
Estuary's length	L	[m]	59000.000	
Tidal period	T	[s]	44712.000	
Tidal amplitude at Guayaquil[1]	$\eta(L)$	[m]	1.852	
HW-HWS phase lag at Guayaquil[1]	$\varepsilon(L)$	[deg]	16.908	
HW-HWS phase lag dwnstr. Guayaquil[1]	ε(10 km)	[deg]	19.324	
HW travel time at Guayaquil[1]	time(L)	[min]	87.000	
HW travel time dwnstr. Guayaquil[1]	time(42.5 km)	[min]	45.000	
Tidal amplitude at the mouth (Bolívar)	$\eta(0)$	[m]		1.330
Cross sectional area convergence length	a	[m]		33651.000
Mean depth at the mouth	h_0	[m]		8.414
Storage width ratio	r_S	[-]		1.000
Manning roughness coefficient	n	[s/m$^{1/3}$]		0.027
Calibration coefficient (O(1))	κ	[-]		1.000
Tidal excursion	E_0	[m]	10624.000	
Tidal prism	P_t	[m^3]	716527384.781	
Velocity amplitude at the mouth	$v(0)$	[m/s]	0.747	

[1] Measurements by Murray et al. (1976)

The solution of the set of equations presented in subsection 2.1.5 applied to the Guayas River estuary is given in Figure 3.3. Due to the limited amount of measurements available, the representativeness of the solution cannot be assessed a priori, nevertheless there is not much disagreement with the available measurements.

The results of Figure 3.3 are estimated based on calibration of the three parameters (a, h_0 and n). A sensitivity analysis was carried out with the aid of Monte Carlo sampling. The performance is assessed with the Nash-Sutcliffe objective function (Nash and Sutcliffe, 1970). The function compares the model results with the measurements by Murray et al. (1976), which are shown in Table 3.1, and evaluates the performance between 0 and 1 ($0 \leq N \leq 1$).

Figure 3.2 displays the model performance for each of the Monte Carlo sampling trials. It can be

seen that the depth at the mouth and the cross sectional convergence length are proven to be the most sensitive parameters. This was expected since they basically define the friction and convergence terms in the damping equation. The calibrated values seem reasonable, in a broad sense the following can be observed:

- At first sight the estuary seems rather straight and uniform in width, especially in the central part, which is consistent with large values of a and b in relation to estuary's length.
- Despite the coarse resolution, the bathymetry in the area surrounding the estuary's mouth (which is available) seems to agree with the calibrated value of h_0.
- The estimation of the Manning friction coefficient is comparable to values for alluvial estuaries presented by Savenije (2006)

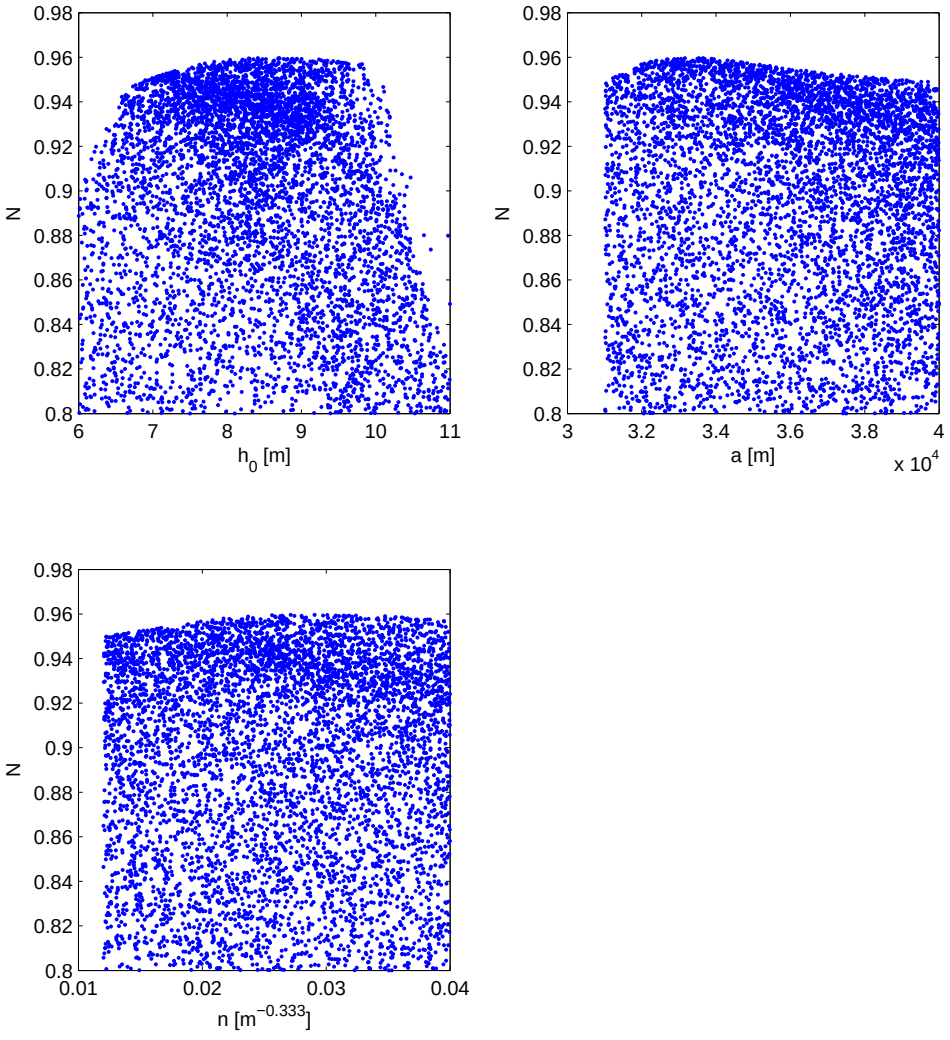

Figure 3.2: Monte Carlo sampling for calibration and sensitivity analysis of the analytical model

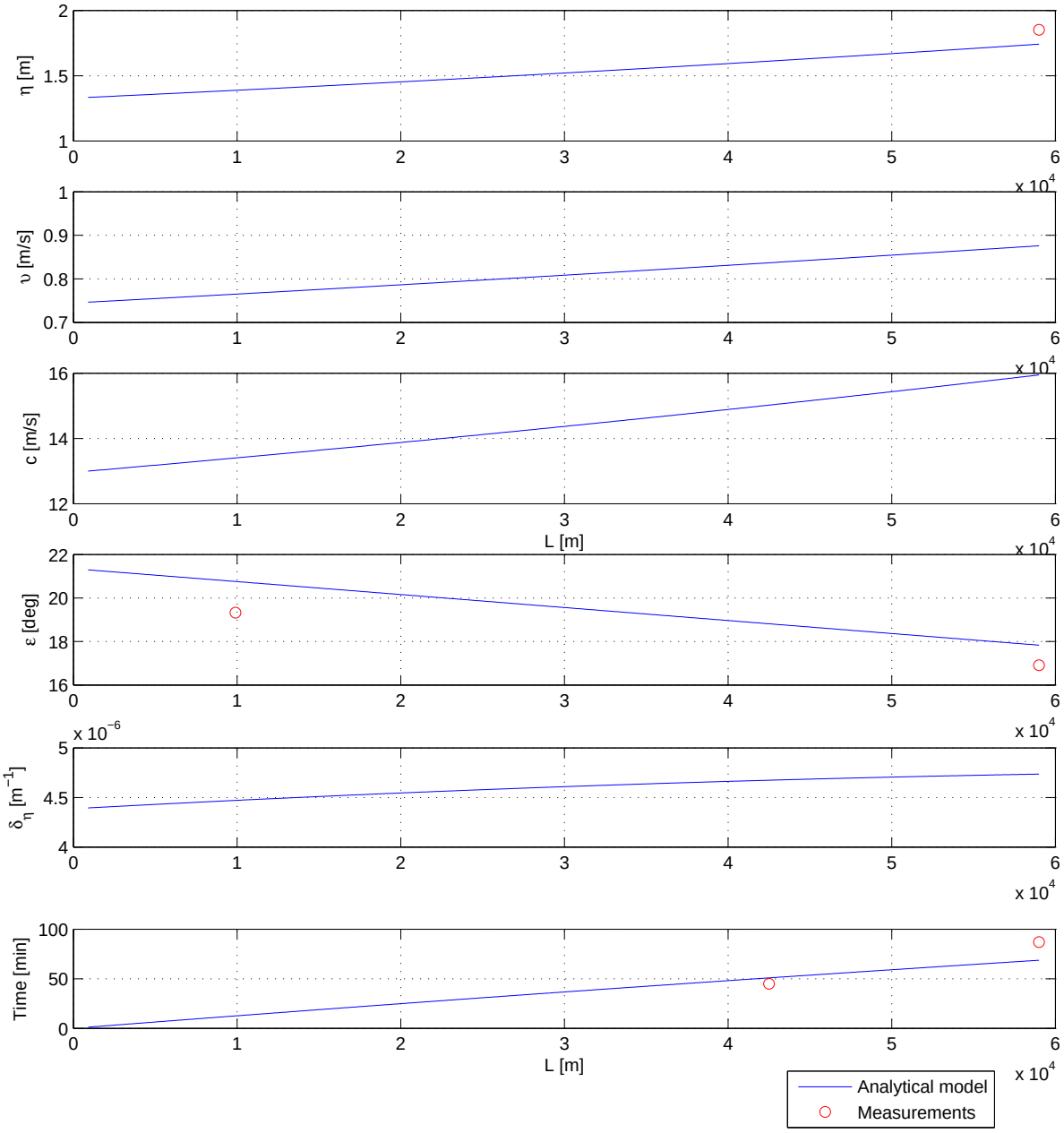

Figure 3.3: Tidal velocity and water level amplitudes, wave celerity, phase lag between HW and HWS, damping rate and time traveled by the tide as it propagates along the Guayas River estuary

3.1.2. DISCUSSION

The tidal amplification of the Guayas River estuary is the result of strong convergence. This is further confirmed since in order to reproduce the measurements the analytical model is more sensitive to the convergence related parameters than to the friction related parameter.

The phase lag between HW and HWS decreases as the tide propagates up the estuary. It is an indication that the tide develops a more standing wave character which is consistent with the increase of the wave celerity. The cross sectional convergence length being larger than the width con-

vergence length, it follows that the estuary's depth increases in the upstream direction. This is also in line with the upstream increasing celerity of the tidal wave.

3.1.3. RELATION TO MORPHOLOGY

The imbalance between convergence and friction can be traced back to the estuary's morphological development. Given the fact that the estuary would tend to reach equilibrium eventually the morphology would evolve accordingly. The equilibrium condition is that of the ideal estuary, that is the estuary is neither amplified nor damped ($\delta_\eta = 0$, $a = b$ and $h = constant$), so lets analyze this condition with the aid of the damping equation:

$$\delta_\eta = \frac{1}{\eta}\frac{d\eta}{dx} = \frac{\frac{1}{a} - f'\frac{v\sin(\varepsilon)}{hc}}{\left(1 + \frac{g\eta}{cv\sin(\varepsilon)}\right)} = 0 \tag{3.1}$$

It is clear that the equilibrium condition can only be reached if the numerator equals zero, which can be identified as the balance between amplification and friction respectively. It is worth noting that the friction term is depth dependent and therefore the key parameters determining damping or amplification are h and b.

$$\frac{1}{b} = \frac{1}{a} = f'\frac{v\sin(\varepsilon)}{hc}$$

The actual amplified condition of the Guayas River estuary states that the left hand side of the above equation is greater than the right hand side. By focusing only on the morphology related parameters the natural development of the estuary would then lead to:

- The relative reduction of the cross sectional convergence length in relation to the width convergence length (either a reduces or b increases).

- A reduction of the estuary's mean depth which would also increase the effect of friction, which is in line with the latter point.

Figure 3.4 shows the equilibrium relation between $b = a$ and h. It also displays the current condition of the estuary and how much it deviates from equilibrium. The curve is obtained by assuming that the values for the Manning friction coefficient and the tidal amplitude at the mouth remain constant.

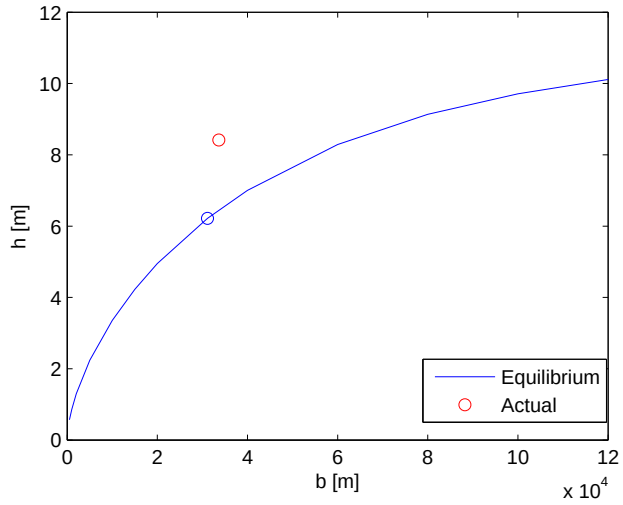

Figure 3.4: Equilibrium relation between mean estuary's depth and convergence length

Considering the interventions carried out within the estuary, fundamentally they make reference to two aspects in particular: changes in the shape due to the decimation of the intertidal flats and changes in the river discharges. From the simple equilibrium perspective presented above, the effects of such interventions can be explained as follows:

- Perhaps the most relevant impact of the construction of shrimp farms is the reduction of the tidal flats. This can be seen as a reduction of the friction term since the average cross sectional mean depth would then increase. This is against the equilibrium condition, so the estuary will tend to deposit more sediment in order to reduce the mean depth.

- The main effect caused by the construction of the Daule-Peripa dam is to reduce the Daule River discharge during the wet season. The river discharge itself has an influence on the shape. For instance, estuaries with large river discharge are more straight and uniform in width , i.e., the have large b. Consequently the introduction of the dam reduces the convergence length, which in turn drives the estuary further away from equilibrium and in doing so it enhances sedimentation.

3.2. THE IMPORTANCE OF THE RIVER DISCHARGE IN RELATION TO THE TIDE

The river discharge influences mainly the occurrences of the slacks (i.e., advancing HWS and delaying LWS) and the salt intrusion. The influence is larger for situations where the amplitude to depth ratio is close to unity ($\eta/h \approx 1$). In a more strict way the importance can be assessed with the Estuary Richardson Number (Equation 2.9) which is a function of the river discharge and the tidal prism. The latter can be computed with the aid of the scaling equation assuming that the tidal range is twice the amplitude ($H = 2\eta$).

From the scaling equation the tidal excursion at the mouth is:

$$E_0 = \frac{2v(0)}{\omega}$$

The tidal prism then is:

$$P_t = A_0 E_0 = B_0 h(0) E_0$$

The results are shown in Table 3.1. Murray et al. (1976) present a distribution of the salinity along the Guayas River estuary. According to data the average density difference between the downstream and upstream part can be estimated at $\Delta\rho$ =15 kg/m^3.

The equation for the Estuary Richardson Number presented in subsection 2.1.2 can now be solved. Three different scenarios are posed based on the hydrographs presented for the Daule and Babahoyo Rivers.

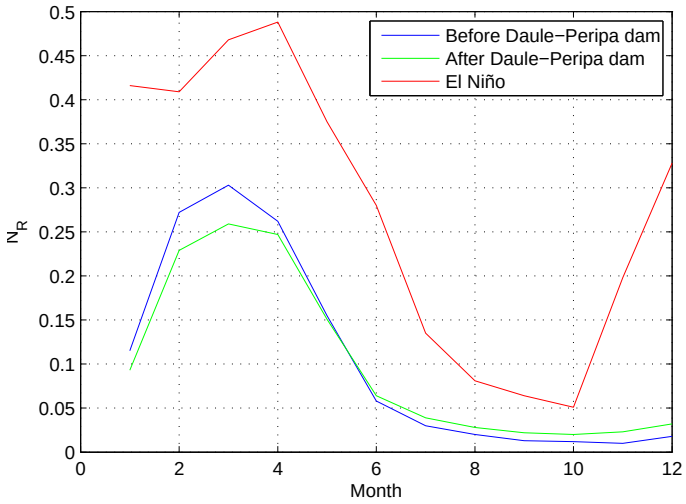

Figure 3.5: Monthly distribution of the estuary Richardson number for different river discharge scenarios

In any case the Richardson number never exceeds the 0.8 threshold which is considered the limit between a partially mixed and a stratified estuary. Indeed, the estuary remains well mixed during the dry season and partially mixed during the wet season. Only during the "El Niño" event the estuary remains partially mixed almost the whole year. It follows that the influence of the river discharge is minor compared to the tide even under extreme conditions, hence the estuary is mainly tide dominated.

4

MODEL SET-UP AND CALIBRATION

4.1. DELFT3D FLOW FLEXIBLE MESH (DELFT3D-FM)

Delft3D-FM is the new hydrodynamic engine that runs on unstructured grids. The numerical concept is based on the combination of 2D/3D finite volume cells with 1D flow networks.

The unstructured character eliminates the restrictions imposed by structured grids, since it is possible to number grid cells in random sequence and construct the network with shapes other than rectangular like triangles or pentagons. The grid layout is then more flexible to mimic complex domain geometries and provides the possibility to achieve an optimal network resolution. This prevents the generation of staircase boundaries and hence avoids the overestimation of flow resistance. Around staircased boundaries, water is suddenly slowed down and changed in direction, which induces artificial mixing of momentum and results in the introduction of flow losses.

In this section a brief overview of the hydrodynamic and morphodynamic modules implemented in Delft3D-FM is presented. For a detailed description of the hydro and morphodynamics, as well as the numerical implementation, the reader is referred to Kernkamp et al. (2011) and Deltares (2015a).

4.1.1. HYDRODYNAMICS

Delf3D-FM solves the two- and three-dimensional shallow water equations. One of the aims throughout this study is to set a 2D depth averaged model. A 3D version could not be implemented since at the time of this research the morphology module was still under development. In depth averaged

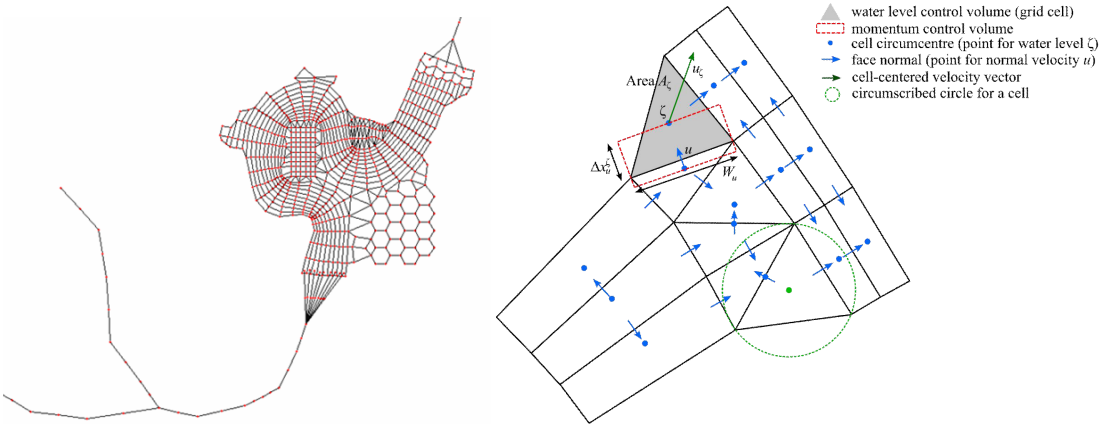

Figure 4.1: Example of the supported unstructured grid, (Kernkamp et al., 2011)

mode, the shallow water equations state the conservation of mass and momentum as:

$$\frac{\partial \zeta}{\partial t} + \nabla\{(h+\zeta)\vec{u})\} = q \tag{4.1}$$

$$\frac{\partial \vec{u}}{\partial t} + \vec{u}.\nabla\vec{u} + g\nabla\zeta - \nu\nabla^2\vec{u} - \vec{T} + \frac{c_f}{h+\zeta} \mid \vec{u} \mid \vec{u} = d \tag{4.2}$$

Where $\vec{u}$ is the depth-averaged velocity vector, h the water depth and ζ the free surface position, both taken from a horizontal reference plane (datum or arbitrary level in which $z = 0$), c_f the bed friction coefficient, ν the kinematic viscosity, g the gravitational acceleration and $\vec{T}$ is the force vector due to subgrid stresses. In the right hand side q and d are the source and external forcing terms respectively.

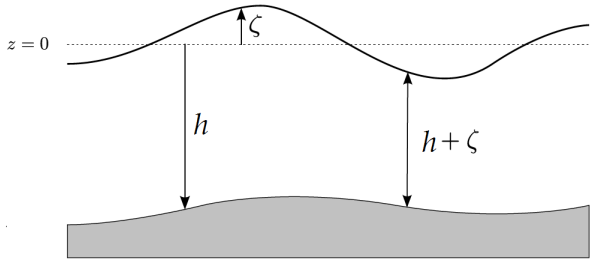

Figure 4.2: Definition of water level (ζ), depth (h) and total depth ($h+\zeta$), (Deltares, 2015a)

NUMERICAL APPROACH

The set of differential equations is solved using an unstructured orthogonal staggered grid. Water level quantities are defined at the cell circumcentre (also called flow nodes) and the velocities are defined at the line segment that connects the flow nodes of two neighboring cells (also called flow links) as shown in the right plot of Figure 4.1.

The grid orthogonality constraint imposes two requirements. First, the flow nodes should lie within the grid cell (i.e., triangles should have acute angles) and second, the flow links should intersect orthogonally the interface between them. Another important aspect to consider is the flow vs grid alignment. A curvilinear grid aligned in the main flow direction is preferred over a fully unstructured grid. In this fashion numerically generated energy losses are minimized, since errors introduced by large velocity gradients are also kept to a minimum. In general, the strategy to lay the grid is to generate as much curvilinear grids aligned in the main flow directions as possible, then merge all of them together with the aid of triangular cells, and finally orthogonalize the coupled grid.

The staggered grid principle is similar to Delft3D. The main difference is that the velocity vector is not decomposed in the m- and n- directions. In this way the 2DH spatial integration becomes one-dimensional.

Time integration unlike Delft3D, which uses the Alternate Direction Implicit method (ADI), is done with the θ-method according to the approach proposed by Kramer and Stelling (2008) with the variant that advection terms are integrated explicitly. The resulting scheme guarantees the conservation of volume and momentum. The stability and efficiency of the model are related to the time step restriction. In this case, since the advection scheme is explicit, the stability is governed by the Courant number.

$$CFL = \frac{\sqrt{gH}\Delta t}{\Delta\lambda} \leq C_{max}$$

Where $\Delta\lambda$ is the flow link length and $H = \zeta + h$ is the total water depth. Delft3D-FM uses a dynamic time-step estimator based on a maximum allowed CFL value which for practical purposes must not be greater than 0.70, i.e., $C_{max} \leq 0.70$.

Besides the aforementioned, an important effect that has inherently a 3D nature is the secondary or helical flow, which is induced by streamline curvature or Coriolis acceleration. Even though its magnitude is small compared to the characteristic horizontal velocity the effect can be considerable on the flow distribution which is directly linked to the morphological changes.Therefore the 2D model must be able to represent this 3D feature. In that regard, Delft3D-FM calculates the secondary flow according to the model proposed by Kalkwijk and Booij (1986). The spiral flow is then accounted for by additional shear stresses that are included into the momentum equations and are coupled to parameters of the depth averaged flow.

The turbulence closure models implemented are based on the eddy viscosity concept.

4.1.2. SEDIMENT TRANSPORT AND MORPHODYNAMICS

The definition of morphodynamics according to Bosboom and Stive (2012) is the adjustment of morphology and hydrodynamic processes involving sediment transport. The Delft3D-FM morphology module includes bed-load and suspended load transports of both cohesive and non-cohesive sediment. It also supports the online bathymetry update which ensures that the hydrodynamic flow computations are carried out with the correct bathymetry. Depending on the transport formulation, a clear distinction is made between suspended and bed-load sediment transport, indeed, they are treated separately. Bed-load is assumed to react instantly to changes in flow velocity and is calculated using a transport formula. Suspended sediment on the other hand, is entrained into the water column by sediment sources and sinks near the bed and is estimated by an advection-diffusion equation. Due to the lack of information, only non-cohesive sediment is considered for this study.

The morphological update obeys the sediment balance at the bed or Exner principle:

$$(1-p)\frac{\partial Z_b}{\partial t} + \frac{\partial (S_{b,x} + S_{s,x})}{\partial x} + \frac{\partial (S_{b,y} + S_{s,y})}{\partial y} = 0 \tag{4.3}$$

where Z_b is the bed level, p is the porosity, S_b and S_s are the bed and suspended sediment transport rates respectively. Delft3D-FM supports several transport formulations for non-cohesive sediment. A summary of them is given in the table below:

Table 4.1: Supported transport formulations, (Deltares, 2015a)

Formula	*Transport*	*Waves*
Van Rijn (1993)	Bedload + suspended	Yes
Engelund-Hansen (1967)	Total transport	No
Meyer-Peter-Muller (1948)	Bedload	No
General formula	Total transport	No
Bijker (1971)	Bedload + suspended	Yes
Van Rijn (1984)	Bedload + suspended	No
Soulsby/Van Rijn	Bedload + suspended	Yes
Soulsby	Bedload + suspended	Yes
Ashida–Michiue (1974)	Total transport	No
Wilcock–Crowe (2003)	Bedload	No
Gaeuman et al. (2009) laboratory calibration	Bedload	No
Gaeuman et al. (2009) Trinity River calibration	Bedload	No

Among the formulations, Engelund-Hansen (1967), Meyer-Peter-Muller (1948) and Van Rijn (1984) are commonly used for river and estuary applications. A description of the transport formulations follows in the next subsection.

TRANSPORT FORMULATIONS

- Engelund-Hansen (1967): The formula estimates the total load (bed and suspended load), is valid for situations in which $w_s/u_* < 1$, $0.19 < D_{50} < 0.93$ mm, and $0.07 < \theta < 6$.

$$S = 0.05 \frac{U^5}{\sqrt{g} C^3 \Delta^2 D_{50}} \tag{4.4}$$

  S_{tot} is the sediment transport per unit width (m^2/s), U is the depth averaged flow velocity (m/s), Δ is the relative mass density of sediment under water, and D_{50} is the median grain size (m).

- Meyer-Peter-Muller (1984): The formula predicts the bedload transport. The main difference with the Engelund-Hansen formula is that it includes the threshold of incipient motion parameter θ_c. The formula is valid for $w_s/u_* > 1$, $D_{50} > 0.40$ mm and $\mu\theta < 0.20$

$$S = 8 D_{50} \sqrt{\Delta g D_{50}} (\mu\theta - \theta_c)^{3/2} \tag{4.5}$$

  θ_c is the critical Shields number for initiation of motion (θ_c= 0.047), μ is the ripple factor, and θ is the Shields number defined as:

$$\theta = \frac{\tau}{(\rho_s - \rho_w) g D_{50}} \tag{4.6}$$

- van Rijn (1984): The total load considers the contribution of bed and suspended load. The formula is used for fine sediment in situations without waves.

$$S = S_b + S_s \tag{4.7}$$

  The bed-load is then computed as:

$$S_b = \begin{cases} 0.053 \sqrt{\Delta g D_{50}^3} D_*^{-0.3} (\frac{\mu\tau - \tau_c}{\tau_c})^{2.1} & if \frac{\mu\tau - \tau_c}{\tau_c} < 3.0 \\ 0.1 \sqrt{\Delta g D_{50}^3} D_*^{-0.3} (\frac{\mu\tau - \tau_c}{\tau_c})^{1.5} & if \frac{\mu\tau - \tau_c}{\tau_c} \geq 3.0 \end{cases} \tag{4.8}$$

  The critical shear stress τ_c is based on the critical Shields number, the efficiency factor is $\mu = (C/C_{D_{90}})^2$ with $D_{90} = 1.5 D_{50}$ and $D_* = D_{50} (\frac{\Delta g}{\nu^2})^{1/3}$.

  The suspended-load transport is computed as:

$$S_s = f_s U h C_a \tag{4.9}$$

  Wherein f_s is an integration factor for the vertical distribution of suspended sediment, and $C_a = 0.015 \frac{D_{50} T^{1.5}}{a D_*^{0.3}}$ is the dimensionless reference concentration at level a measured from the bed, and $T = \frac{(C/C')^2 \theta - \theta_c}{\theta_c}$ is a bed shear stress parameter.

MORPHOLOGICAL ACCELERATION FACTOR

In order to breach the difference between hydrodynamic and morphological time-scales, a morphological acceleration factor is introduced in the equation for mass sediment conservation as follows:

$$(1-p) \frac{\partial Z_b}{\partial t} + MorFac \left[\frac{\partial S_{tot,x}}{\partial x} + \frac{\partial S_{tot,y}}{\partial y} \right] = 0 \tag{4.10}$$

The use of this technique is justified since the adaptation times of the morphology and the flow differ by orders of magnitude. Even though the estimation of this factor is a matter of judgment, one must consider that pushing this value too far might result in inaccurate results which are not realistic. Moreover, it might make the model prone to instabilities.

A key aspect to keep in mind is that the interpretation of the morphological factor depends on the application. For coastal or tide dominated situations that are characterized by periodic conditions, it can be considered as a factor that influences the morphological developments after each tidal cycle, i.e., the changes experienced after one tidal cycle with a factor of 10 are similar to those experienced after 10 tidal cycles with a factor 1. In river situations no such periodicity is involved. The morphological factor then must be viewed as a speed-up factor of the hydrodynamics, i.e., a morphological factor of 10 implies that a 10 day flood event is reduced to a 1 day event.

The 2D implementation involves additional assumptions in relation to the 3D version. These assumptions refer mainly to velocity profiles, turbulent mixing profiles, and sediment adaptation time scales.

4.2. MODEL SET-UP

4.2.1. GRID AND DOMAIN EXTENT

The model domain covers the whole Gulf of Guayaquil from the limit with the continental shelf at the seaward side up to the tidal signature in the Babahoyo and Daule Rivers at the landward side, which is approximately 50 km from the city of Guayaquil following each river. The area of interest for this study is the Guayas River estuary which is outlined in Figure 4.3. The main reason to choose the extent of the domain is related to the lack of information regarding boundary conditions in the area of interest. As explained before, there is only a limited amount of tidal and discharge gauging stations from which information can be retrieved. Moreover, the effect of disturbances at the boundaries is kept to a minimum by choosing the boundaries quite far from the area of interest. Mosselman and Le (2016) argue that erroneous morphodynamic solutions can be imposed by the effect of sediment entry errors if boundaries are too close to the area of interest, therefore the 50 km distance to the boundaries is deemed enough to make the model domain suitable for morphological computations. Within this context Delft3D FM offers great versatility when it comes to outlining the complex geometry of the Gulf while trying to achieve an acceptable grid resolution in order to limit computational efforts.

The grid consists of 21800 nodes and 20037 grid cells. It has a typical grid cell size of approximately 80 m to 200 m around the area of interest, and 200 m up to 6500 m in the outer zone of the Gulf. The resolution is chosen such that a balance between computational time, scale of processes and level of detail is achieved. The grid is constructed according to the strategy presented in subsection 4.1.1, i.e., the domain is covered with a curvilinear rectangular grid as much as possible and triangular cells are used only when strictly needed. The size of the grid cells depends on the characteristic length scale of the model geometry and the bathymetry one is trying to resolve. A minimum of 5 grid cells is needed to capture morphological features. Regarding the level of detail around the interest zone it is assumed that the characteristic length scale of such morphological features is 1/4th the channel width, which gives a total of 20 grid cells. In general the length of the grid cells is larger than or equal to the width. Cells become larger as the grid moves away from the interest area. In any case, the aspect ratio is never larger than 4.

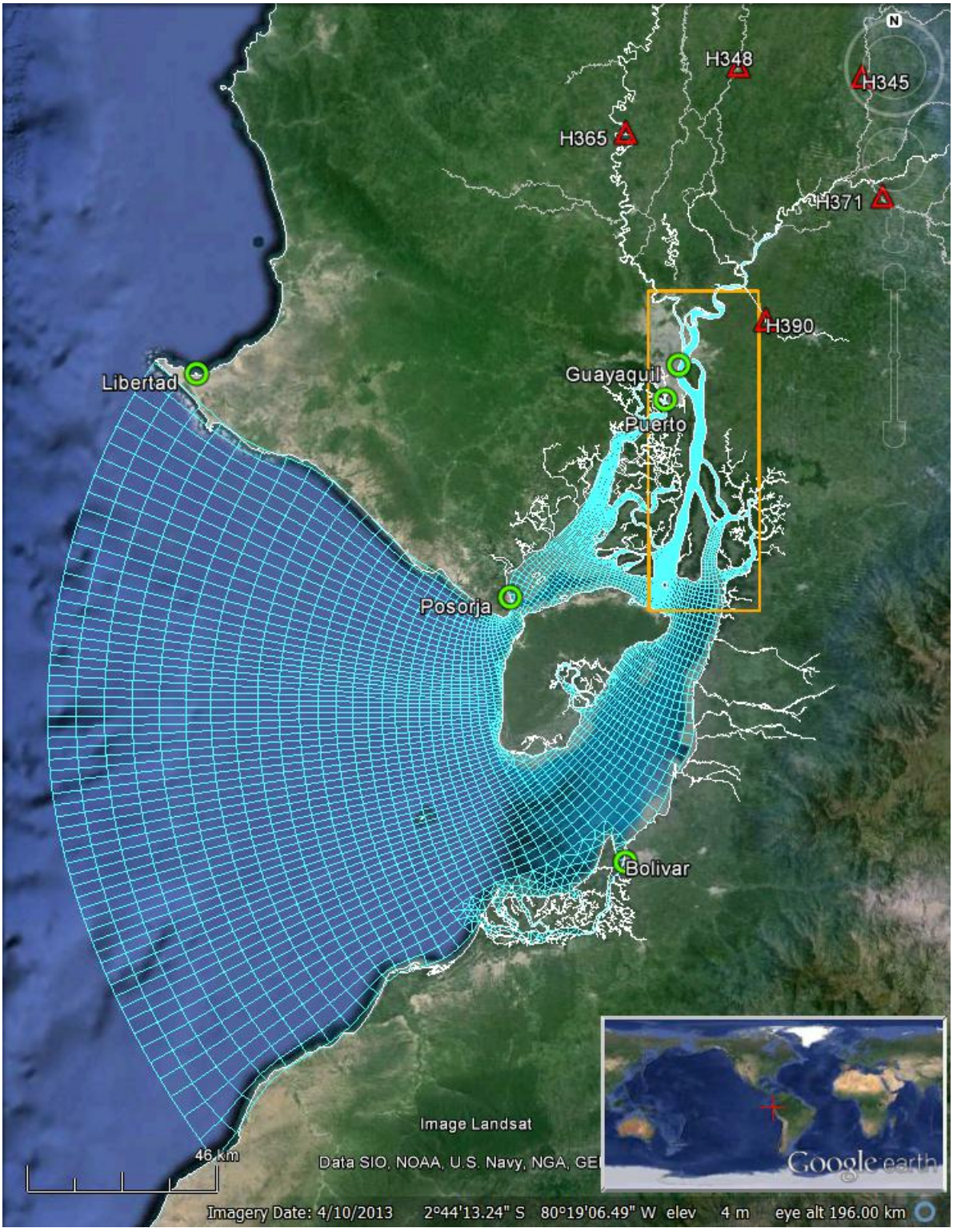

Figure 4.3: Numerical grid of the Delft3D FM model of the Gulf of Guayaquil and the Guayas River estuary. Tidal stations (green), river gauging stations (red) and area of interest (orange)

4.2.2. BOUNDARY CONDITIONS AND MODEL PARAMETERS

The open boundaries at the seaward and landward ends of the model are subjected to boundary conditions derived directly from the tidal and riverine information available.

In case of the seaward boundary, it was tempting to use the information from the "La Libertad" tidal station as boundary condition. Nevertheless, as the boundary spans over 200 km, which falls within the same order of magnitude as the tidal wave length, a single station is not representative over the entire extension. A space varying boundary condition is derived in that regard from the global model of ocean tides TPXO 7.2. The boundary is subdivided in 7 segments of approximately equal length for which tidal constituents are prescribed.

The discharge boundary condition for the Babahoyo and Daule Rivers stem directly from Figure 2.7.

For longer-duration morphological simulation the forcing conditions are simplified. The tide is simplified to a mean "morphological tide" and the river discharges are scaled accordingly. Both simplification schemes are treated in the following subsection.

A list of the most relevant model parameters is presented in Table 4.2. The only parameter subjected to calibration is the Manning friction coefficient. The information of the 5 available tidal stations are used as the calibration targets to determine this coefficient. This is further treated in the next chapter.

Numerical parameters such as the maximum CFL condition are chosen to ensure the stability and accuracy of the model. Currently, the subgrid scale model (Horizontal Large Eddy Simulation) for 2D turbulence used in Delft3D is not yet supported in Delft3D-FM. Instead the Smagorinsky horizontal model has been implemented. For a depth averaged simulation the horizontal eddy viscosity should contain the contribution of the vertical variation of the flow. The background horizontal eddy viscosity should then be chosen accordingly. Both the Smagorinsky constant and the background eddy viscosity are deemed as calibration parameters in practice. For this study however, not much effort was put towards the exact determination of these values, since there are not sufficiently detailed data available that allow for a proper calibration. Their choice was rather based on typical values from literature and discussions with colleagues at Deltares.

During this study 2 types of morphological simulations were carried out, i.e., a long-term simulation in order to derive the initial bed topography and mid-term morphological simulations to reproduce the actual evolution of the Guayas River estuary. Within this framework the choice of the morphological acceleration factor is also dependent on the duration of the simulation. The use of a morphological factor is valid as long as the bed level changes remain sufficiently small so that the nonlinear interactions with the hydrodynamics stay also small. Van der Wegen et al. (2008) state that in general the use of large $MorFac$ values may lead to large discrepancies for individual spatial points, however the patterns are likely to be properly captured. Van der Wegen and Roelvink (2012) validate the use of morphological factors up to 400 for the Western Scheldt estuary in the Netherlands. In the present study a $MorFac$ of 100 is chosen to derive the initial bed topography, and a smaller value of 15 is chosen for the subsequent mid-term morphological simulations. This is further elaborated in subsection 4.2.3.

A uniform sediment fraction is defined for the model namely 'sand'. The characteristic sediment size is chosen according to what is presented in Figure 2.9. In line with the limited available data, the Engelund-Hansen transport formulation is selected for simplicity. This formulation does not discriminate between suspended and bed-load transport, which is a drawback since the settling lag effect of especially fine suspended sediment is not considered. According to Mosselman (2005), spatial lag effects are important if the corresponding adaptation lengths are 5 times the length of a computational cell or more. Hence, the use of the Engelund-Hansen formulation can be justified as long as the processes of sediment suspension and deposition take place within 5 grid cells. Considering the sediment settling velocity roughly at 0.04 m/s and depths around 8 m, it would take a

sediment particle 200 m to settle which falls within the range of cell sizes in the finer areas of the grid.

The direction of the sediment transport can deviate from that of the mean flow due to the effect of secondary flow or due to the action of gravity on the sediment on transverse slopes. Mosselman and Le (2016) show that the morphological changes are sensitive to the inclusion of the bed slope effect, in the sense that less diffusive patterns develop when this effect is omitted. Delft3D-FM adjusts the direction of the sediment transport vector for bed slopes according to the formulation presented by Van Rijn (1993). The formula is adjustable through a factor α_{bn}. Van der Wegen and Roelvink (2012) performed a sensitivity analysis on this factor and suggested a value in the order of 10 in the case that the Engelund-Hansen predictor is used. The same value is adopted.

Finally, in order to account for the effects of bank erosion or erosion of potentially dry cells that may arise along the morphological simulation, Delft3D-FM applies a simple algorithm in which a dry cell starts to erode when erosion occurs in a neighboring wet cell. For this study it is considered that 50% of the erosion of a wet cell is to be spread over neighboring dry cells.

Table 4.2: Input model parameters

Description	*Parameter*	*Unit*	*Value*
Maximum Courant Number	CFL_{max}	-	0.50
Smagorinsky horizontal turbulence model constant	$c_{Smagorinsky}$	-	0.20
Background eddy viscosity	v_{back}	[m^2/s]	10
Manning friction coefficient	n	[$s/m^{0.333}$]	0.0165
Morphological acceleration factor	MorFac*	-	100 & 15
Sediment transport predictor	EH	-	-
Median sediment diameter	D_{50}	[μm]	300
Transverse bed gradient factor for bedload transport	α_{bn}	-	10
Fraction of erosion to assign to adjacent dry cells	θ_{SD}	-	0.5

4.2.3. MORPHOLOGY SETTINGS AND SCHEMATIZATION

In order to complete the simulation within an acceptable time frame, besides the acceleration of the morphological changes achieved through the morphological factor, some input reduction techniques are used to schematize the boundary conditions. Due to the implementation of these techniques the speed of the morphological model is increased significantly reducing the computation time for long-term simulations from days or even weeks to a few hours.

MORPHOLOGICAL TIDE

The aim of this technique is to select a single "morphological tide" which is able to reproduce the same morphological changes as the complete tidal signal over a representative period, e.g., the spring-neap cycle. The idea of this input reduction technique is supported by what was discussed in subsection 2.1.4, i.e, for the purpose of long term morphodynamic modelling it is enough to consider the main semi-diurnal constituents. This is justified since the net tide-induced bed-load transport is mainly caused by their contribution. The effect of the other constituents would average out in the long term.

A common approach to determine the representative tide is based on the idea presented by Latteux (1995) who argues that a single representative tide can be chosen such that the patterns of morphological change over the tidal period matches that of the full tide climate over a spring-neap tidal cycle. Lesser (2009) improved this idea considering not only one tide but the residual transport that stems from the interaction of the M_2 with its overtides, and the O_1 and K_1 tidal constituents. He

points out that the residual sediment transport caused by this non-linear interaction can be more important than the well known residual transport due to the non-linear interaction of the M_2 tide and its overtides.

Assuming that the sediment transport is proportional to U^3, Lesser (2009) finds a simplified term representing the sediment transport due to the aforementioned interaction:

$$\left\langle U^3_{O_1 K_1 M_2} \right\rangle = \frac{3}{2} O_1 K_1 M_2 \cos(\phi_{O_1} + \phi_{K_1} - \phi_{M_2}) \tag{4.11}$$

Where O_1, K_1 and M_2 are the amplitudes, ϕ_{O_1}, ϕ_{K_1} and ϕ_{M_2} are the phases and $\langle\rangle$ represents the long term-average quantity. To replace the O_1 and K_1 components by an artificial diurnal constituent (i.e., with a tidal period twice that of the M_2 component) C_1 is introduced as follows:

$$\left\langle U^3_{C_1 M_2} \right\rangle = \frac{3}{4} C_1^2 M_2 \cos(2\phi_{C_1} - \phi_{M_2}) \tag{4.12}$$

Where the amplitude C_1 and phase ϕ_{C_1} are:

$$C_1 = \sqrt{2 O_1 K_1} \quad and \quad \phi_{C_1} = \frac{\phi_{O_1} + \phi_{K_1}}{2} \tag{4.13}$$

Besides the latter analysis based on the tidal action alone, also the interaction with a mean flow is addressed in the same study. A factor f_2 is introduced that scales only the amplitude of the M_2 component in order to account for the sediment transport caused by the combined action of the tide and the residual current. A practical manner to determine this factor is by comparisons against a brute-force simulation.

Based on the above the method the determination of the morphological tide can be summarized as follows:

- Select the M_2 (with its overtides M_4 and M_6 if this is the case) plus the O_1 and K_1 constituents from the range of components of the tidal signal.
- Next, compute the amplitude and phase of the artificial diurnal C_1 component with Equation 4.13.
- Determine the scaling factor f_2 of the M_2 component based on trial and error comparisons with a brute-force simulation for the duration of the spring-neap cycle.
- The morphological tide then consists of $f_2 M_2 + C_1 + (M_{2_{overtides}})$.

The factor f_2 is a parameter that has to be determined through calibration. For the derivation of the initial bed topography, since there is no information to appropriately calibrate f_2, the scaling factor is determined such that the energy of the full astronomical tide is conserved:

$$f_2 = \sqrt{\frac{(M_2^2 + S_2^2 + N_2^2 + O_1^2 + K_1^2 + ...) - C_1^2}{M_2^2}} \tag{4.14}$$

Applying the equation above to the tide prescribed at the seaward bounday it is found that $f_2 = 1.08$, which is consistent with typical values from literature, e.g. Lesser (2009). Once the initial bed topography is assessed, for purposes of mid-term morphological computations in the order of years, this factor is determined as explained above. This is further elaborated in subsection 5.4.2.

RIVER DISCHARGE SCHEMATIZATION

The use of the morphological factor to speed up the computation time has a different interpretation for coastal and river applications. While for coastal applications only the overall simulation time is affected by this factor, for river applications it also involves changing the time scale of the time-varying boundary conditions. For a combination of both applications, as in an estuary, there is not such a clear interpretation. In that regard, 2 ways to schematize the river input are proposed. The first considers a constant discharge and the second considers the shape of the hydrograph and couples it to the period of the morphological tide. The initial topography is then derived following each schematization separately. Ultimately, the selection of either approach is based on whichever yields the best results.

- **Constant discharge**: The derivation is based on the assumption that the total transport over the duration of the hydrograph T must be captured by the constant value as follows:

$$\overline{Q_s}T = \int_0^T Q_s dt \tag{4.15}$$

From the basic continuity equation and the momentum balance for flow in equilibrium conditions plus the expression for the transport formulation, the relation between the sediment discharge Q_s and the flow discharge Q can be derived. Following the same nomenclature as subsection 2.1.2 we have:

$$\left.\begin{array}{l} Q = BhU \\ U = C\sqrt{h\frac{\partial Z_b}{\partial x}} \\ Q_s = Bd_sU^n \end{array}\right\} Q_s = d_sB^{\left(1-\frac{n}{3}\right)}C^{\frac{2n}{3}}\left(\frac{\partial Z_b}{\partial x}\right)^{\frac{n}{5}}Q^{\frac{n}{3}} \tag{4.16}$$

Considering a similar relation for $\overline{Q_s}$, i.e., using the the average discharge $\overline{Q}$ instead of Q, the expression for the average discharge reads:

$$\overline{Q} = \left(\frac{1}{T}\int_0^T Q^{n/3}dt\right)^{3/n} \tag{4.17}$$

In case of the Engelund-Hansen transport predictor $n = 5$. Since the aim is to derive the bed topography prior to the construction of the Daule-Peripa dam, the hydrographs used to estimate the average discharges are chosen accordingly (refer to Figure 2.7). The obtained average discharges for the Daule and Babahoyo Rivers then are 389.77 m^3/s and 611.82 m^3/s respectively.

One has to keep in mind that this simple approach lumps the seasonality of the hydrograph. Given that the estimation of the initial bed topography involves a long-term morphological simulation in the order of hundred of years, this simplification is deemed acceptable.

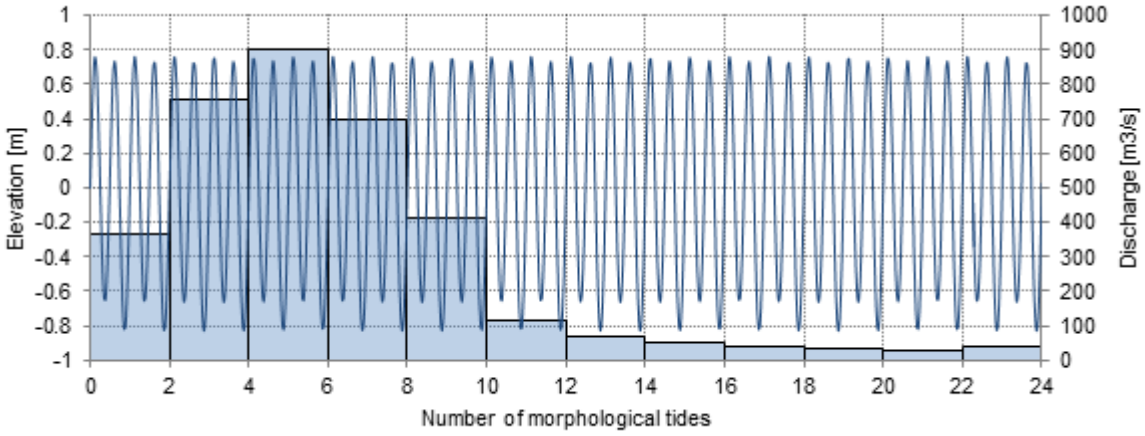

Figure 4.4: Schematization of the sea and river boundary conditions for one year of morphological development

- **Maintaining the shape of the hydrographs**: The idea behind this approach is to relate the time scales of the tidal and riverine forcing conditions. The constant discharge value that represents each month must be converted into a morphological simulation of the month length. This is done via the morphological factor. Each monthly discharge is simulated over the duration of 2 morphological tide periods (approximately 2 days), $MorFac$ is then chosen such that the morphological duration of those 2 tidal periods matches the duration of the month, i.e., $MorFac \approx 15$. In this way the durations of the river hydrographs are scaled to match the duration of 24 morphological tides. Figure 4.4 shows an illustration of the schematized sea and river boundary conditions for a year of morphological development. Months are assumed to have equal duration, i.e., 2 morphological tide periods.

5

CALIBRATION AND VALIDATION

5.1. CALIBRATION OF HYDRODYNAMICS

The calibration consists of tuning the the Manning friction coefficient in order to reproduce the observed water level signals at the location of the different tidal stations. The calibration is done prior to the determination of the initial bed topography of the Guayas River estuary. Therefore the Guayaquil tidal station is not taken into account. It will serve rather as validation data to contrast the results of the model once the initial topography is derived.

The data of the 4 remaining stations are used (Libertad, Posorja, Bolivar and Puerto). The aim is to reproduce the water levels during a spring-neap tidal cycle at these locations. Values between 0.012 s/m$^{1/3}$ and 0.030 s/m$^{1/3}$ were considered. The performance of the model is assessed with the root mean square error ($rmse$) and the coefficient of determination (R^2). The former provides an idea of the accuracy of the model and the latter indicates whether the trend of the measurements is captured.

The best results were obtained with a Manning friction coefficient of 0.0165 s/m$^{1/3}$. Figure 5.1 displays the corresponding observed and modelled water levels at each location and Table 5.1 presents the corresponding $rmse$ and R^2 values. At the Libertad and Posorja stations it can be said that the signals coincide almost at every instance. At the Bolivar and Puerto stations the major discrepancies are found. The differences can be ascribed to the fact that in the area surrounding the Puerto tidal station the resolution of the topographic data is coarse and therefore not as representative of the real conditions. Nevertheless the overall performance of the model is good considering the limited available information.

A final remark is that Figure 5.1 is evidence of the tidal amplification due to convergence, which is consistent with the funnel shape of the Gulf of Guayaquil.

Table 5.1: Evaluation of the model performance

Tidal Station	R^2	*rmse [m]*
Puerto	0.907	0.359
Bolivar	0.879	0.280
Posorja	0.955	0.151
Libertad	0.996	0.039

A further check of the model performance is done with a tidal analysis of the computed water levels over the duration of the calibration period. For a reliable tidal analysis at least 6 months of data are needed in order to properly resolve all the tidal constituents. In this case, however, due to the short length of the calibration period, the attention is focused only on the most energetic components. The results of the analysis for each station are contrasted with the corresponding observed values from Table 2.1. The comparison in shown in Table 5.2.

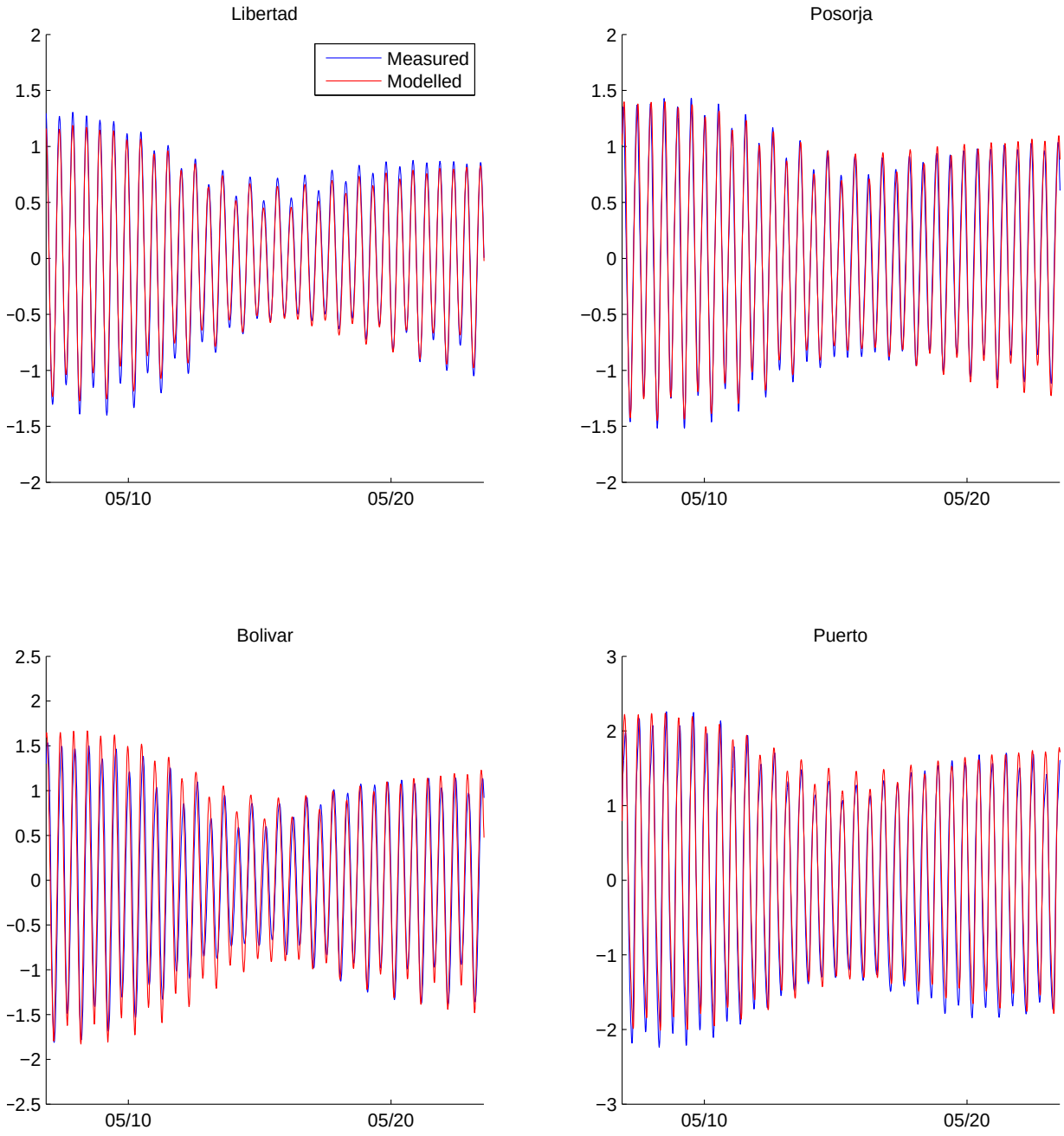

Figure 5.1: Observed and modelled water levels at the tidal station location

The model is able to reproduce reasonably well the tidal components. In general, amplitudes do not defer more than 10% and phases not more than 10 deg from the observed values. Large differences are perceived only for the small components K_2 and P_1 particularly at the Bolivar and Puerto stations. In part this might also be attributed to the uncertainty of the tidal analysis.

Table 5.2: Computed and observed tidal constituents at the Puerto, Bolivar, Posorja and Libertad tidal stations

Tidal Station	*Constituent*	*Amplitude*		*Ratio*	*Phase*		
		Observed [cm]	*Computed* [cm]		*Observed* [deg]	*Computed* [deg]	*Difference* [deg]
Puerto	M_2	148.30	150.94	1.02	324.20	332.80	8.60
	S_2	42.00	33.89	0.81	27.10	36.20	9.10
	N_2	28.20	26.74	0.95	292.20	305.40	13.20
	K_1	11.90	13.01	1.09	47.00	75.00	28.00
	K_2	11.40	14.83	1.30	27.50	61.60	34.10
	P_1	3.90	4.12	1.06	46.60	78.30	31.70
Bolivar	M_2	102.20	107.94	1.06	298.60	278.20	-20.40
	S_2	30.10	29.86	0.99	326.00	325.90	-0.10
	N_2	20.60	22.00	1.07	278.50	250.10	-28.40
	K_1	16.90	12.47	0.74	47.60	49.10	1.50
	K_2	8.20	8.76	1.07	326.40	341.30	14.90
	P_1	5.60	4.07	0.73	47.20	50.40	3.20
Posorja	M_2	91.40	96.18	1.05	288.20	297.00	8.80
	S_2	19.30	22.79	1.18	341.90	345.60	3.70
	N_2	18.60	18.75	1.01	260.40	266.70	6.30
	K_1	12.10	11.81	0.98	48.90	55.90	7.00
	K_2	5.20	7.05	1.36	342.30	12.80	-30.50
	P_1	4.00	3.79	0.95	48.50	58.00	9.50
Libertad	M_2	78.60	74.28	0.95	251.70	250.40	-1.30
	S_2	23.10	22.35	0.97	299.20	295.00	-4.20
	N_2	17.50	16.06	0.92	223.20	222.00	-1.20
	K_1	11.40	11.43	1.00	42.10	40.80	-1.30
	K_2	6.30	5.98	0.95	296.90	294.60	-2.30
	P_1	3.30	3.55	1.07	39.60	39.80	0.20

5.2. DERIVATION OF THE INITIAL BED TOPOGRAPHY IN THE AREA OF INTEREST

Before starting to analyze the behavior of the estuary itself all the boundary conditions of open and closed boundaries need to be defined first. From the gathered data the information for open boundaries such as water levels and river stages can be retrieved. In addition, the bed topography for the outer estuary is also well defined. However, as mentioned in subsection 2.3.1, in absence of measurements and due to the coarse resolution of the GEBCO topographic data set, it is not possible to define a priori the initial bed topography for the Guayas River estuary.

The approach adopted to derive the bed topography is similar to what is proposed by Van der Wegen and Roelvink (2012) for the Western Scheldt estuary in the Netherlands. The main premise is that under steady forcing conditions stable morphological features evolve as the result of the interaction between the forcing, the estuary's geometry and the available sediment. This is in line with what was presented in chapter 3 that the estuary is developing towards an equilibrium condition for which changes in the shape are the estuary's response to the hydrodynamic forcing.

5.2.1. APPROACH

Starting from a flat bed in the area lacking topographic information, the model is forced until the formed channel-shoal patterns resemble the observed patterns from satellite photographs. Visual comparisons however might be somewhat subjective, therefore a more strict criterion is needed to validate the generated bed topography. For this, use is made of the influence on the hydrodynamics caused by the morphology and the fact that under stable conditions the estuary develops towards an equilibrium state.

In summary the validation criteria namely consist of three parts:

- **Visual comparisons with satellite images:** Use is made of the 1970 satellite image of the estuary.
- **Equilibrium state condition:** The model is run until some sort of stable patterns are generated. In order to assess this 'stability condition', the development of the estuary's depth (averaged over the domain) and the sedimentation/erosion volumes with respect to the initial condition are computed.
- **Hydrodynamic validation:** Once a positive evaluation of the previous items is obtained, the model is run again for the spring-neap calibration period with the new bathymetry. This time the records from the Guayaquil tidal station are contrasted with the model results at that same location. The bathymetry is deemed acceptable based on the level of agreement between the observed and modelled water level signals.

In this manner it is assured that the model, with the new bed topography, is calibrated for present-day conditions.

5.2.2. INITIAL AND FORCING CONDITIONS

Van der Wegen and Roelvink (2012) argue that the larger amount of available sediment of a shallower initial bathymetry favors the formation of large intertidal areas with a single straight deep channel. This can be explained from the perspective of the tide propagation, since the formation of intertidal areas stimulates ebb dominance, which in turn enhances the excavation of a single channel. At the other end, an initial deeper topography is not so much influenced by the amount of sediment available but by the estuary's geometry instead. Thus, a good assessment of the initial condition is key to obtain a good estimate. In general deep initial conditions render better results, however the deeper the initial condition the longer time it would take to reach equilibrium. In this case the initial flat bed level is set equal to the equilibrium condition determined with the analytical model shown in Figure 3.4, approximately 6 m below mean sea level.

The forcing conditions consist of the morphological tide at the seaward boundary (taken as $1.08*M_2+C_1+M_{2_{overtides}}$) and the schematizations for the river discharges discussed in subsection 4.2.3, in addition the morphological factor is set to $MorFac = 100$. Both schematizations are treated separately and the one that yields the best results is ultimately chosen.

The morphological boundary conditions are imposed such that there is a zero concentration gradient at the boundaries. In this way little accretion or erosion is experienced at the boundaries.

5.2.3. RESULTS

Figure 5.2 shows the morphodynamic evolution of the estuary. The **a** and **b** indexes indicate the river discharge schematizations with a constant value and with the variation according to the hydrograph's shape, respectively. The subscripts 1 to 4 indicate the situation after 0, 50, 100 and 200

years. The final situation for both cases stems from the first and second validation criteria mentioned before, which are further elaborated in the following paragraphs.

In general, it can be seen that during the first 50 years the morphological evolution is relatively fast and is already comparable to the final situation. Besides, there are not significant differences between the **a** and **b** runs, which underlines the minor influence of the river discharge compared to that of the tidal forcing, at least for long-term simulations.

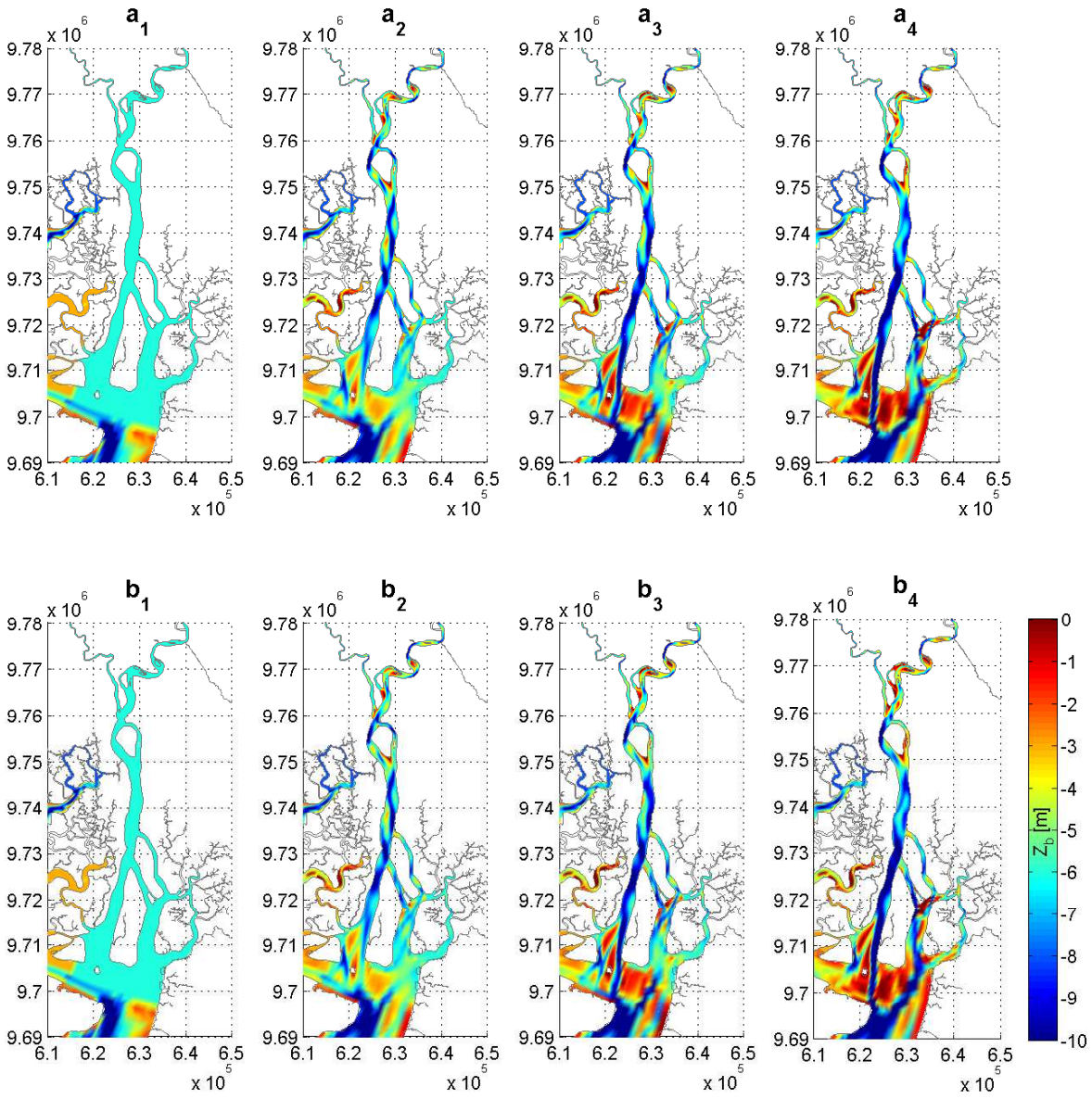

Figure 5.2: Bed level development: **a** is the case with a constant river discharge and **b** is the case with varying discharges according to the hydrographs of the Daule and Babahoyo Rivers

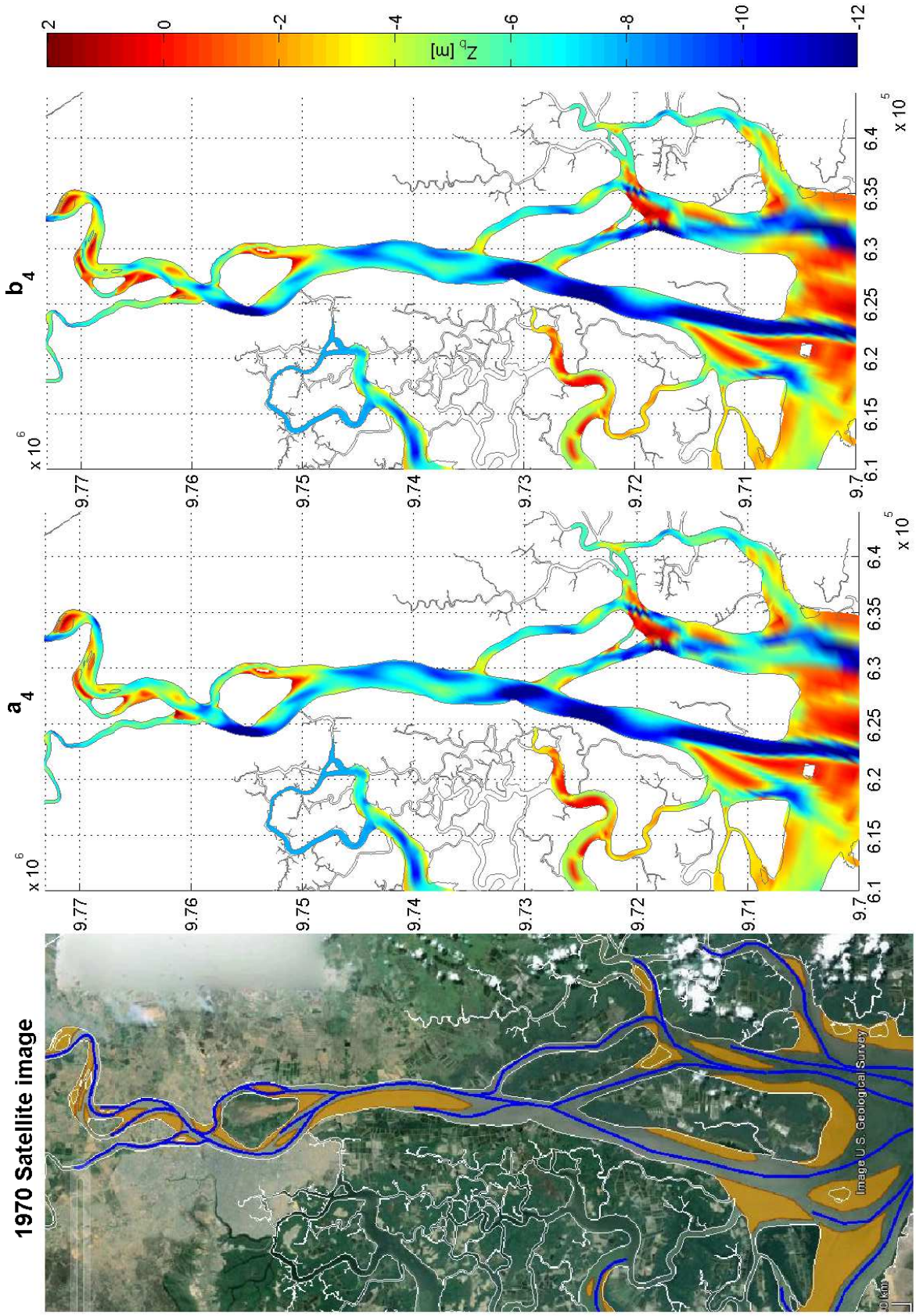

Figure 5.3: Comparison of the obtained $\mathbf{a}_4$ and $\mathbf{b}_4$ bathymetries with the 1970 Satellite image (channels in dark blue and shoals in orange)

VISUAL COMPARISONS

Figure 5.3 presents the obtained $\mathbf{a}_4$ and $\mathbf{b}_4$ bathymetries and the 1970 satellite image of the Guayas River estuary. After a close inspection, the main morphodynamic features have been outlined in the satellite image. The resemblance with the model simulations is remarkable in the northern and middle parts of the estuary. The southern part is where larger differences are found. In both simulations, the model in the southern part develops a single straight deep channel while in reality the distinction between channel and shoals is not that pronounced.

In the northern and middle parts, the effects of curvature induced secondary flow on the morphology is evident, i.e., deeper channels in outer bends and shallower areas in inner bends. This is, to a large extent, properly captured by the model. Indeed, to further corroborate the quality of the simulations the majority of islets at inner bends, that are well discerned as permanent dry areas, were purposely included into the domain as active wet grid cells. At almost every instance the location and shape of the islets are well seized by the model.

From a visual assessment practically there is no difference between the derived bed topographies. It can be said though that both are a fairly good representations of the 1970 situation.

EQUILIBRIUM CONDITION

In Figure 5.2 it can be seen that for both case **a** or **b** the morphological evolution is quite fast over the first 50 years. Afterwards the morphological patterns remain more or less stable. Indeed there is not much appreciable difference between the 100 and 200 years bathymetries for both cases. This suggests that the estuary is reaching some sort of equilibrium under the prescribed forcing. A depiction of the development of the estuary over time is presented in Figure 5.4. The left plot presents the evolution of the average bed level. In both cases a rapid development can be seen over the first decades, on average the estuary continuously deepens the first 100 years, after which it stabilizes at a slower rate. The difference between case **a** and **b** is now evident. The schematization of the river discharge as a constant value leads to a deeper estuary. However case **b** seems to reach the end of the simulation period in a more stable manner.

The latter is further confirmed with the estimation of the sedimentation and erosion volumes (right plot of Figure 5.4). The volumes are calculated by subtracting the initial condition (i.e., $\mathbf{a}_1$ and $\mathbf{b}_1$) from the computed bed levels through time. The trend of the net volume curves reflects the same behavior observed for the average depth curves. The practically constant trend reached by case **b** indicates that no more sediment is being imported nor exported, hence a high degree of stability has been reached. A closer look into the sedimentation/erosion volumes reveals that the difference between both cases in the first 100 years is mainly due to larger erosion volumes of case **a** and in the last 100 years due to smaller sedimentation volumes of the same case.

The schematizaion of the river discharge for case **a** was based on a flow transport relation that relates the transport rates to the discharge powered to an exponent 5, i.e, $n = 5$. The river discharges thus computed (389.77 m^3/s and 611.82 m^3/s for the Daule and Babahoyo rivers respectively) are larger than the yearly averaged values (292.44 m^3/s and 469.13 m^3/s). This means that on average more water flows out of the estuary due to this schematization, hence the estuary needs to adapt to this larger volume of water by deepening its bed. This highlights the importance of capturing the seasonality of the river hydrographs and constitutes a sound argument for choosing the case **b** river discharge schematization and consequently the resulting $\mathbf{b}_4$ bed topography.

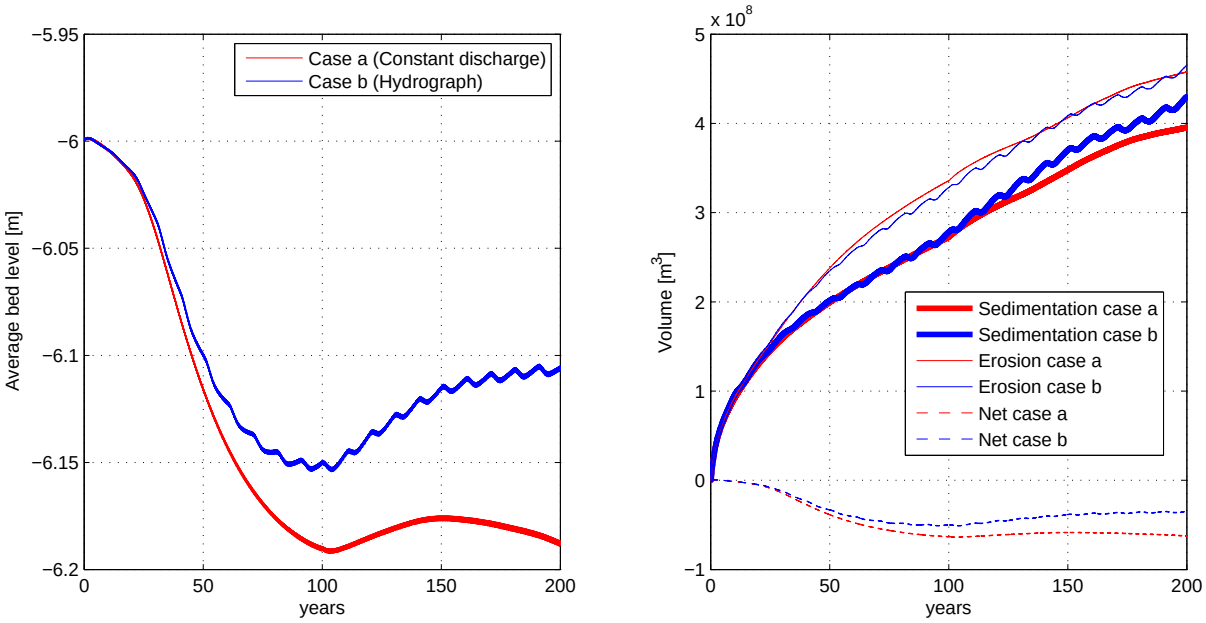

Figure 5.4: Evolution of the estuary's average depth and sedimentation/erosion volumes

Hypsometric curves provide information about the wetted topographic area that is under a certain level. Figure 5.5 presents the curves corresponding to the case **b** bed topographies shown in Figure 5.2. Again, the first 50 year period is when most of the significant changes take place. The evolution is such that the average bed level of Figure 5.4 is proven to be the middle point of the curves around which shallow areas become shallower and deep areas become deeper in time.

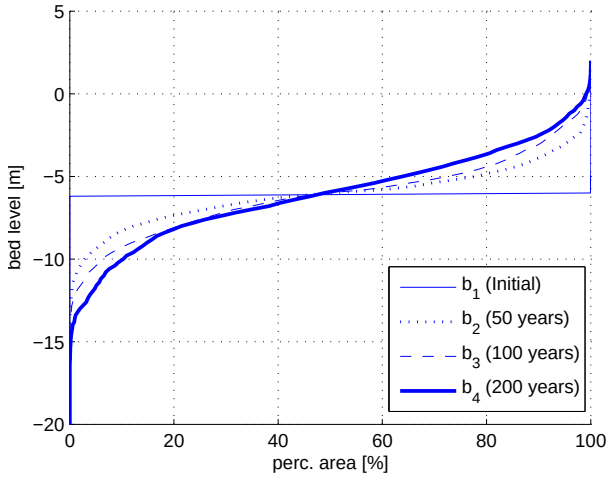

Figure 5.5: Evolution of hyspometric curves for case **b**

HYDRODYNAMIC VALIDATION

The final stage to validate the derived intial topography $\mathbf{b}_4$ is to contrast the computed water levels with those of the Guayaquil tidal station. The correlation and error between measured and modelled water levels are $R_2 = 0.96$ and $rmse = 0.221$ m. Furthermore, tidal analysis of the modelled signal results in the respective tidal constituents that can be contrasted against those of Table 2.1.

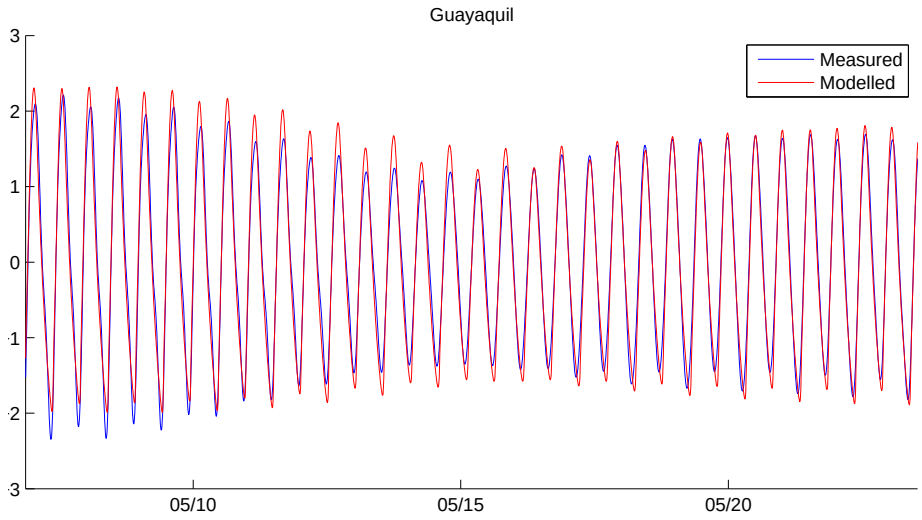

Figure 5.6: Observed and modelled water levels at the Guayaquil tidal station

The comparison of the most energetic components is shown in Table 5.3. All the component amplitudes agree generally well with the measurements. The main difference stems from the computed phases for components N_2 and K_2.

Table 5.3: Computed and observed tidal constituents at the Guayaquil tidal station

	Amplitude			*Phase*		
Constituent	*Observed* [cm]	*Computed* [cm]	*Ratio*	*Observed* [deg]	*Computed* [deg]	*Difference* [deg]
M_2	150.40	157.24	1.05	20.90	17.92	-2.98
S_2	34.80	29.46	0.85	67.50	77.77	10.27
N_2	25.00	26.70	1.07	21.10	346.21	-34.89
M_4	14.60	23.72	1.62	313.40	324.00	10.60
MU_2	13.90	12.96	0.93	119.80	141.09	21.29
L_2	11.20	11.53	1.03	17.50	43.82	26.32
K_2	9.50	9.49	1.00	67.90	119.83	51.93
K_1	8.80	10.25	1.16	92.10	98.00	5.90
MS_4	8.10	11.81	1.46	3.00	9.63	6.63
MSF	7.90	6.52	0.83	10.30	30.86	20.56
M_6	6.90	3.85	0.56	143.60	153.06	9.46

5.3. TIDAL PROPAGATION THROUGHOUT THE GULF OF GUAYAQUIL

During October and November, 1970, Murray et al. (1976) carried out a measuring campaign in order to determine the velocity field during a tidal cycle throughout the Gulf. Their measurements are synthesized in a series of velocity field maps for different tidal current stages. Similar results are found applying the current model.

The coupling between the vertical and horizontal tide is shown every 2 lunar hours over the duration of a tidal cycle in Figure 5.7. Starting from the low water slack situation at lunar hour 0, it can be seen that by the second hour flood currents prevail throughout the Gulf, moreover the flow converges at the entrance of the Guayas River in the northern part of the Puna island. By lunar hour 4, major flood currents prevail mostly in the northern part of the Gulf, i.e. the Guayas River and

the Estero Salado estuaries. High water slack is reached at lunar hour 6, however still strong flood currents are present in the Guayas River. Ebb currents are predominant by lunar hour 8 and the flow in the northern part of the Puna Island is now divergent. The peak of the ebb currents in most of the Gulf is reached by the tenth hour.

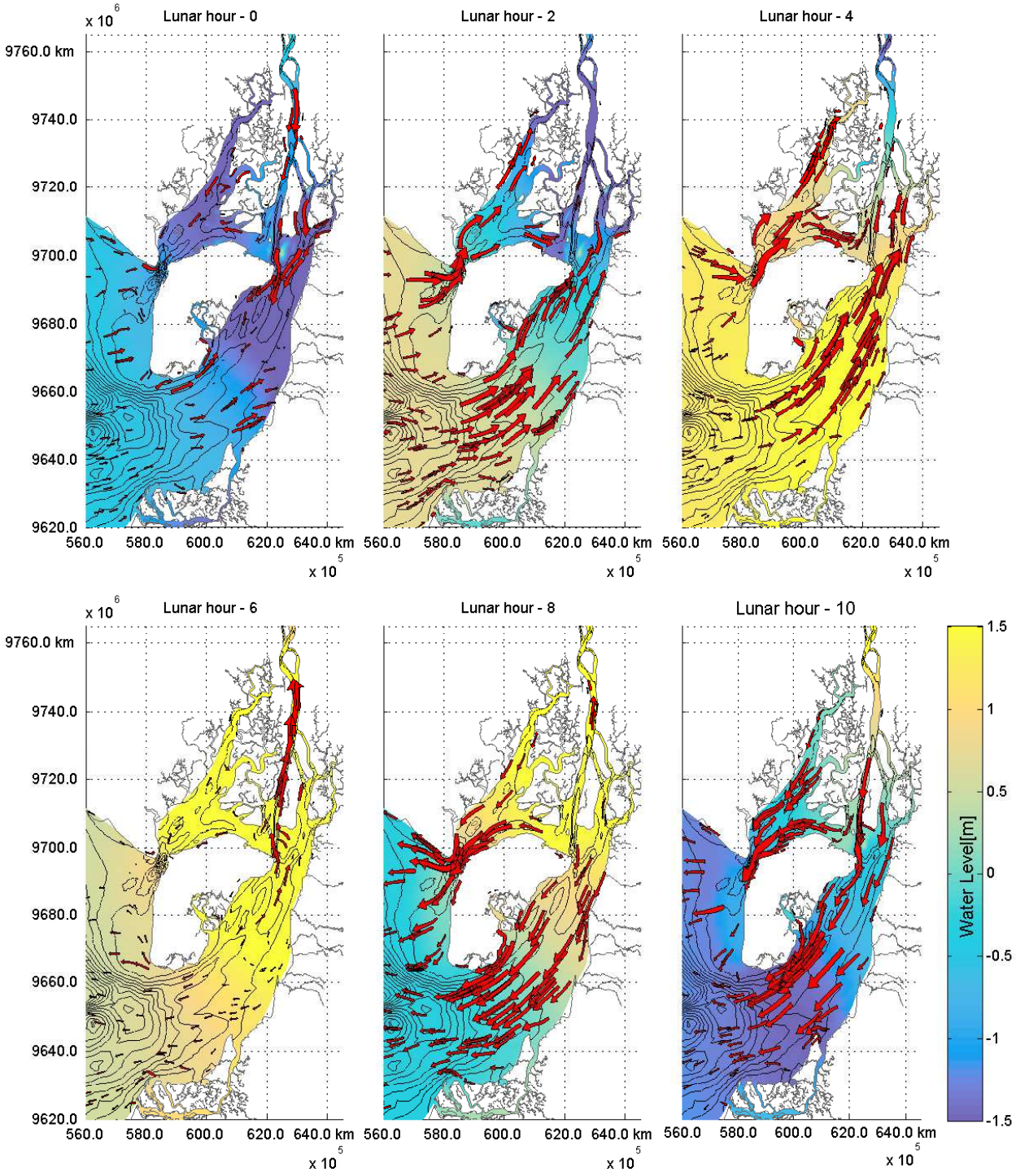

Figure 5.7: Tidal current velocity field over a tidal cycle

The amplification of the tidal wave can also be analyzed with the aid of the model. The sum of the amplitudes $M_2 + S_2$ is a good estimate of the amplitude at spring tide. By performing a tidal harmonic analysis at every grid point it is possible to map the spring tidal amplitude throughout the Gulf, as shown in Figure 5.8. It becomes clear now how the tide is amplified due to the convergence of the banks and as the bathymetry becomes shallower. The maximum amplitude, found at the city of Guayaquil at the confluence of the Daule and Babahoyo Rivers, nearly doubles the values of the outer part of the Gulf. In particular, the amplitude increases from 1.58 m to 1.93 m along the Guayas River.

In addition, by analyzing the horizontal tide, the relative phase lag ε between HW and HWS for the M_2 constituent can also be mapped in order to illustrate the character of the wave at every location. Values of ε close to 90 degrees indicate that the wave has a propagating character which is typical of deep prismatic channels. At the other end, the standing wave character is dictated by values of ε close to 0 degrees, characteristic of short tidal embayments. Both types of behavior of the tide are clearly discernible by comparing the Estero Salado and the Guayas River estuaries. The former can be deemed as a tidal embayment since it lacks the input of fresh water, the latter on the other hand has a more straight shape and deeper bathymetry that agrees with a more propagating behavior in relation to the Estero Salado.

What essentially can be seen from Figure 5.8 is that the character of the tide becomes more standing-wave-like towards the upstream part of the Gulf. In the Guayas River ε remains fairly constant at approximately 30 degrees, i.e., the phase lag between HW and HWS is roughly 1 hour.

Besides, by mapping the co-tidal lines (lines that connect points of equal phase angles for the vertical tide) the propagation of the tide can be visualized. These lines (red lines) are presented in the right plot of Figure 5.8 every 10 minutes i.e., approximately every 5 deg. A close examination of these lines reveals that it takes about 90 minutes for the tide to travel from the Guayas River estuary mouth (northern from the Puna island) up to the Guayaquil tidal station. This is in line with the measurements by Murray et al. (1976).

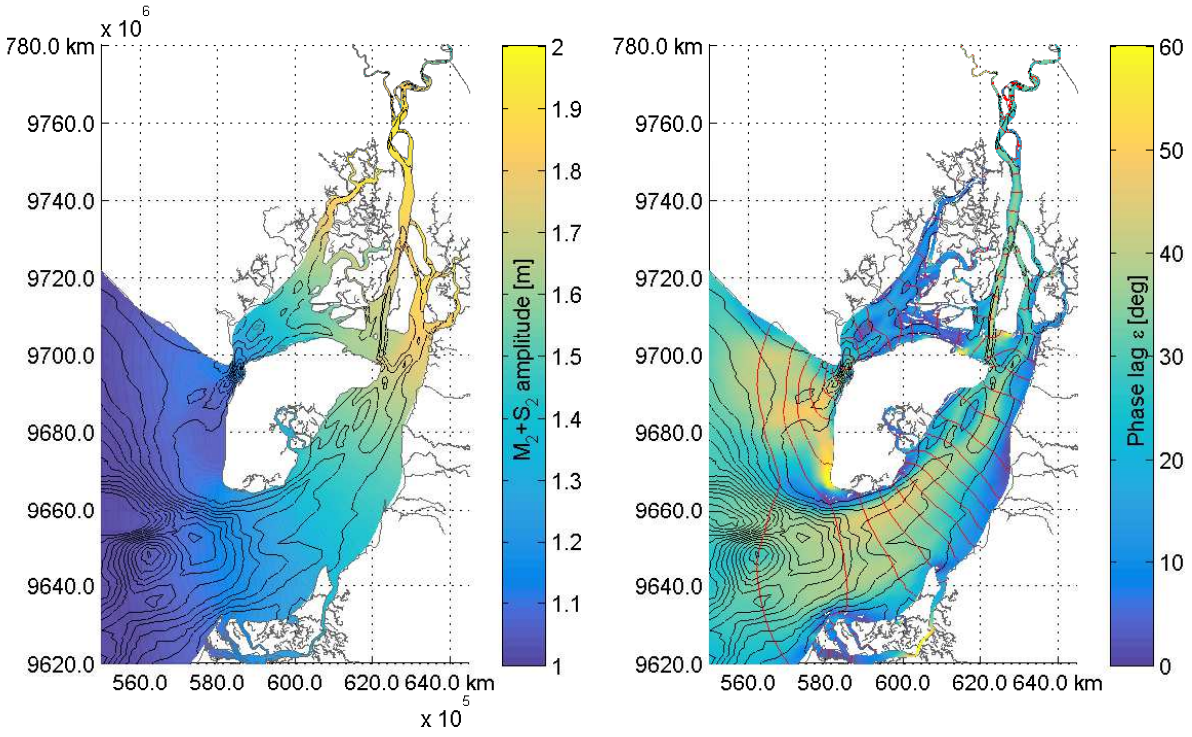

Figure 5.8: $M_2 + S_2$ tidal amplitude and HW - HWS phase lag

The above discussed results are consistent with what was presented in chapter 3 with the analytical model for the Guayas River estuary, which in a sense validates the use of the Delft3D-FM model as well.

5.4. CALIBRATION OF THE MORPHOLOGICAL TIDE

In order to perform mid and long term simulations in acceptable computational times, the forcing conditions were schematized. The accelerated simulation makes use of these schematized forcing conditions in addition to the morphological acceleration factor. To determine and validate the use of the morphological tide, the results obtained with the schematized conditions are compared with a brute force simulation that is performed over 2 spring-neap tidal cycles, i.e., approximately one month according to the **Maintaining the shape of the hydrographs** forcing schematization described in subsection 4.2.3.

5.4.1. BRIER SKILL SCORE

The Brier Skill Score (BSS) described by Sutherland et al. (2004) objectively quantifies the accuracy of a model prediction relative to a baseline prediction, i.e., the skill of the model. The BSS reads:

$$BSS = 1 - \frac{\langle (Y - X)^2 \rangle}{\langle (B - X)^2 \rangle} \tag{5.1}$$

Where $\langle\rangle$ denotes the arithmetic mean, Y is the prediction, B is the baseline prediction and X is an observation. For judging the decrease of skill caused by the introduction of the morphological tide schematization, B is defined as the initial sedimentation/erosion volumetric change map which is zero, Y is the sedimentation/erosion volumetric map prediction (relative to the initial bathymetry derived in section 5.2 with the schematized tide, and X is the 'perfect' sedimentation/erosion volumetric map obtained with the full tidal signal. The BSS then is:

$$BSS = 1 - \frac{\langle (\Delta vol_{morphological-tide} - \Delta vol_{brute-force})^2 \rangle}{\langle (\Delta vol_{brute-force})^2 \rangle} \tag{5.2}$$

A BSS of 1.0 indicates a perfect prediction of the morphological changes. At the other end, a value of 0.0 means that the model prediction is no better than the baseline model, i.e, no morphological change. A negative BSS points out that the prediction is less accurate than the baseline model. For morphodynamic studies Van Rijn et al. (2003) qualify the BSS according to Table 5.4.

Table 5.4: BSS qualification for morphodynamic studies

Qualification	*BSS*
Excellent	1.0 - 0.8
Good	0.8 - 0.6
Reasonable/fair	0.6 - 0.3
Poor	0.3 - 0.0
Bad	< 0.0

5.4.2. CALIBRATION OF THE f_2 SCALING FACTOR

The morphological tide consists of the sum of some of the tidal components given by $f_2 M_2 + C_1 + (M_{2_{overtides}})$, for the derivation of the initial bed topography the scaling factor was taken as $f_2 = 1.08$. Assuming that the topography $\mathbf{b}_4$ thus derived is reality, the factor can now be properly calibrated.

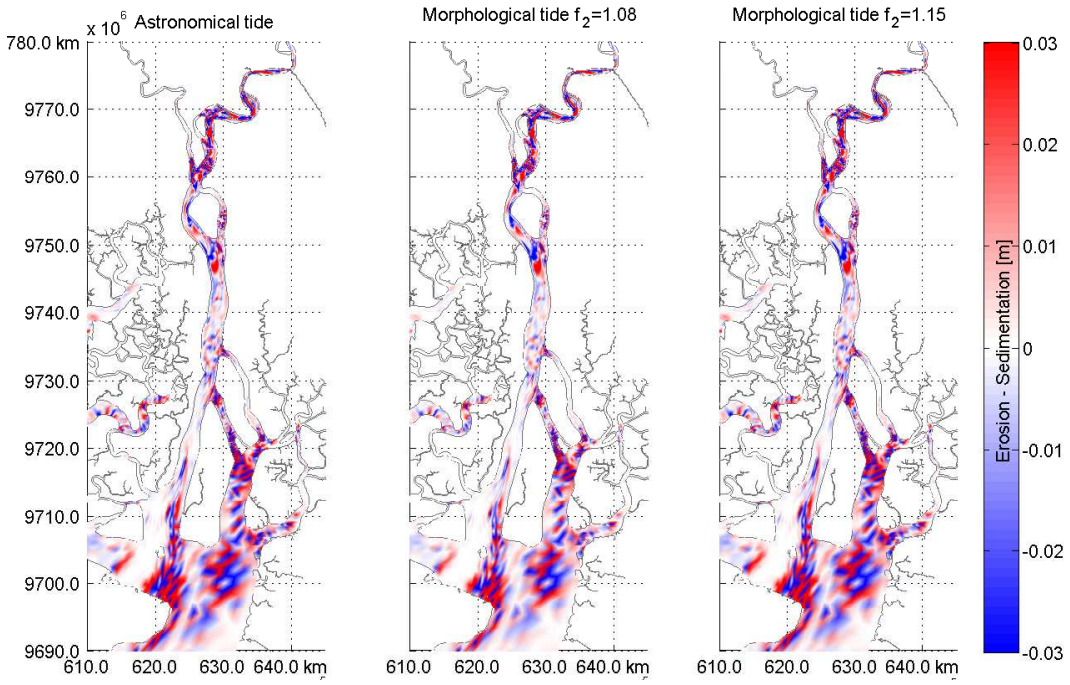

Figure 5.9: Sedimentation and erosion patterns computed using the full astronomical tide and the morphological tide over 2 spring-neap tidal cycles

Table 5.5 shows the BSS results for the initial and calibrated f_2 values, in addition, Figure 5.9 presents the erosion/sedimentation maps. The calibration is focused on the Guayas River estuary. The BSS is computed for the overall area and, in order to detect the most sensitive zones, the estuary is further dived in 3 parts of roughly the same length (upstream, middle and downstream sections) for which the BSS is computed individually as well.

The tuning of the scaling factor renders excellent results. The optimum value is $f_2 = 1.15$, which reproduces basically the same sedimentation/erosion patterns as for the full astronomical tide. Reiterating, with this schematization of the forcing conditions, the duration of the simulation has been significantly reduced to a 6.67% of the time, i.e., one month of morphological development is reduced to 2 days of simulation.

The initial value of 1.08 reproduces the same patterns but a little less intense. It is an excellent approximation already, hence its use for the derivation of the initial bed topography is justified. However, for the following simulations $f_2 = 1.15$ is used.

From the results it can also be inferred that the most morphologically active zones are slightly better reproduced. Besides it can also be said that the model is not so sensitive to the scaling factor. This might be attributed to the fact that the seaward boundary is located far away from the Guayas estuary (about 170 km), and a slight change in the amplitude of the tide does not affect significantly any wave transformations that might take place over the large travel distance.

Table 5.5: BSS for different values of the f_2 scaling factor

Morphological tide	*BSS*			
	Overall	*Downstream*	*Middle*	*Upstream*
$1.08M_2 + C_1 + (M_{2_{overtides}})$	0.954	0.953	0.943	0.971
$1.15M_2 + C_1 + (M_{2_{overtides}})$	0.995	0.997	0.963	0.966

6

ANALYSIS

6.1. APPROACH

From the results obtained in the previous chapter, it can be said that the model is able to reproduce at least in a qualitative way the observed bed topography. Therefore, it can be assumed that the model is able to predict the sediment transport patterns relatively well. In this chapter the emphasis is put towards reproducing and explaining the evolution of the estuary in a broader sense, that is, a detailed representation of morphological features is not a priority. Instead, the effects of interventions are assessed by interpreting the differences between pairs of model simulations. With this in mind, a number of scenarios is proposed, each of which represents a particular intervention [1] or phenomenon experienced by the estuary. The approach is as follows:

- Simulations are run for a period of 6 years. The first year is taken as spin up time, during which all conditions are the same for every case scenario.
- All simulations are performed starting with the $\mathbf{b}_4$ bed topography.
- A total of 6 case scenarios is analyzed based on the identified causes of sedimentation discussed on subsection 1.2.1, namely:

  GRE01. Reference scenario: The morphological tide constitutes the seaward boundary conditions and the river discharges are those pertaining to the situation prior to 1979, i.e., without the influence of any of the interventions nor El Niño events. The model domain **does not include** the intertidal areas either, i.e., the model resembles the situation after the construction of the shrimp farms (left image of Figure 6.1).

  GRE02. Situation prior to shrimp farms construction and mangrove deforestation: In this case the boundary conditions remain the same as for the previous case, however the shape of the estuary is modified to include the intertidal areas that have been occupied by the increasing aquaculture practices over the last decades.

  The right image of Figure 6.1 displays the modified domain. The extent of the intertidal areas is unknown, the only available information is that of online satellite images. Therefore it is assumed that the intertidal areas, especially in the middle part of the estuary, match those areas that are currently occupied by the shrimp farms. In addition, to account for the mangrove forest in the intertidal flats, the Manning friction coefficient is locally increased to 0.030 $s/m^{1/3}$ and the bed level elevation is set to MSL.

[1] The term 'intervention' is used as a reference to any of the 5 considered events, i.e., decimation of tidal flats, El Niño, Daule-Peripa dam, the 'Puente de la Unidad Nacional' bridge and sediment overload due to deforestation of the upper basin

The inclusion of the intertidal flats is supposed to affect mainly the tide propagation, hence the exchange of sediment with the rest of the domain is restricted by setting these areas as not morphologically active.

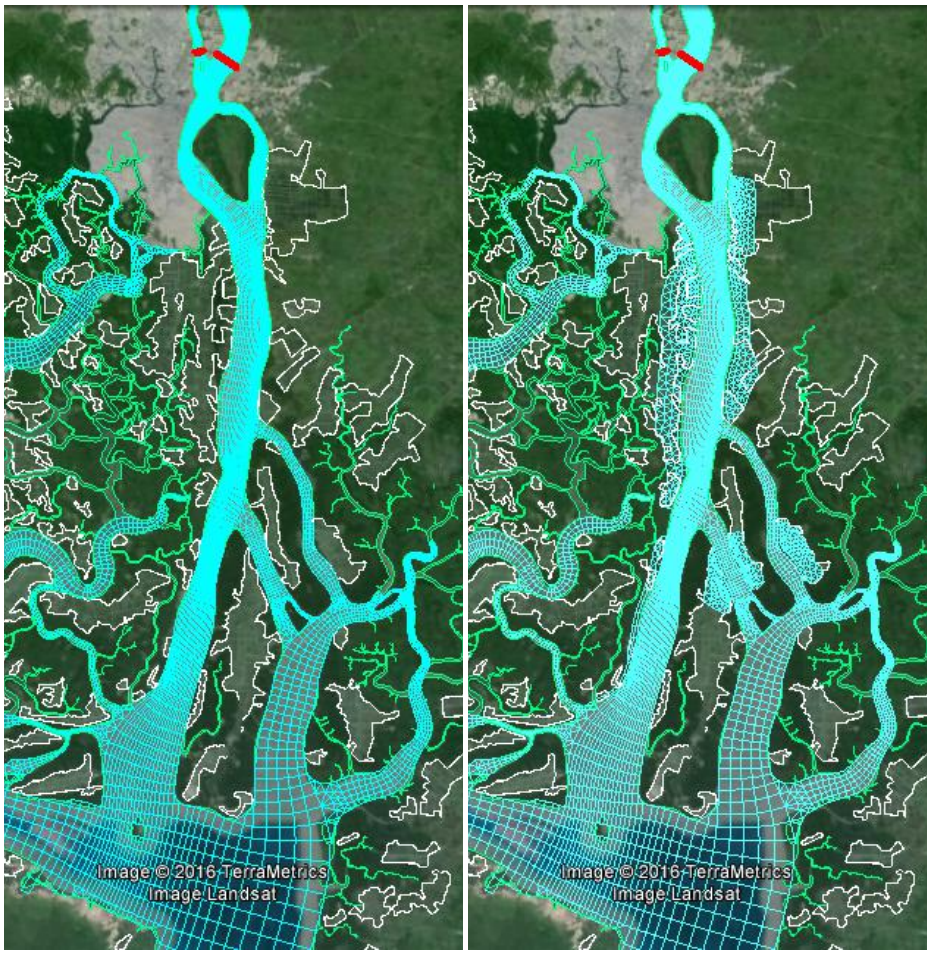

Figure 6.1: Reference (left) domain and modified (right) model domain (light blue) that includes the intertidal and mangrove forest areas currently occupied by shrimp farms (white). 'Puente de la Unidad Nacional' bridge (red)

GRE03. El Niño events: This scenario includes the effects on the river hydrographs caused by the El Niño events. The set-up is similar to case **GRE01** with the difference that in the third year of the simulation the hydrographs of the Daule and Babahoyo rivers are modified according to a 'typical' El Niño year according to Figure 2.7.

GRE04. Daule-Peripa dam project: The regulation effect of the Daule-Peripa dam on the discharges of the Daule River is taken into account by changing the shape of the hydrograph to that after the construction of the dam, Figure 2.7.

GRE05. The 'Puente de la Unidad Nacional' bridge: The 'Puente de la Unidad Nacional' is a set of bridges over the Daule and Babahoyo Rivers that connect Guayaquil with the cities of Samborondón and Durán and it is located near the confluence of the rivers. The location is shown in Figure 6.1. The design of the bridges is such that the foundations block over 20% of the width of both rivers. In that regard, the bridge piers are modelled as thin dams. The rest of the set up for this scenario is the same as for case **GRE01**.

GRE06. Deforestation of the upper basin: Erosion processes are accelerated in the upper

basin of the Guayas River estuary due to deforestation. Since the effects of erosion have not been yet formally quantified, it is assumed that the related increase of the sediment load is 20% more than the transport capacity of the rivers at the boundaries. In all previous cases, the morphological boundary conditions at the rivers are chosen such that the sediment input equals the transport capacity, and thus, the bed level at the boundaries experiences little to non changes. In this case, in contrast, the sediment input at the rivers is 1.20 times that of the previous cases.

6.2. TIDAL ASYMMETRY AND RESIDUAL SEDIMENT TRANSPORT

The effect of the different interventions on the tidal asymmetry and the residual bed-load transport is treated in this section. For this a tidal analysis is performed in all the points along the profile defined in the lower plot of Figure 6.3. The profile is taken along the Guayas River estuary and starts at the mouth, near the Puna island (km 0.00), up to the confluence of the Babahoyo and Daule Rivers (km 64). The harmonic tidal analysis aims at obtaining the amplitudes and phases of the main horizontal tidal components M_2, M_4 and M_6, as well as the magnitude of the residual flow u_0 previously discussed in subsection 2.1.4.

Once the components are determined for each point along the profile, with the aid of Equation 2.13, the time averaged bed-load transport can be computed as well as its main contributors, that is terms (1), (2) and (3) on the right hand side of the equation. In this way the relative impact on the sediment transport caused either by the effect of the residual flow (e.g. river discharges) or the tidal distortion can be assessed for each one of the cases described above. The total load transport formulation of Engelund-Hansen, used for Delft3D-FM model, assumes a relation of the form $S \propto U^5$, however, the analysis presented in this section follows the approach by Van de Kreeke and Robaczewska (1993) which assumes a relation of the form $S \propto U^3$. In reality the power exponent is always greater or equal than 5. However the simpler approach is analytically more convenient since it provides a direct insight into the causes of asymmetry. Moreover, the results correlate with the actual annual residual transport computed by the model for the different scenarios (presented in Appendix B), which validates the soundness of the analysis.

Figure 6.3 shows the average annual residual sediment transport S and its contributor terms (1), (2) and (3), which have been normalized by the cubed amplitude of the M_2 component. Positive and negative values mean that the sediment transport is directed upstream or downstream, respectively. The two bottom plots of Figure 6.3 show the relative difference of the profiles of terms (1) and (2) with respect to those of case **GRE01**. Positive and negative values indicate the direction towards which the sediment transport is affected in relation to the reference case, i.e., in the upstream or downstream direction. The following can be stated:

- Term (3) is almost negligible in every case, as expected, and therefore not really relevant for the analysis.

- In all case scenarios term (2), which is related to the distortion of the tidal wave due to the interaction of the M_2 and M_4 components, shows a flood dominant character at every point along the profile that continuously increases in the upstream direction.

- Case **GRE02** presents the major impact on term (2) in relation to the other cases. This is attributed to the addition of the intertidal areas, which provides additional friction that slows down the propagation of the high tide. Moreover, water levels are higher during flood and the volume that is stored in the intertidal areas needs to flow out during ebb, when the water levels are lower. This implies that the ebb velocities must be increased, which results in a less flood dominant situation. Term (1) is also significantly affected, although there is not a clear

trend, the effect is more local. In any case the difference is less than for the wave distortion related transport, which is the most influenced transport mechanism for this scenario.

- The large river discharges associated with the "El Niño" have a significant impact on promoting ebb dominance in case **GRE03**, particularly the part related to the residual flow. This can be explained from the increased seaward velocities that result from the larger discharges of the Daule and Babahoyo Rivers during an "El Niño" event. The effect is more prominent in the upstream part of the estuary where the influence of the rivers is larger.

  Regarding the tidal distortion, the effect is opposite. Large river discharges tend to compress the tidal wave as it propagates upstream. This reduces the flood period which in turn intensifies flood dominance. However, this is overwhelmed by the latter effect on the residual flow, which is the dominant mechanism in this case.

- **GRE04** presents a slight reduction of the residual flow associated transport in relation to **GRE01**. The situation is opposite to the previous case. The regulated discharge of the Daule River by the Daule-Peripa dam decreases the influence of the river on the residual flow and the tidal distortion.

- The 'Puente de la Unidad Nacional' bridge (km 64 and shown in Figure 1.5) in **GRE05** has also a minor impact on the residual transport, the effect is more local. Term (1) is enhanced in the downstream direction in a stretch of approximately 20 km from the bridge. This can be attributed to the local acceleration that water experiences due to the width constriction in order to comply with the continuity requirement. In contrast, the residual transport related to term (2) is slightly increased in the upstream direction at a 50 km distance from the estuary's mouth. The bridge produces a backwater effect in both upstream and downstream directions. This might be visualized by the relative changes in the mean water levels along the estuary which are presented in Figure 6.2. The slightly decreased mean water level from km 0.0 up to km 50 explains the changes in the transport related term (2), since the effect of friction will be enhanced particularly for lower water levels which in turn will reduce the ebb velocities.

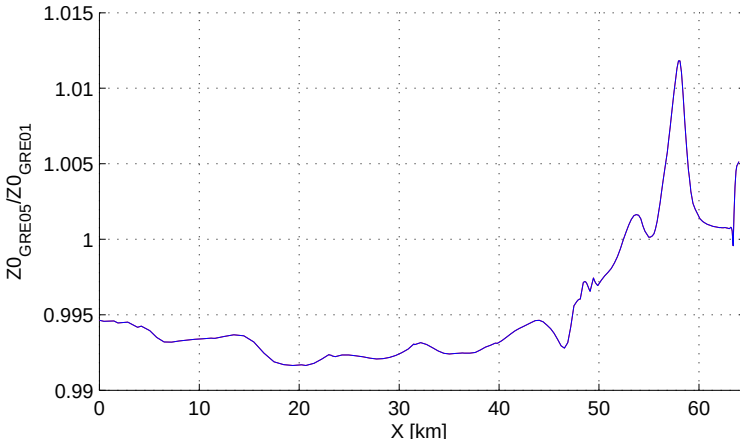

Figure 6.2: Mean water level profile of case **GRE05** in relation to case **GRE01**

- Case **GRE06** presents no differences with the reference. The effect of an increase in the sediment load at the the rivers has no influence on the residual sediment transport. The model boundaries are located about 65 km upstream the confluence of the rivers, which is a large travel distance for the amount of sediment prescribed at the boundaries to reach the zone of interest. A quick assessment of the order of magnitude of the time T_s needed can be done by

assuming equilibrium conditions in the rivers, i.e., there are no gradients in sediment transport along the L = 65 km distance. The transport capacity then equals the sediment load. Assuming the averaged flow velocity U = 1 m/s, the averaged depth h = 5 m, a mean Chézy coefficient C = 50 $m^{0.5}/s$, Δ = 1.65, D_{50} = 0.3 mm and with the aid of the Engelund-Hansen formula we have:

$$T_s = \frac{Lh}{S} = \frac{Lh}{\frac{0.05U^5}{\sqrt{g}C^3\Delta^2 D_{50}}} \approx 65 years \tag{6.1}$$

Therefore, it can be concluded that the effects of this case have minimum impact on the morphology, at least for periods of short to medium term in the order of decades.

6.3. SEDIMENT BALANCE

To determine the sediment balance the estuary has been divided in 13 macro cells. The macro cells enclose areas within which the residual sediment transport has approximately the same magnitude and direction. The sediment balance quantifies the erosion and sedimentation volumes in each of these cells as well as the sediment exchange between them. The calculations are done on a yearly basis as well as over the duration of the wet (December to May) and dry (June to November) seasons, i.e., the volume change of a cell over a year (or season) is computed as the difference between the sediment passing thorough the seaward and landward boundaries correspondingly. Upstream or landward sediment transport is considered positive whereas downstream or seaward is negative. The results are summarized in Figure 6.4, Figure 6.5 and Figure 6.6. A more detailed description can be found in Appendix B where, besides the sediment balance, the patterns of erosion-sedimentation are also shown.

During the dry season, regardless of the case scenario, with the exception of macro cells 1 and 2, the net sediment transport through the cells is directed upstream. Things change during the wet season when basically depending on the magnitude of the river discharges, the direction is reversed for most of the estuary, especially the area upstream macro cell 3. This underlines the fact that the resulting magnitude and direction of the net transport is dependent on the relative riverine influence with respect to that of the tide. During the dry season the tidal influence is the greatest and during the wet season the latter is reduced significantly or even surpassed by the rivers.

The following remarks can be made by comparing the case scenarios:

- No significant differences can be discerned by comparing **GRE01** with **GRE04**. Since the only difference between this cases is the changes in the Daule River hydrograph it can be inferred that the influence of the Daule River is minor in relation to that of the Babahoyo River. During the wet season the larger differences appear, especially in the macro cells downstream the confluence of the rivers, i.e, cells 3, 4, 5, 6 and 9. The Daule-Peripa Dam regulates the Daule River discharge such that less water flows during the wet season compared to **GRE01**, hence the transport capacity in the ebb direction is reduced. In contrast, during the dry season the dam delivers additional water to the river which enhances the transport capacity in the ebb direction.

- By inspecting the volume change of the cells in Figure 6.4 it can be concluded that the impact of the 'Puente de la Unidad Nacional' bridge (**GRE05**) on the morphology is somewhat stronger than the construction of the Daule-Peripa Dam (**GRE04**). A comparison of both cases reveals that in the former case larger sedimentation and erosion quantities occur downstream of the bridge from cell 4 up to cell 6. The lower part experiences less erosion, viz., cells 1, 2, 3 and 12. Unlike **GRE04**, for **GRE05** the differences occur particularly during the dry season.

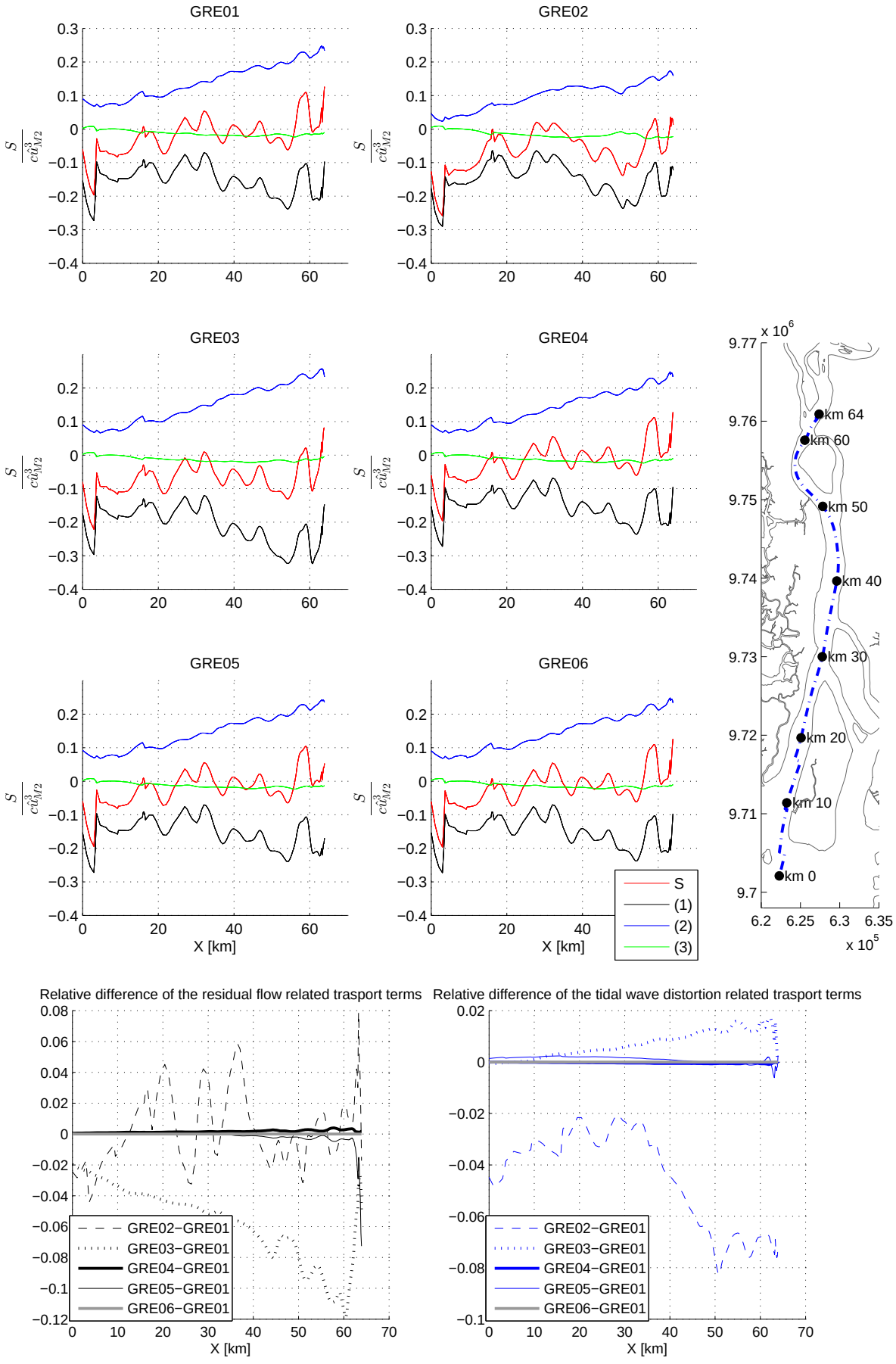

Figure 6.3: Normalized bed-load sediment transport profiles along the Guayas River estuary for the modelled case scenarios computed according to equation (2.13)

As explained before, the bridge has an impact on the tidal asymmetry related to the distortion of the tidal wave and the effect of a residual current. The former effect then becomes more prominent when the discharges are smaller.

- It is confirmed what was mentioned before that the sediment overload at the boundaries in scenario **GRE06** does not produce any significant changes.
- Cases **GRE02** and **GRE03** are the most influential. There is not only a change in the direction of the residual sediment transport in most of the estuary, but also significant changes in the sedimentation and erosion patterns occur.
- In case **GRE02**, the estuary changes from flood to ebb dominant in the middle and upper zones (cells 4 to 8), and the export of sediment is strengthed in the lower sections. The intertidal flats favor ebb dominance regardless of the season, hence during the dry period the upstream directed transport is severely reduced and during the wet period the sediment transport is even reversed in the downstream direction in almost the entire estuary. Regarding the volume changes, the inclusion of these areas leads to an increased erosion and decreased sedimentation almost in the entire estuary, i.e., eroding macro cells erode even more and accreting cells accrete less. Only for macro cells 3 and 6 the situation is reversed.
- The main effect of "El Niño" (**GRE03**) is to promote ebb dominance. During the dry season the upstream directed sediment transport is slightly reduced all over the estuary. The real effects are felt during the wet season when the flood dominant character of the estuary in the upper and middle part changes abruptly. The differences are even more obvious than the previous case. In particular, the contribution of the Daule River is significantly larger. Sedimentation is promoted particularly in the middle sections 3 and 4, and erosion in the upper part before the confluence of the Daule and Babahoyo Rivers.

6.4. REMARKS REGARDING THE SEDIMENTATION AROUND GUAYAQUIL

The sedimentation around Guayaquil has been a controversial topic due to the associated side effects previously discussed on section 1.2. Multiple hypotheses on what the causes are and possible measures to be undertaken have been discussed without really reaching a compelling consensus.

This research attempts to provide with such compelling argument. Indeed, from the previous results it can be seen that albeit sedimentation is the natural tendency of the estuary in this area, the interventions have definitely aggravated the situation. The sediment balance for the zone near Guayaquil, identified as macro cells 5, 6 and 9, confirms the latter statement.

Table 6.1: Sediment volume change inside macro cells 5, 6 and 9 (positive = sedimentation, negative = erosion)

Season	*Unit*	*GRE01*	*GRE02*	*GRE03*	*GRE04*	*GRE05*	*GRE06*
Dry	[m^3/6 months]	897	-8610	-8840	-447	3402	897
Wet	[m^3/6 months]	365	-5677	-13190	3723	1726	365
Yearly	[m^3/year]	1262	-14287	-22029	3276	5128	1262

Table 6.1 reveals that either recovering the intertidal areas or the effect of the river discharge would help mitigate the problem. Hence, any strategy for implementing a suitable solution should take these aspects into consideration. The following remarks can be made:

- From Table 6.1 the effect of the Daule-Peripa dam is even more evident, and also it can be identified that actually the problem worsens during the wet season. The regulation of the

Daule River leads to erosion during the dry season, but the reduced discharges during the wet period lead to a severe increase in sedimentation. In view of this, it is advised to carry out a further investigation towards determining how the operation of the dam could be managed especially during the wet season.

- Again, the intensive shrimp farming has caused the greatest impact on this area. The situation prior to the decimation of intertidal areas reveals that actually erosion was predominant. An assessment of the possibility of recovering some of these tidal flats as well as the mangrove forest could also lead to a suitable solution for the sedimentation problem around Guayaquil.
- Changes in the operation scheme of the Daule-Peripa dam and recovery of the intertidal areas might have adverse economical repercussions. These are related to the cost of hydropower generation, and the profits from aquaculture activities. Therefore the alternative of dredging must also be considered. From Figure 6.4 it can be seen that on a yearly basis the sedimentation problem affects particularly macro cell 6. Therefore, most of the dredging efforts should be focused around this area.

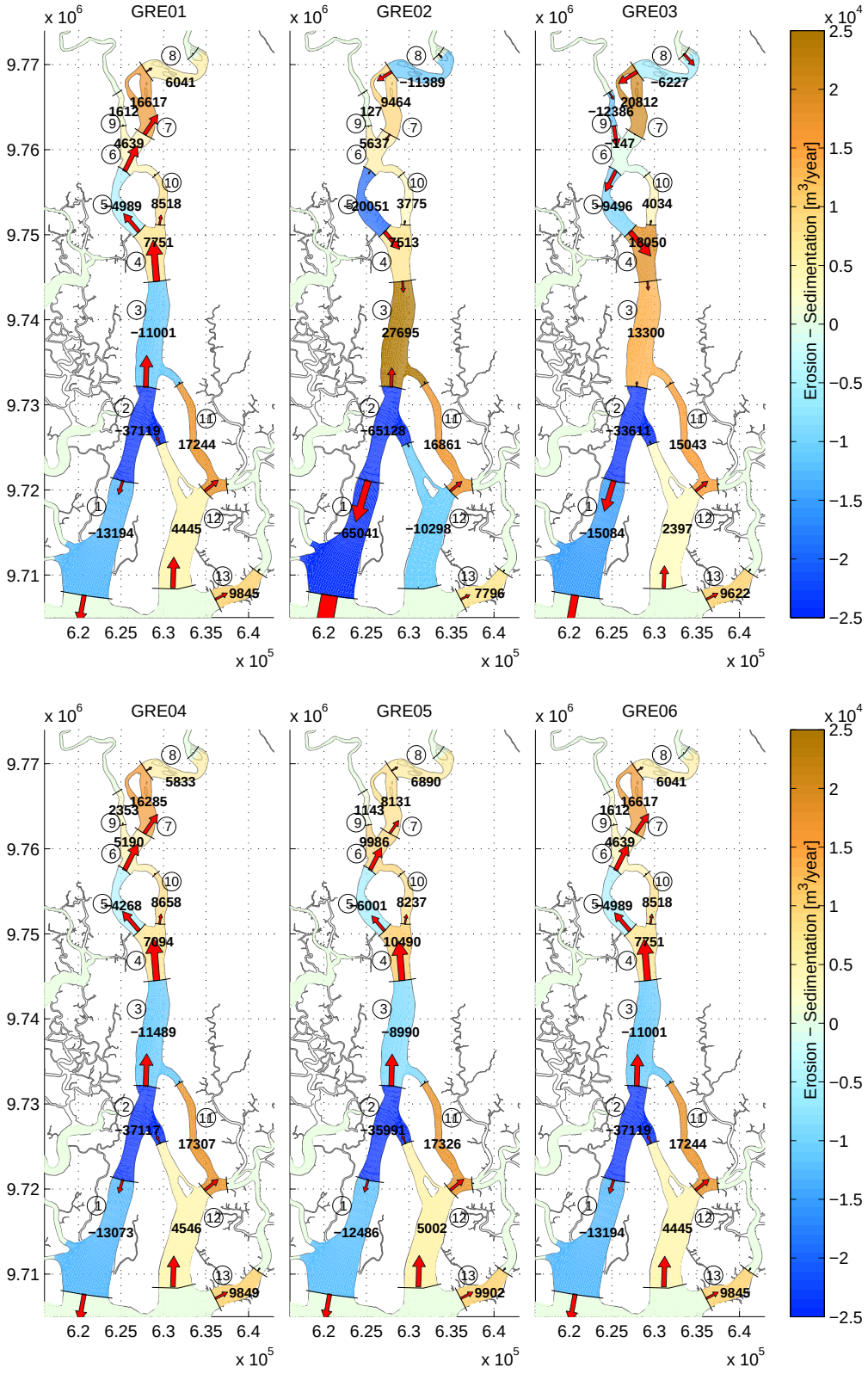

Figure 6.4: Yearly sediment balance for all case scenarios. Volume change inside macro cells (**bold**) and upstream or downstream sediment exchange across the cell boundaries (arrow sizes scaled according to exchange volumes between macro cells)

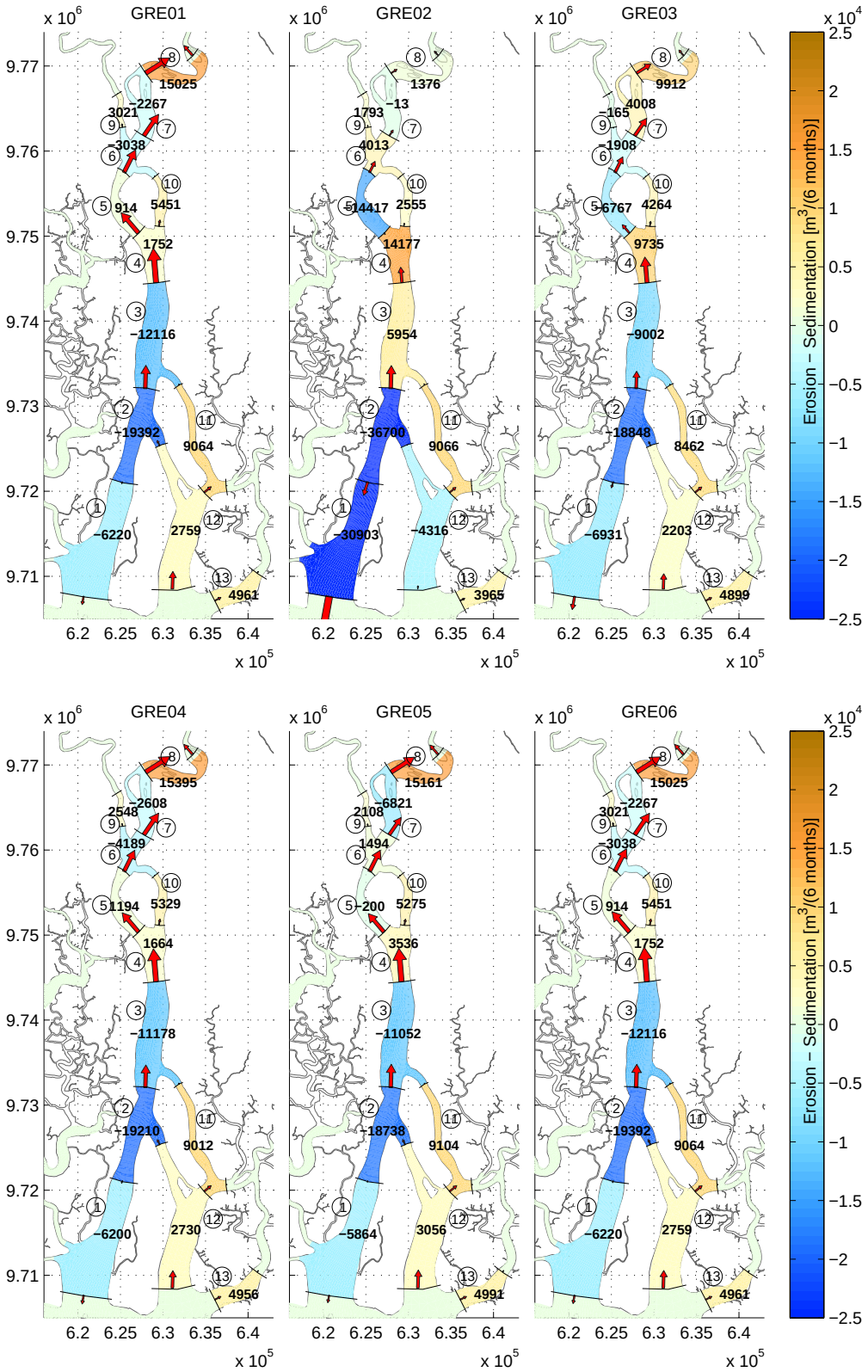

Figure 6.5: Sediment balance for all case scenarios during the dry season. Volume change inside macro cells (**bold**) and upstream or downstream sediment exchange across the cell boundaries (arrow sizes scaled according to exchange volumes between macro cells)

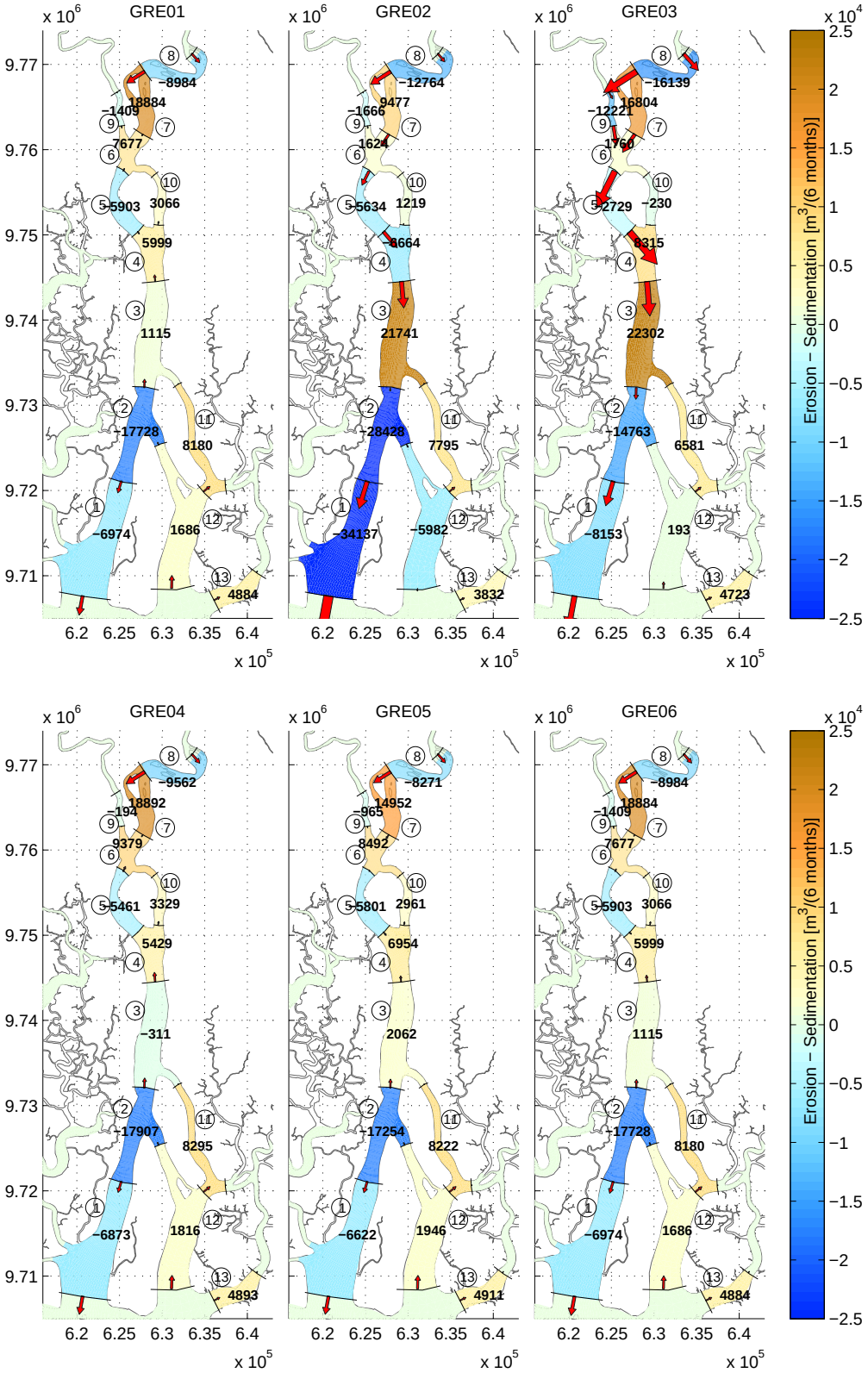

Figure 6.6: Sediment balance for all case scenarios during the wet season. Volume change inside macro cells (**bold**) and upstream or downstream sediment exchange across the cell boundaries (arrow sizes scaled according to exchange volumes between macro cells)

7

CONCLUSIONS & RECOMMENDATIONS

7.1. CONCLUSIONS

The morphological development of the Guayas River estuary in Ecuador and the processes behind its evolution have been studied with the implementation of a morphodynamic numerical model using the software Delft3D-FM. The estuary has not been subject to many studies related to morphology, and even though a thorough literature review has been carried out to gather all the relevant information, still some data are lacking, especially that related to bed topography. In that regard, a long term morphological simulation in the order of hundred of years has been done to derive the bed topography. This is the basis to set up the model for the different case scenarios considered that simulate natural events and anthropic interventions carried out within the estuary.

The central topic of this research is to understand the estuarine system from the hydrodynamic and morphology perspectives.

With respect to the former, it was shown that the tide is amplified as a result of the strong bank convergence. Relative to the estuary mouth(northern part of the Puna island), the amplitude is 1.22 times larger near the city of Guayaquil (about 60 km from the mouth). In addition, the tidal wave also develops a more standing wave character as it travels up the Gulf of Guayaquil. The phase lag of approximately 1 hour between HW and HWS remains fairly constant along the Guayas River estuary. Moreover, even though the estuary is tide dominated, the discharges of both the Babahoyo and Daule Rivers, play a significant role in the asymmetry of the horizontal tide in particular. Depending on the magnitude of the discharges the predominant flood dominant character of the estuary is either reduced or even shifted towards ebb dominance. This can be evidenced during the wet season, when the hydrographs peak, especially in the upper parts near the confluence of the rivers.

7.1.1. REGARDING THE MAIN RESEARCH QUESTIONS

To investigate the effects on the morphology, a total of 5 scenarios was defined. Each scenario addresses a certain intervention carried out during the last decades within the estuary or in its upper basin. Plus the effect of a natural phenomenon characteristic of the zone, "El Niño", is also taken into consideration. An additional reference scenario is also defined for comparison purposes, in which none of the aforementioned interventions are taken into account.

The different interventions are simulated by changing the model boundary conditions according to the following:

- Modifiying the river hydrographs
- Changing the shape of some parts of the estuary by including intertidal areas that have been decimated over the years due to aquaculture practices.

- Increasing the sediment load of the rivers.
- Constricting the width of the rivers near the confluence, which is attributed to the blockage caused by the foundations of a major bridge.

The analysis of the different scenarios sets the tone for answering the proposed research questions in section 1.4:

What are the sedimentation and erosion patterns due to fluvial and tidal processes?

The sedimentation and erosion patterns for all cases are presented in the figures of Appendix B. From the figures it can be observed that the upper zone of the estuary is the most morphologically active. In some instances major shifts in the patterns occur between the wet and dry season ,i.e., eroding areas during the wet season become accreting areas during the dry season and vice versa.

What is the relative impact on the sediment balance and the morphology of the estuary caused by the different interventions carried out in the Guayas River basin and the estuary itself and how sensitive is the system to them?

The effects on the sediment balance is a direct consequence of the changes in the residual sediment transport caused by the interventions, which in turn are related to the changes in the tidal asymmetry. The two sources of asymmetry that are directly linked to sediment transport stem from the influence of residual currents and the distortion of the tidal wave.

It was shown that changes in the river hydrographs affect principally the first source of asymmetry. This is easily appreciable particularly during the wet season when the discharges are larger.

The second source of asymmetry is significantly influenced when the shape of the estuary is modified. In that regard, the addition of the intertidal areas causes the most prominent effect on this source of asymmetry.

Finally the sediment overload at the river boundaries does not induce any changes on the sediment balance.

The sensitivity of the estuarine system to the different interventions is classified from the most to the least influential as follows:

1. **GRE02 Situation prior to shrimp farms construction and mangrove deforestation:** The additional intertidal areas (included in this scenario) decrease the flood dominant character of the tide during the dry season and promote ebb dominance during the wet period. On an annual basis, the most prominent change related to the reference case (i.e, after the construction of shrimp farms), is that sedimentation is promoted in the central part of the estuary (identified as macro cell 3).

2. **GRE03 The "El Niño" phenomenon:** The associated large river discharges during the wet season change the annual residual sediment transport direction in almost the entire estuary towards downstream. Sedimentation is also promoted in the middle section. In contrast to the previous case, where the influence is permanent, "El Niño" is an episodic event therefore it is deemed less influential.

3. **GRE05 The "Puente de la Unidad Nacional" bridge:** The influence is mild in comparison to the previous cases. The bridge affects mainly the tidal asymmetry related to the distortion of the wave. It enhances the transport in the upstream direction in most of the estuary especially during the dry season. This leads to more sedimentation in the section next to the city of Guayaquil right at the confluence of the rivers (identified as macro cell 6).

4. **GRE04 Daule-Peripa Dam:** The regulation effect of the dam on the Daule River discharge is such that it delivers more water during the dry season and less during the wet season compared to the situation before its construction. Therefore the upstream and downstream directed transports are enhanced during the wet and dry seasons respectively. Again, as a result the sedimentation is increased next to the city of Guayaquil on an annual basis.

5. **GRE06 Sediment overload due to erosion of the upstream basin:** This does not influence what so ever the tidal asymmetry, the residual sediment transport nor the sediment balance. Any possible effect would be perceived after decades.

Besides the identified causes of sedimentation by previous studies, is the estuary importing sediment from the adjacent coast?

The annual residual sediment transport figures presented in Appendix B show that even though in most of the estuary the direction is towards upstream, the downstream areas of the main branch (identified as macro cell 1) actually export sediment to the adjacent coast regardless of the scenario. The magnitude of the sediment export is the only thing that differs from scenario to scenario. In that regard, the addition of the intertidal areas also induces the greatest impact, causing the export quantities to significantly increase.

What are the possible measures to be taken in order to control the sedimentation in the Guayas River, especially around the city of Guayaquil?

The sedimentation problem around Guayaquil is also related to the tidal asymmetry. The mitigation measures to be undertaken must be directed towards increasing the effect of the residual currents and minimizing the effect of the distortion of the wave. In that regard, three alternatives are proposed by the author (or a combination of them) as potential mitigating measures. The first is to manage the operation of the Daule-Peripa dam in a fashion that more water is delivered especially during the wet season. The second is to reforest and recover some the intertidal flats that have been decimated by the aquaculture practices. The third is to dredge the area of the estuary close to Guayaquil.

The final solution requires a more detailed study. However, it will involve a compromise between the cost of dredging and the decreased profit from hydro power generation and aquaculture. Further research must be done to define and evaluate the extent, viability, socio-economic and environmental impacts related to each of them.

7.1.2. REGARDING THE SECONDARY RESEARCH QUESTION

Appendix C addresses the secondary objective regarding the testing and diagnosing of problems with the implementation of the Delft3D FM morphology module. Hence the related research question can now be answered:

Is Delft3D-FM able to reproduce similar results for sediment transport and morphology as the previous structured grid version of Delft3D, in relation to the effects caused by spiral flow and sediment transport over fixed-layers?

Yes, the identification and diagnosis of problems related to this particular features helped the Deltares developer team to implement suitable solutions. The proof that similar results, as those obtained with Delf3D, are reproduced by Delft3D-FM is disclosed in the test bench cases of Appendix C.

7.2. RECOMMENDATIONS

In this section some recommendations are given regarding future research on the topic. The goal is to point out shortcomings, simplifications and assumptions that were done throughout this research. Besides, suggestions on what is it that needs to be done and how are also provided in order to overcome these issues.

- In chapter 3 it was concluded that the estuary is well mixed, the effects of density were then assumed to be of minor importance and were not taken into account for the Delft3D-FM model. In reality, the longitudinal density gradient in well mixed estuaries also drives a secondary flow referred as gravitational circulation (which is explained in subsection 2.1.3). The resulting residual upstream directed near bottom current continuously transports marine sediment into the estuary. Besides, the process of floculation of fine sediment, which is transported as wash load, as soon as it gets in contact with saline water is also not taken into account in the current model. As pointed out by Savenije (2006), the action of both processes would lead to mud or sand bar formation at the limit of the salt intrusion. This effects related to density differences could be further analyzed for instance with the aid of a 3D computation, however by the time of this research the 3D version of Delft3D-FM was not yet available.

- In absence of measured data, the results and the consequent analysis were derived based on an initial bed topography which was obtained through a long-term morphological simulation. This approach is justified since hydrodynamics and morphology are coupled in the sense that hydrodynamic forcing produces sediment transport. Morphological features then emerge and evolve due to spatial sediment transport gradients. These features in turn influence hydrodynamic processes and the feedback loop starts again until equilibrium is reached. Even though the so derived initial topography seem to correlate with observed patterns from satellite images, it is an approximation that still remains to be validated with bathymetric survey data. In that regard, the Brier Skill Score (BSS described in subsection 5.4.1) provides a good objective criterion for evaluation. Moreover, in order to calibrate the sediment transport predictors, it is advised to follow the evolution of an excavated trench at some cross sections along the estuary.

- To assess the effects and importance of the interventions, an individual scenario was defined for each one of them. However, the combined effect remains yet to be studied as well. For this, a scenario could be defined in which the timing and duration of each of the interventions would also play an important role. In this manner, the morphological evolution up until the current state could be more accurately reproduced, which would give a sound basis to predict and assess the effect of future developments.

- The effects of El Niño were only taken into account by modifying the respective hydrographs of the Daule and Babahoyo Rivers. The effects on the sea level response were largely disregarded.

  El Niño is the central Pacific ocean response to the atmospheric forcing. Preceding its occurrence strong southeast trade winds lead to the accumulation of warm water in the western Pacific. As soon as the wind strength decreases water flows back. The consequent rapid drop of the sea level in the west leads to a peak in the sea level in the east. Wyrtki (1977) studies the sea level response associated to the 1972 El Niño event. He shows the stricking effects on the sea level at the Galápagos Islands (approximately 1100 km west of the continental Ecuadorian territory). The mean sea level increases 20 cm above the long-term value around December. According to Wyrtki (1975) the same patterns are to be expected for the continental coastal areas of Ecuador.

Intuitively, a sea level rise would mean an increase of the tidal prism and a decrease of the intertidal areas which is translated into a reduction of friction and hence a contribution to flood dominance. However, the complete picture about the impacts of mean sea level rise on the estuary morphology remain yet to be studied. This could be achieved by defining additional tidal components as boundary conditions at the seaward side.

- Due to the subgrid dimensions of the 'Puente de la Unidad Nacional' bridge piers, they were represented as thin dams (thin objects that prohibit flow exchange between adjacent grid cells). This schematization largely simplifies the shape of the foundations and the drag forces acting on them. A closer representation of the piers can be achieved by locally refining the grid and defining dry cell instead at the location of the piers.

BIBLIOGRAPHY

Arias-Hidalgo, M., Villa-Cox, G., Griensven, A., Solórzano, G., Villa-Cox, R., Mynett, A., and Debels, P. (2013). A decision framework for wetland management in a river basin context: The "Abras de Mantequilla" case study in the Guayas River Basin, Ecuador. *Environmental Science & Policy*, 34:103 – 114. Management of wetlands in river basins: the {WETwin} project.

Armijos, M. M. and Montolío, T. S. (2008). Ecosistema Guayas (Ecuador), Medio ambiente y Sostenibilidad. *Revista Tecnológica-ESPOL*, 21(1).

Arriaga, L. (1989). The Daule-Peripa dam project, urban development of Guayaquil and their impact on shrimp mariculture. *Coastal Resources Center, University of Rhode Island, Narragansett, RI, USA*, 17.

Benites, S. (1975). Morfología y sedimentos de la Plataforma Continental del Golfo de Guayaquil. *Tesis ESPOL. Guayaquil, Ecuador*, 112.

Bolle, A., Wang, Z. B., Amos, C., and De Ronde, J. (2010). The influence of changes in tidal asymmetry on residual sediment transport in the Western Scheldt. *Continental Shelf Research*, 30(8):871–882.

Bosboom, J. and Stive, M. J. (2012). *Coastal Dynamics I: Lectures Notes CIE4305*. VSSD, Delft.

Briére, C., Giardino, A., and Winterwerp, H. (2011). Analyse de la morphologie du chenal de Nantes et etude de sa restauracion. Technical report, Deltares.

CAMAE (2013). Problemas que afectan la Navegabilidad en el Río Guayas. *Informar*.

CELEC (2013). Revista 25 Años de la presa Daule - Peripa. Technical report, CELEC EP-HIDRONACIÓN.

Changuán, P. S. (2010). Estudios y Diseños del Muelle de Servicio Isla Santay. Technical report, Ministerio del Ambiente del Ecuador.

Cucalón, E. (1989). Oceanographic characteristics off the coast of Ecuador. *A sustainable shrimp mariculture industry for Ecuador, pp. University of Rhode Island, Narragansett, RI: Coastal Resources Center*.

Deltares (2015a). Delft3D Flexible Mesh user manual.

Deltares (2015b). Validation Document Delft3D-Flexible Mesh. *Version*.

Dumont, J., Santana, E., Soledispa, B., and King, A. (2007). El Islote El Palmar, resultado de una evolución a largo plazo de la distribución del drenaje entre los Ríos Daule y Babahoyo en la Cuenca del Guayas. *Acta Oceanográfica del Pacífico*.

GEBCO (2015). Gridded bathymetry data. [`http://www.gebco.net/data_and_products/gridded_bathymetry_data/`; accessed 15-September-2015].

Gobierno Autónomo Descentralizado Provincial del Guayas (2013). Plan de desarrolo de la Provincia del Guayas. Technical report, GADPG, Guayaquil.

Hasselaar, R., de Boer, W., Luijendijk, A., et al. (2013). Optimizing harbour maintenance strategies using Delft3D and D-flow flexible mesh. In *Coasts and Ports 2013: 21st Australasian Coastal and Ocean Engineering Conference and the 14th Australasian Port and Harbour Conference*, page 364. Engineers Australia.

Holthuijsen, L. H. (2010). *Waves in oceanic and coastal waters*. Cambridge University Press.

IGM (2015). Cartografía de libre acceso. [`http://www.geoportaligm.gob.ec/portal/index.php/descargas/cartografia-de-libre-acceso/`; accessed 01-September-2015].

INAMHI (Instituto Nacional de Meteorología e Hidrología, E. Anuarios hidrológicos 1984-2012.

Jaillard, E. (1993). La sedimentación en los deltas, los estuarios y las cuencas deltaicas.

Kalkwijk, J. P. T. and Booij, R. (1986). Adaptation of secondary flow in nearly-horizontal flow. *Journal of Hydraulic Research*, 24(1):19–37.

Kernkamp, H. W., Van Dam, A., Stelling, G. S., and de Goede, E. D. (2011). Efficient scheme for the shallow water equations on unstructured grids with application to the continental shelf. *Ocean Dynamics*, 61(8):1175–1188.

Kramer, S. C. and Stelling, G. S. (2008). A conservative unstructured scheme for rapidly varied flows. *International journal for numerical methods in fluids*, 58(2):183–212.

Laraque, A., Cerón, C., Magat, P., and Pombosa, R. (2002). Informe del primer estudio del impacto de la marea sobre el estuario del Río Guayas. Technical report, INOCAR-INAMHI.

Latteux, B. (1995). Techniques for long-term morphological simulation under tidal action. *Marine Geology*, 126(1):129–141.

Lesser, G. R. (2009). *An approach to medium-term coastal morphological modelling*. UNESCO-IHE, Institute for Water Education.

Liu, H., Chang, F. F., and Skinner, M. M. (1961). *Effect of bridge constriction on scour and backwater*. Civil Engineering Section, Colorado State University.

Mosselman, E. (2005). Basic equations for sediment transport in CFD for fluvial morphodynamics. *Computational fluid dynamics: applications in environmental hydraulics*, pages 71–89.

Mosselman, E. and Le, T. B. (2016). Five common mistakes in fluvial morphodynamic modeling. *Advances in Water Resources*.

Murray, S. P., Conlon, D., Siripong, A., and Santoro, J. (1976). *Circulation and salinity distribution in the Rio Guayas estuary, Ecuador*. Coastal Studies Institute, Center for Wetland Resources, Louisiana State Univ.

Nabi, M., Ottevanger, W., and Giri, S. (2016). Computational modelling of secondary flow on unstructed grids. *Unpublished*.

Nash, J. E. and Sutcliffe, J. V. (1970). River flow forecasting through conceptual models part i—a discussion of principles. *Journal of hydrology*, 10(3):282–290.

Pawlowicz, R., Beardsley, B., and Lentz, S. (2002). Classical tidal harmonic analysis including error estimates in MATLAB using T_TIDE. *Computers & Geosciences*, 28(8):929–937.

Riebeek, H. (1985). El Niño, la Niña, and Rainfall.

Savenije, H. H. (2006). *Salinity and tides in alluvial estuaries*. Elsevier.

Soledispa, B. (2002). Estudio de los sedimentos del sector donde convergen los ríos Daule y Babahoyo, y las posibles causas que están formando un nuevo islote en ese sector.

Struiksma, N. (1999). Mathematical modelling of bedload transport over non-erodible layers. In *Proceedings IAHR Symp. River Coastal and Estuarine Morphodynamics, Genova*, volume 1, pages 89–98.

Sutherland, J., Peet, A., and Soulsby, R. (2004). Evaluating the performance of morphological models. *Coastal engineering*, 51(8):917–939.

Twilley, R., Cárdenas, W., Rivera-Monroy, V., Espinoza, J., Suescum, R., Armijos, M., and Solórzano, L. (2000). 17 The Gulf of Guayaquil and the Guayas River Estuary, Ecuador. *Coastal Marine Ecosystems of Latin America*, 144:245.

Twilley, R. R. (1989). Impacts of Shrimp Mariculture Practices on the Ecology of Coastal Ecosystems in Ecuador. *Establishing a Sustainable Shrimp Mariculture Industry in Ecuador*, page 91.

Twilley, R. R., Montaño, M., Valdivieso, J. M., and Bodero, A. (1999). The environmental quality of coastal ecosystems in Ecuador: implications for the development of integrated mangrove and shrimp pond management. *Mangrove Ecosystems in Tropical America. IUCN/NOAA/Instituto de Ecologia, Xalapa, Mexico*, pages 199–230.

Van de Kreeke, J. and Robaczewska, K. (1993). Tide-induced residual transport of coarse sediment; application to the Ems estuary. *Netherlands Journal of Sea Research*, 31(3):209–220.

Van der Wegen, M. and Roelvink, J. (2012). Reproduction of estuarine bathymetry by means of a process-based model: Western Scheldt case study, the Netherlands. *Geomorphology*, 179:152–167.

Van der Wegen, M., Wang, Z. B., Savenije, H., and Roelvink, J. (2008). Long-term morphodynamic evolution and energy dissipation in a coastal plain, tidal embayment. *Journal of Geophysical Research: Earth Surface (2003–2012)*, 113(F3).

Van Rijn, L., Walstra, D., Grasmeijer, B., Sutherland, J., Pan, S., and Sierra, J. (2003). The predictability of cross-shore bed evolution of sandy beaches at the time scale of storms and seasons using process-based profile models. *Coastal Engineering*, 47(3):295–327.

Van Rijn, L. C. (1990). *Principles of fluid flow and surface waves in rivers, estuaries, seas and oceans*, volume 11. Aqua Publications Amsterdam, The Netherlands.

Van Rijn, L. C. (1993). *Principles of sediment transport in rivers, estuaries and coastal seas*, volume 1006. Aqua publications Amsterdam.

Wang, Z. B., Jeuken, C., and De Vriend, H. (1999). Tidal asymmetry and residual sediment transport in estuaries: a literature study and application to the Western Scheldt. Technical report, Deltares (WL).

Wyrtki, K. (1975). El Niño-the dynamic response of the equatorial Pacific oceanto atmospheric forcing. *Journal of Physical Oceanography*, 5(4):572–584.

Wyrtki, K. (1977). Sea level during the 1972 El Niño. *Journal of Physical Oceanography*, 7(6):779–787.

A

SUMMARY OF THE GATHERED INFORMATION

Most of the information needed to realize the present work has been the result of a thorough literature review of studies on the area, most of which were realized decades ago. The compiled information includes data generated by independent sources and mainly data available by the Ecuadorian governmental entities. A summary of all the sources and data is disclosed in the following sections as well as a suggestion of what is still needed to further improve the implementation of the Delft3D-FM model.

A.1. MODEL OUTLINE AND CLOSED BOUNDARIES

A.1.1. LAND BOUNDARIES

The outline of land boundaries of the Gulf of Guayaquil and the principal channels of the Guayas, Daule and Babahoyo Rivers were obtained from the Ecuadorian Geographic Institute of the Navy (IGM, 2015) by merging 1:50000, 1:100000 and 1:250000 cartographic charts available in standard shape file format. Still lacking is the information about the extent of the tidal flats, historic development of shrimp farms and the reclamation of the mangrove forest along the Guayas River.

A.1.2. BED TOPOGRAPHY

The General Bathymetric Chart of the Oceans (GEBCO, 2015), provides bathymetric information as samples points in a 30 arc-second resolution grid. This is sufficient for the outer part of the Gulf of Guayaquil, nevertheless for the area of interest, i.e., the Guayas River estuary, such a resolution is too coarse. For this part then the bed topography is obtained by performing a long term mophological simulation starting from a flat bed. Although the so derived bed topography seems to visually correlate with observed patterns identified in satellite images, it is sill a mere approximation of reality. In order to validate or improve this, at least cross sectional profiles must be measured in a 5 to 10 km interval in the most downstream part of the Guayas River and in a 1 to 2 km interval in the more upstream part up to the confluence of the Daule and Babahoyo rivers, which is the most morphologically active zone. Ideally, multibeam echosounder recordings would be the best option. Along the Daule and Babahoyo Rivers, due to the model grid resolution, detailed information is not required. A profile along the axis of each river will suffice. These profiles should go from the city of Guayaquil up to the city of Babahoyo (approximately 50 km) in the Babahoyo River, and from Guayaquil to La Capilla gauging station in the Daule River (approximately 75 km). Attention must be paid to the datum used for the measured data (i.e., LAT (Lowest Astronomical Tide), MSL (Mean Sea Level), MLWS (Mean Low Water Spring), etc.), particularly when coupling the information from various sources. Throughout this study all elevations are referenced to MSL.

In addition to the deliniation of intertidal areas, their topography is also of interest in order to expand the model domain.

A.2. OPEN BOUNDARY CONDITIONS

The model domain and locations of tidal and discharge gauging stations are shown in Figure 4.3. The Guayas River estuary is enclosed in the orange box.

A.2.1. WATER LEVELS AND CURRENTS

There are 5 tidal gauging stations scattered around the Gulf that are supported by the International Hydrographic Organization (IHO): Libertad, Posorja, Puerto Bolivar, Puerto Maritimo and Guayaquil. The information is retrieved in the form of tidal constituents for each station. This is used mainly for calibration and validation purposes. Out of the 5 stations, Libertad is the one that is closest to the seaward model boundary. At the beginning, it was tempting to use the information from this station as the boundary condition. However due to the extent of the seaward boundary(that spans over 200 km), which is in the same order of magnitude as the length of the tidal wave, a single station is not representative for the entire boundary. Hence a space varying boundary condition was derived form the global model of ocean tides TPXO 7.2.

The Ecuadorian Oceanographic Institute of the Navy (INOCAR) holds and maintains the same 5 stations plus 3 additional ones: Anconcito, Data Posorja and Puna. The data are available on its website as time series plots, however only for visualization. If retrievable, these data could be further harmonically analyzed to determine the tidal constituents or simply used as a raw time series for further calibration and validation of the model. A record length of at least six months is necessary to achieve a reliable tidal analysis and properly resolve the tidal components.

No information of tidal currents is available. Murray et al. (1976) through a field measuring campaign in October and November, 1970, determined the velocity field throughout the Gulf. The results are presented in a very simple schematized way. At particular locations, they also present some information about the tide propagation such as HW-HWS phase lags and tidal phase velocities, but also in no great detail.

A.2.2. RIVER DISCHARGE

The location of the river boundaries is chosen at the limit of the tidal signature in both rivers. This is intended to avoid reflection of the wave at the boundaries.

The river discharge data are obtained from the hydrological yearbooks published between 1984 and 2012 by the Ecuadorian National Institute of Meteorology and Hydrology (INAMHI). The discharges are given as monthly averaged values. In case of the Babahoyo River, there is not a unique gauging station from which the information can be derived. Instead the existent gauges are located at the 4 main tributaries (H345, H348, H371, H390). These tributaries connect at different points along the Babahoyo, however for practical reasons only the total contribution is considered as the prescribed discharge. In case of the Daule River the information is directly obtained from a single gauge (H365) which is located exactly at the model boundary.

The information is not continuous, indeed, for some years several months exist with missing data. Moreover some of the gauging stations lack more information than others. Therefore a prior revision of these data is important. If possible a direct request to the source, either INOCAR or INAMHI is advised to obtain more reliable information.

A.3. SALINITY

Twilley et al. (2000) deem the Guayas River estuary as partially mixed, nevertheless a more recent study by Laraque et al. (2002) proves that the estuary is actually well mixed. During the study a measurement campaign was conducted at the beginning of May 2002, which can be considered as the peak of the wet season, when the estuary is more prone to stratification. Salinity profiles are determined at the confluence of the Daule and Babahoyo Rivers over the period of a tidal cycle. The profiles show a slight variation in the salinity in the first couple of metres of the water column below which the profiles remain constant. As a result for this study the estuary was assumed as fully mixed in its entire length and the effects of density differences were discarded. To validate this assumption salinity profiles further downstream are needed.

A.4. SEDIMENT CHARACTERISTICS AND MORPHOLOGY

Based on the sediment distribution presented by Benites (1975), which roughly maps a mean sediment grain size between 0.20 and 0.40 mm along the estuary, the sediment size for the model was assumed as a unique value of 0.30 mm. This is a large simplification, in reality it is very likely that multiple sediment fractions and muddy areas are encountered. This could also be further addressed by analysis of soil samples at different parts along the estuary. Besides, suspended sediment concentrations are also of interest to if the scope of model is to be extended to analyze the influence of fine sediment. For example, how does the wash load impact the development of shallow areas like tidal flats.

Additionally, of utmost importance for the morphological development is also the identification of zones of non-erodible layers, like peat layers, stiff clay and rock. These areas can be included in the model by adjusting the sediment availability per grid cell. According to Van der Wegen and Roelvink (2012), the location of non-erodible substrates largely impacts the development of morphological patterns.

A.5. HISTORICAL DATA

Historical data are important to infer morphological trends. Perhaps the most relevant are those related to bed level changes. A sequence of maps gives a good impression of the long-term morphological development. Historic maps can be obtained from the appointed Ecuadorian entity INOCAR or relevant nautical charts. As an example. Dumont et al. (2007) on his study about the "El Palmar islet" located at the confluence of the Daule and Babahoyo rivers, describes the evolution of the islet based the bathymetric surveys carried by INOCAR from 1982 to 2001.

B

RESULTS

B.1. GRE01

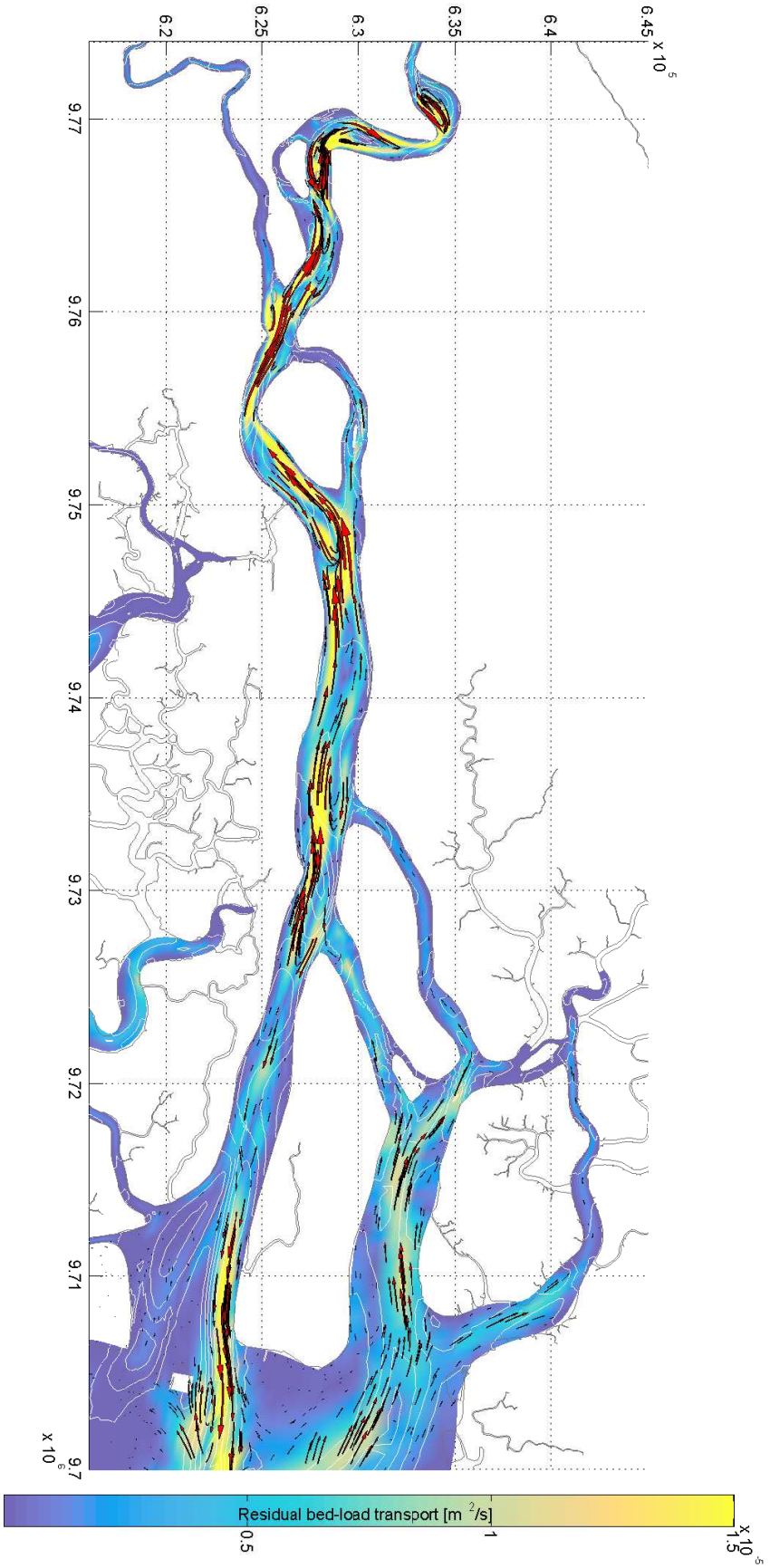

Figure B.1: GRE01. Magnitude and direction of the annual residual sediment transport

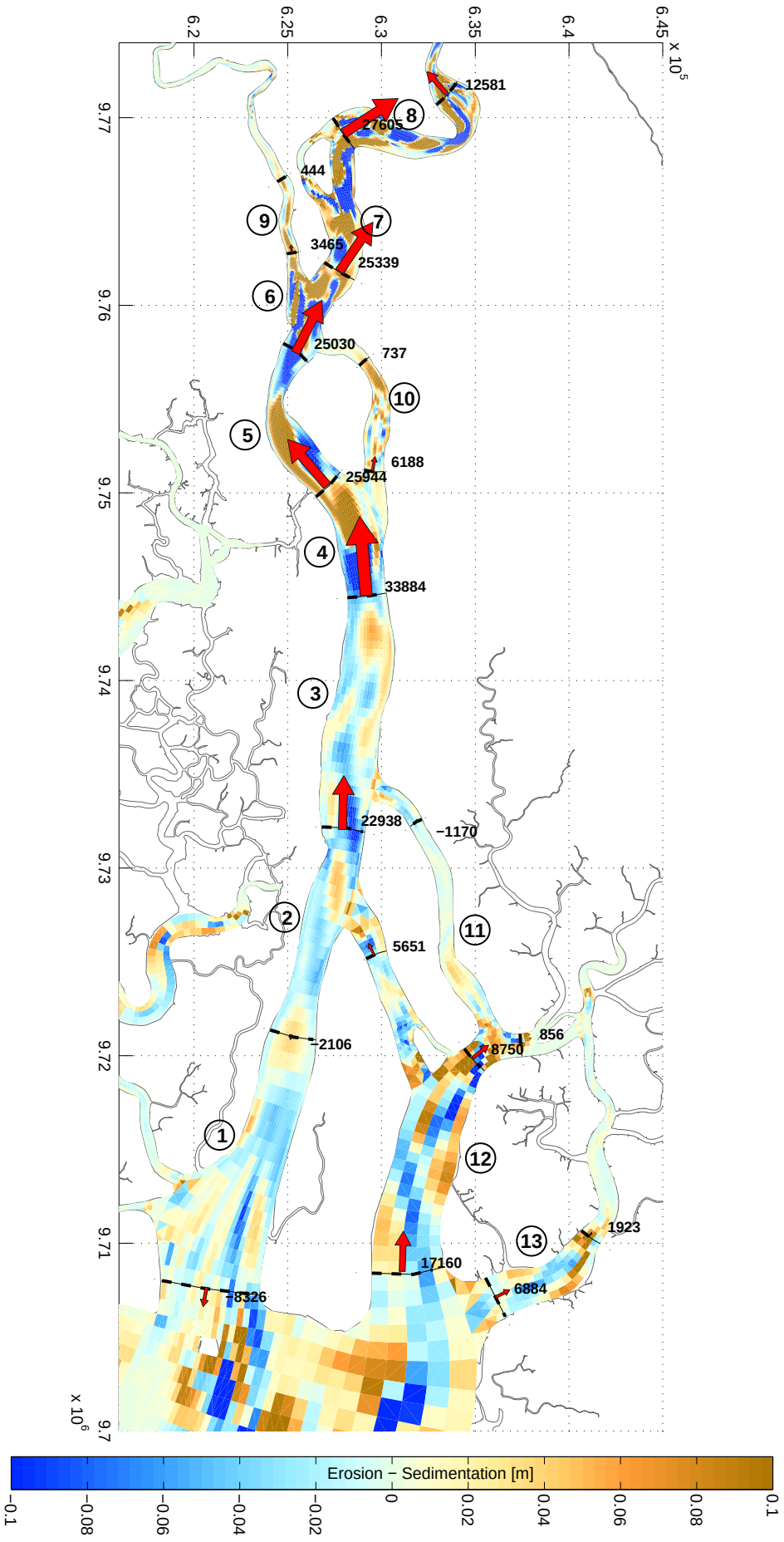

Figure B.2: GRE01. Sedimentation and erosion patterns, and volume exchange of sediment between macro cells during the **dry** season

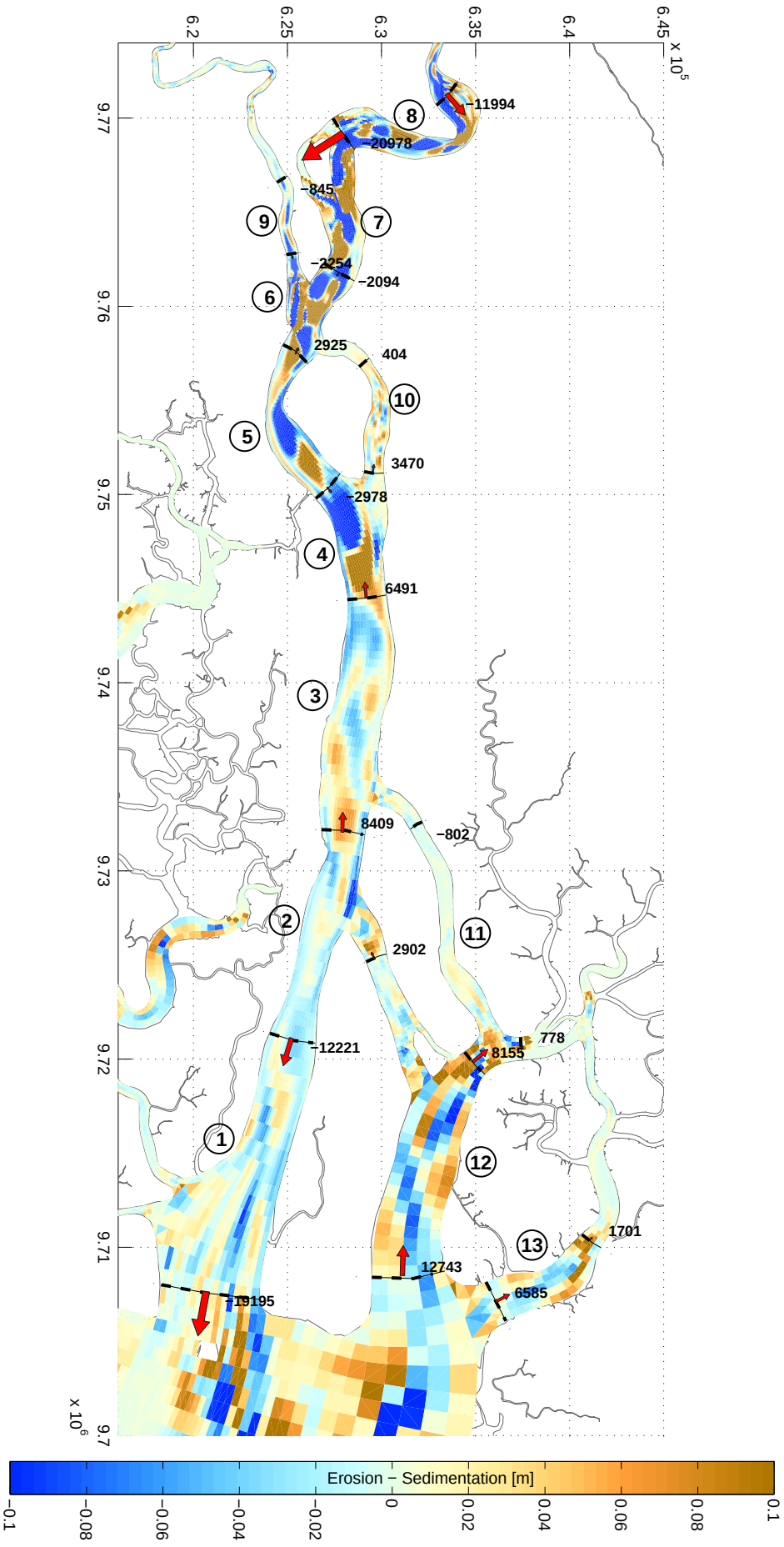

Figure B.3: GRE01. Sedimentation and erosion patterns, and volume exchange of sediment between macro cells during the **wet** season

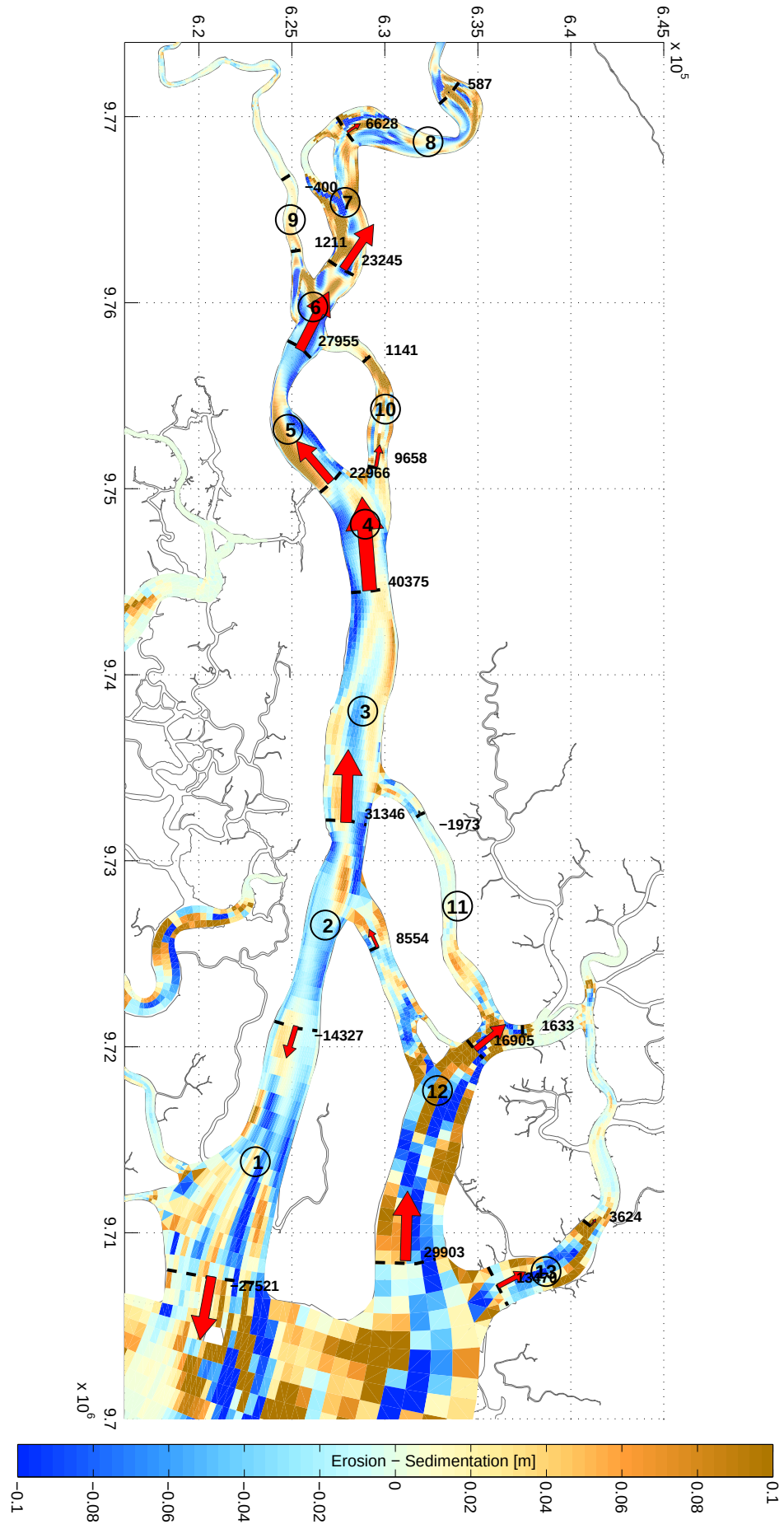

Figure B.4: GRE01. Sedimentation and erosion patterns, and volume exchange of sediment between macro cells in a **yearly** basis

B.2. GRE02

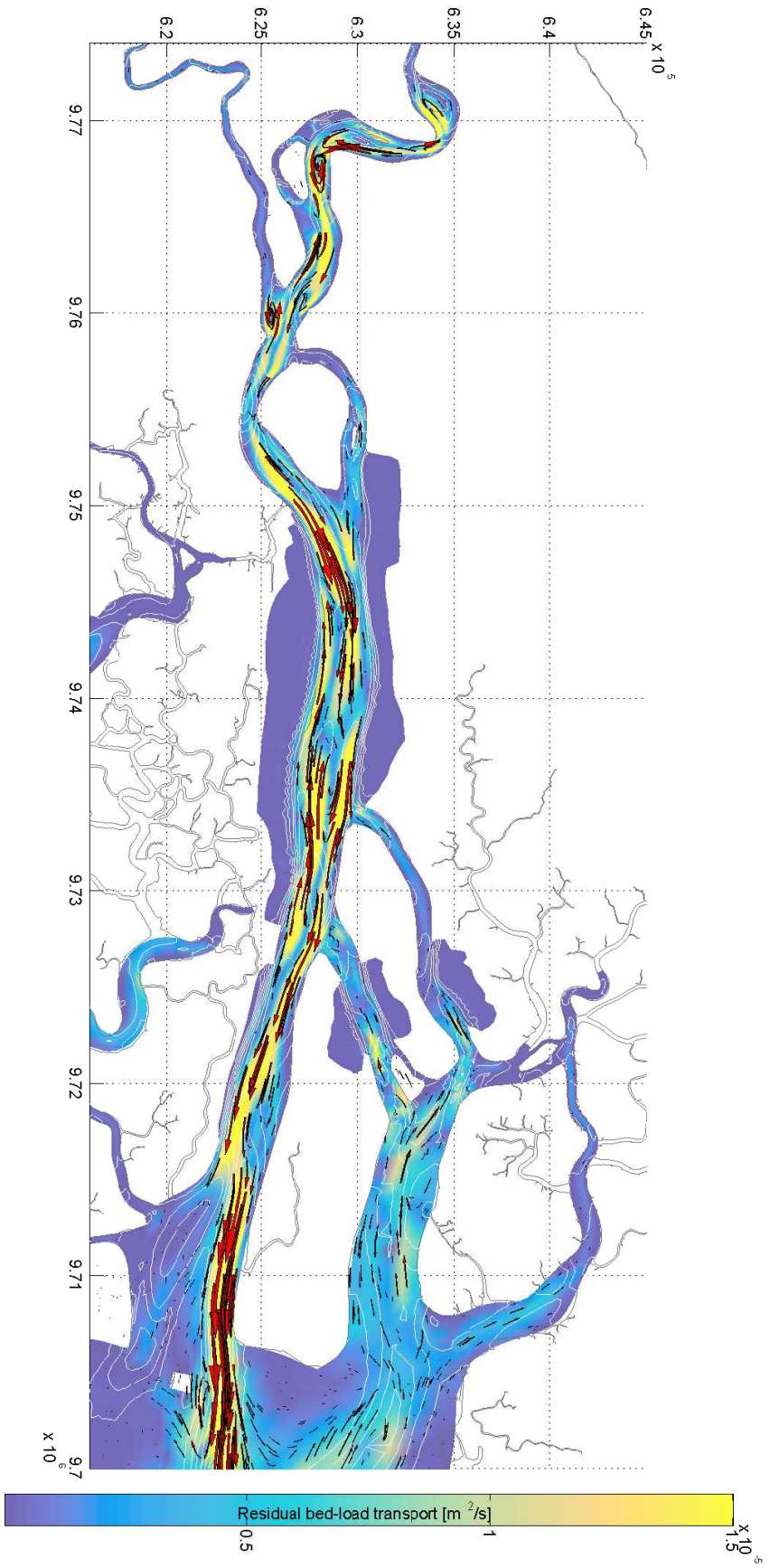

Figure B.5: GRE02. Magnitude and direction of the annual residual sediment transport

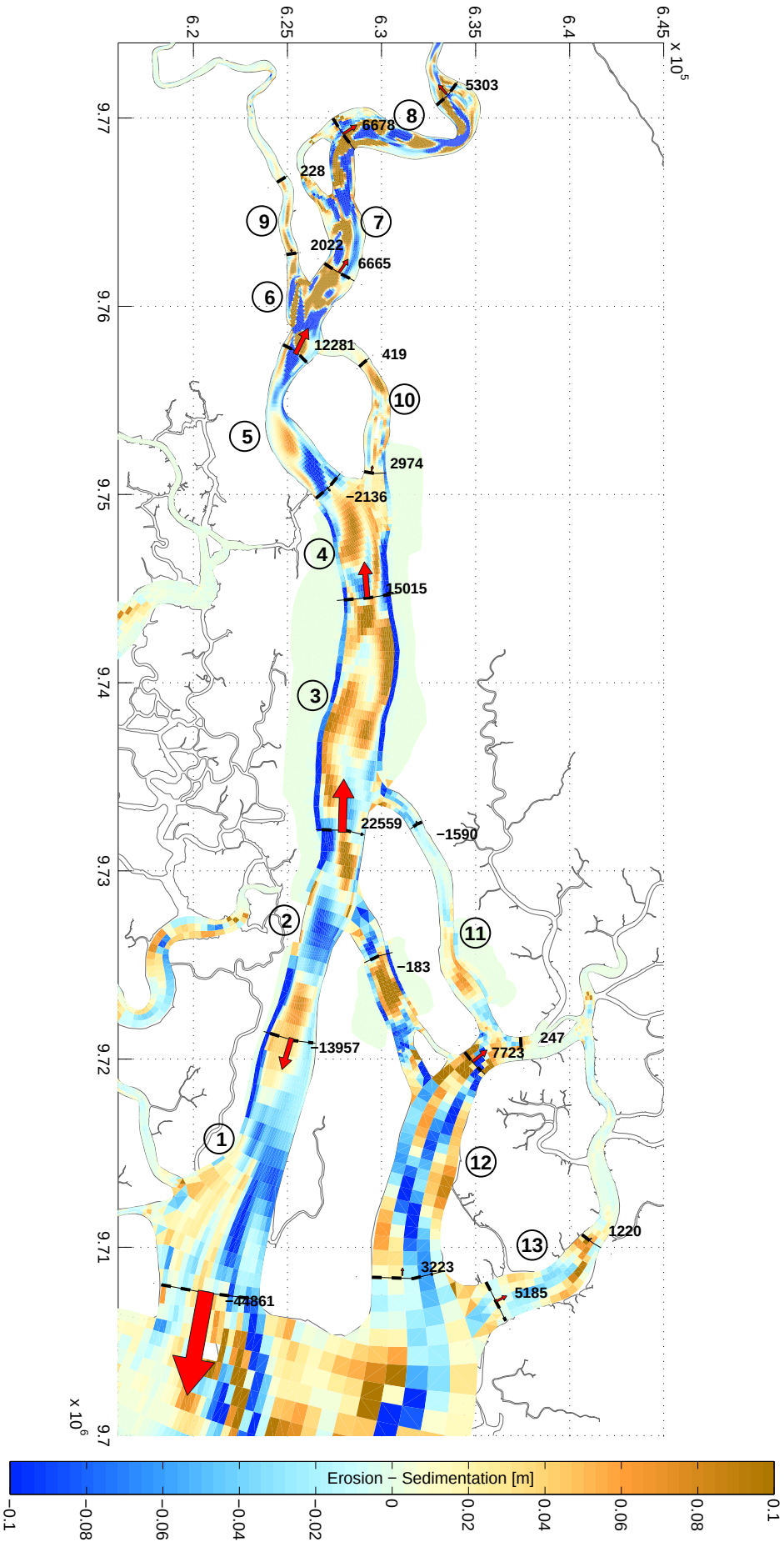

Figure B.6: GRE02. Sedimentation and erosion patterns, and volume exchange of sediment between macro cells during the **dry** season

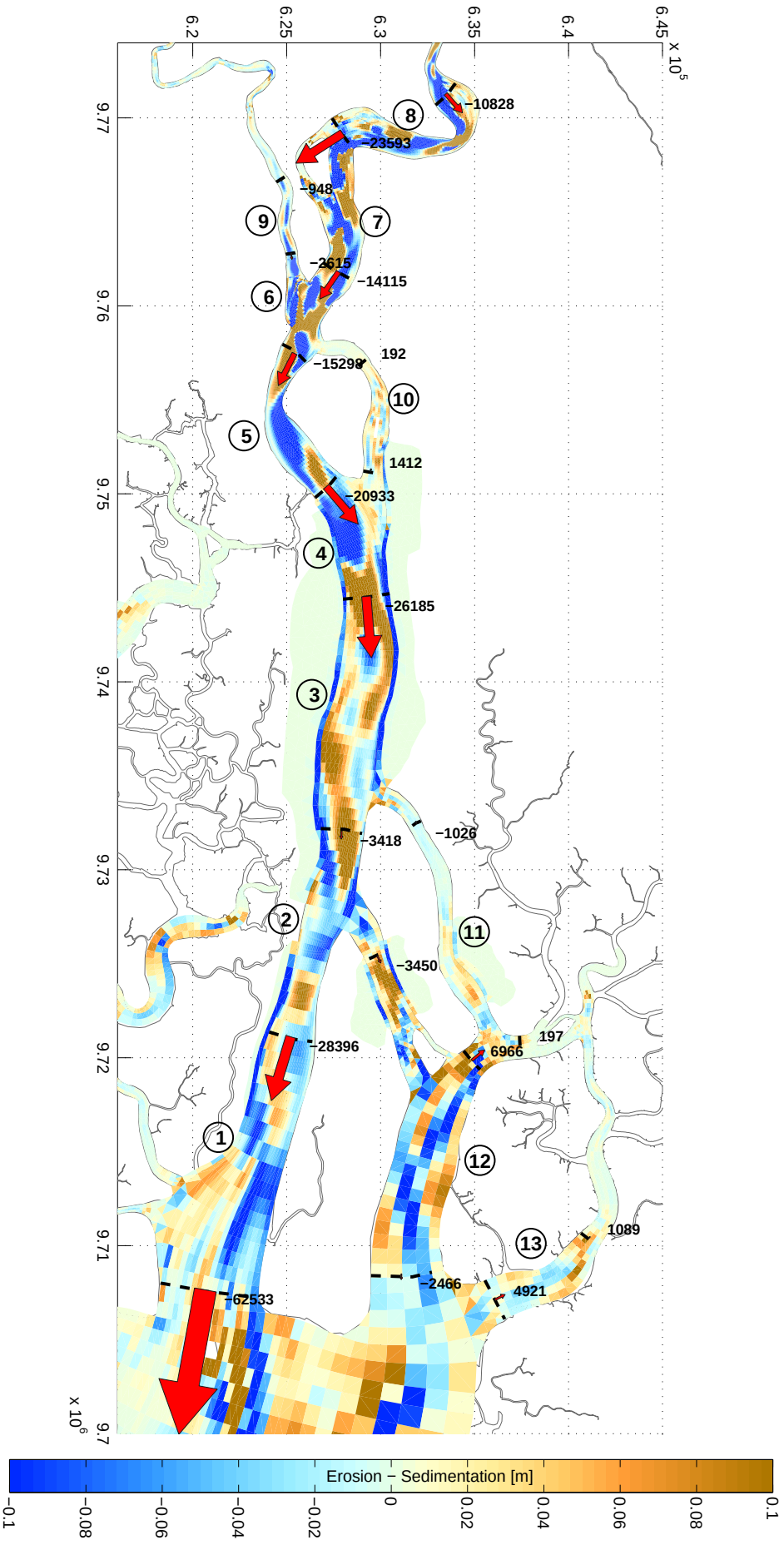

Figure B.7: GRE02. Sedimentation and erosion patterns, and volume exchange of sediment between macro cells during the **wet** season

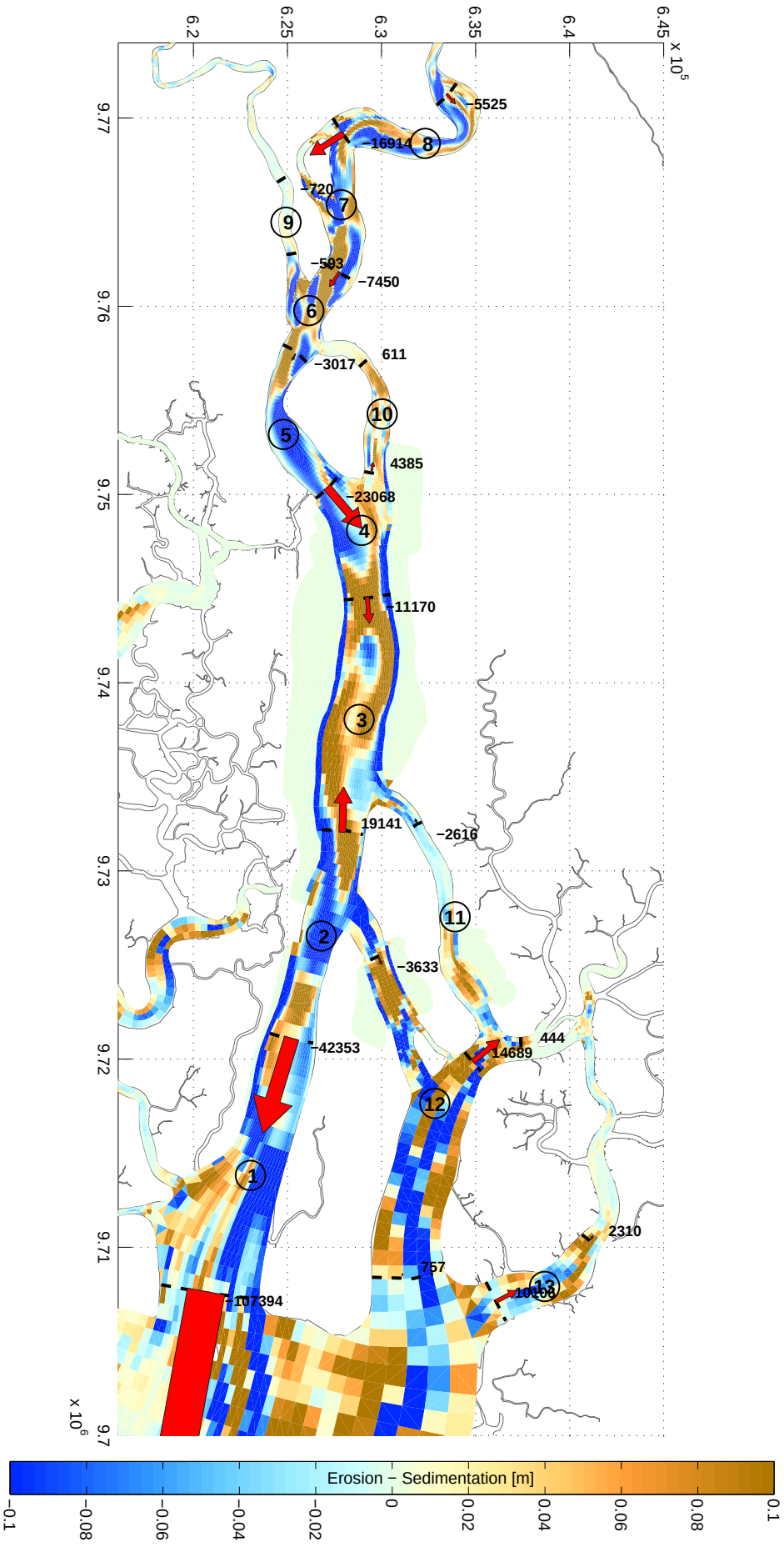

Figure B.8: GRE02. Sedimentation and erosion patterns, and volume exchange of sediment between macro cells in a **yearly** basis

B.3. GRE03

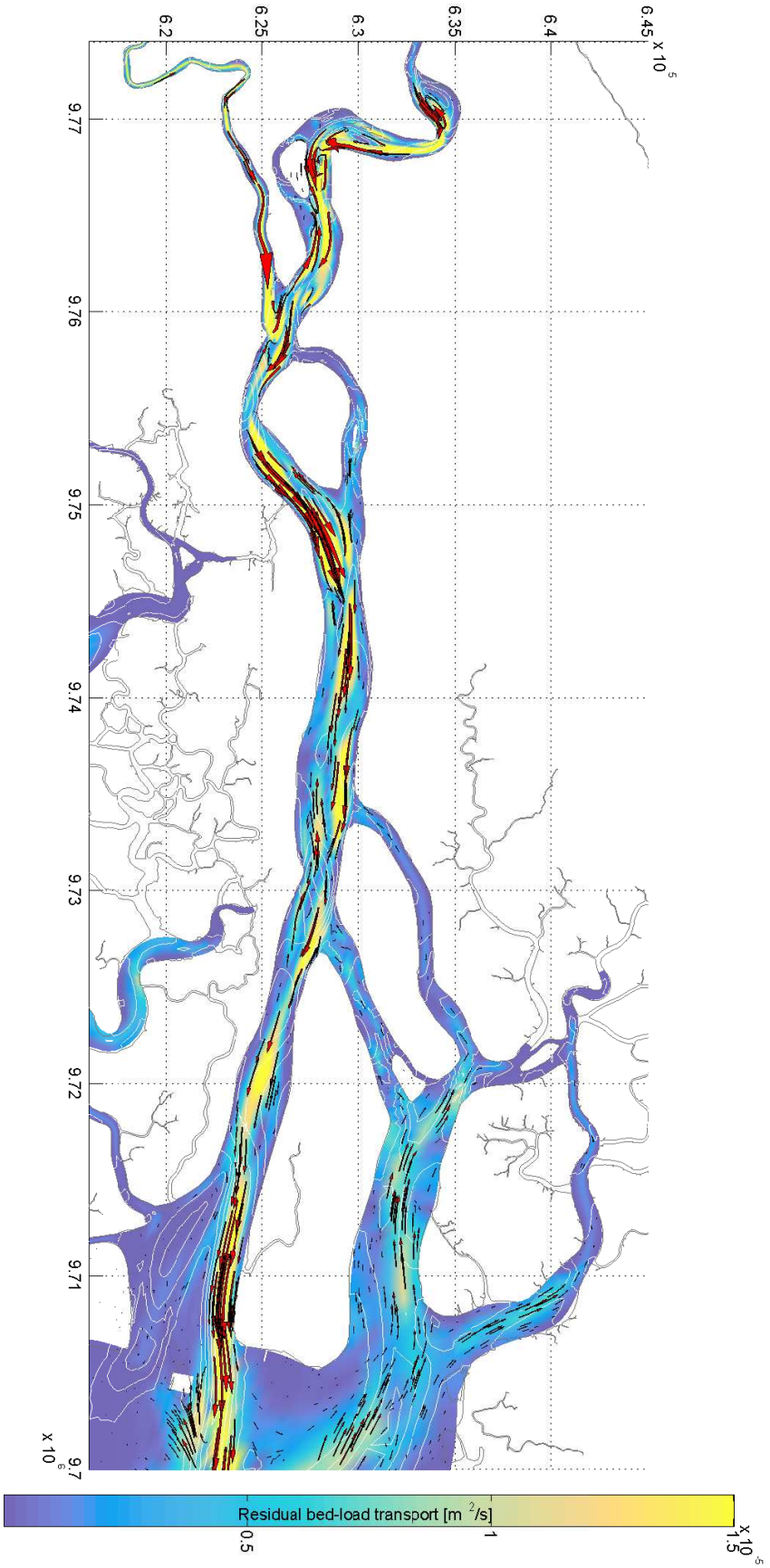

Figure B.9: GRE03. Magnitude and direction of the annual residual sediment transport

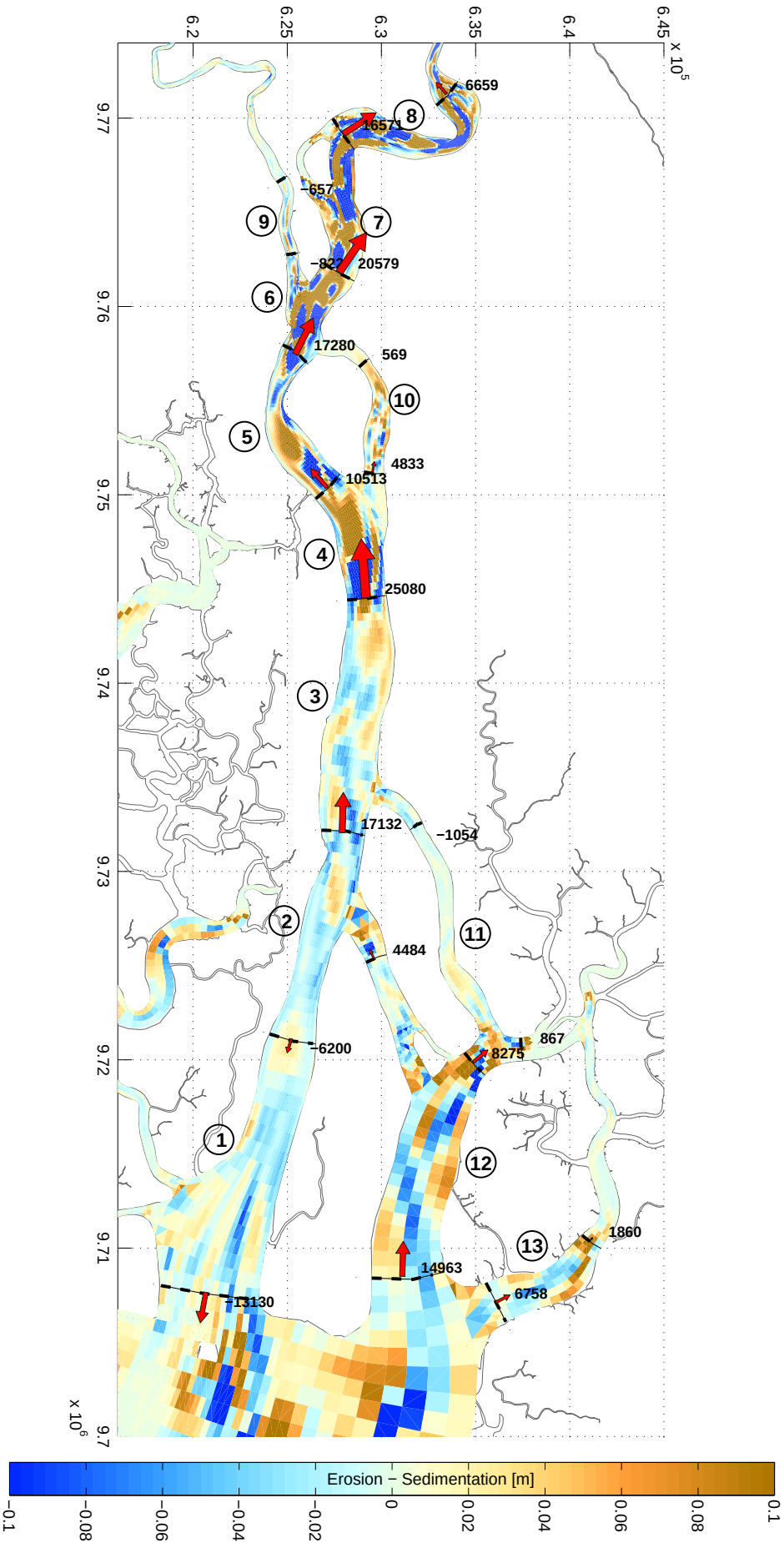

Figure B.10: GRE03. Sedimentation and erosion patterns, and volume exchange of sediment between macro cells during the **dry** season

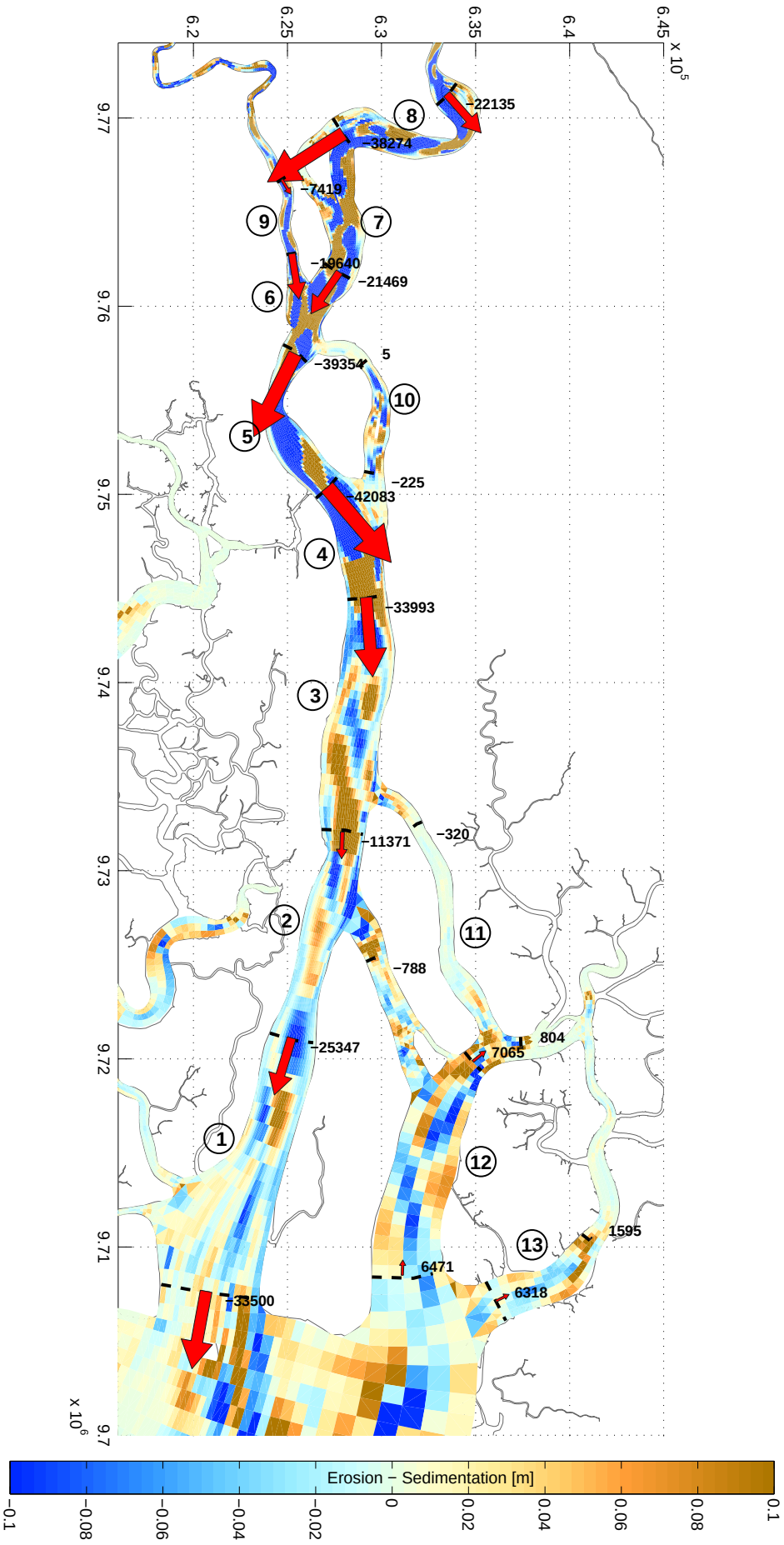

Figure B.11: GRE03. Sedimentation and erosion patterns, and volume exchange of sediment between macro cells during the **wet** season

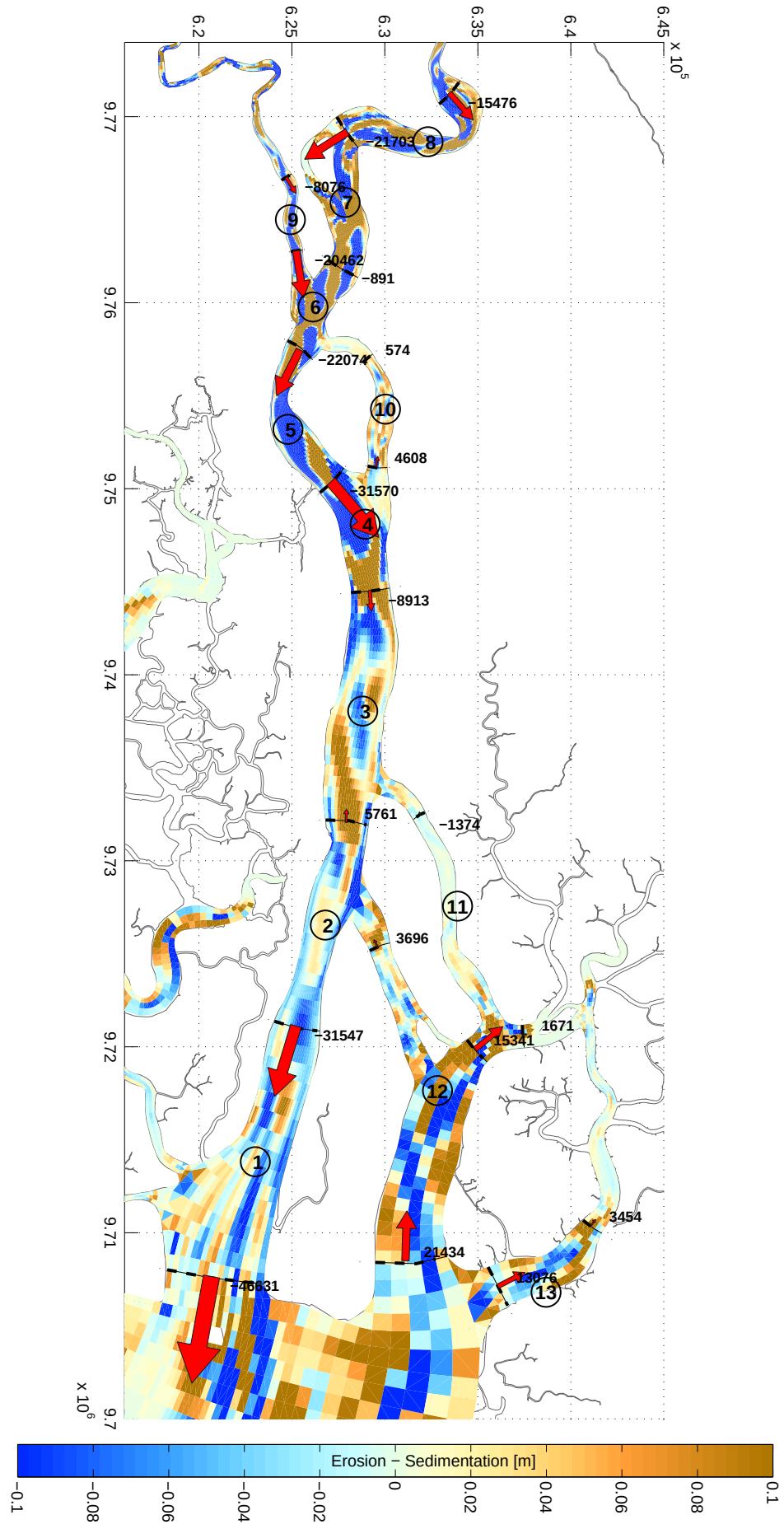

Figure B.12: GRE03. Sedimentation and erosion patterns, and volume exchange of sediment between macro cells in a **yearly** basis

B.4. GRE04

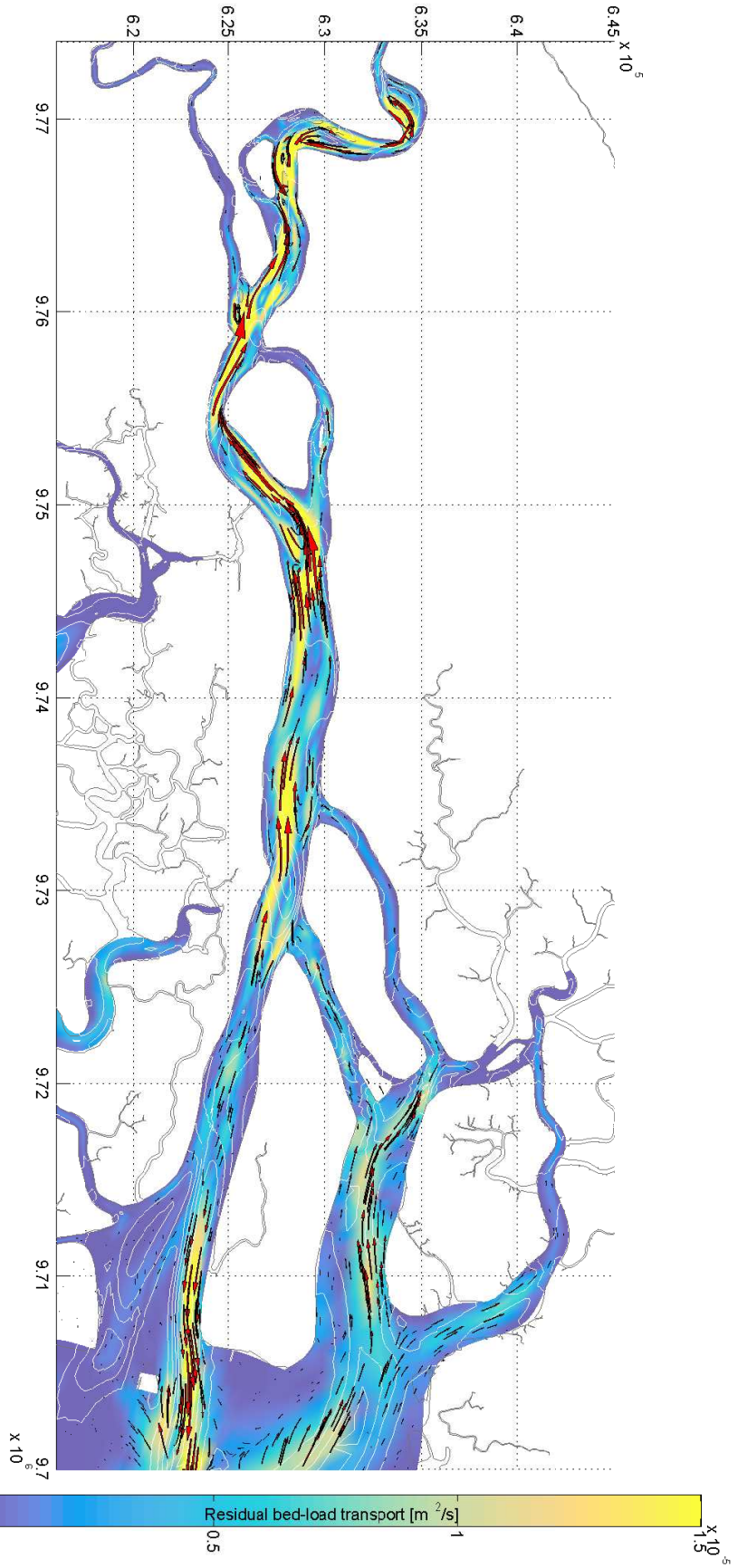

Figure B.13: GRE04. Magnitude and direction of the annual residual sediment transport

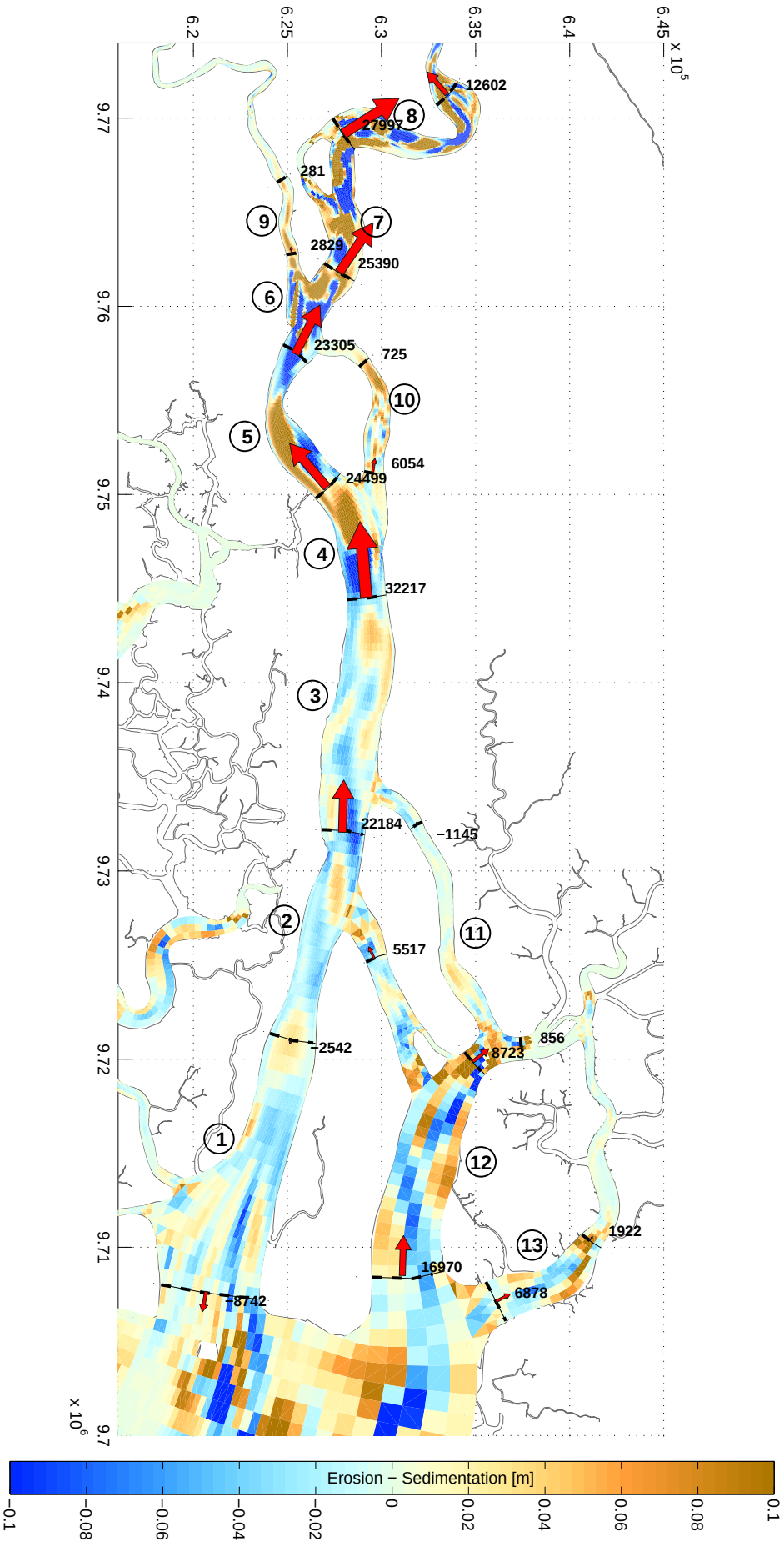

Figure B.14: GRE04. Sedimentation and erosion patterns, and volume exchange of sediment between macro cells during the **dry** season

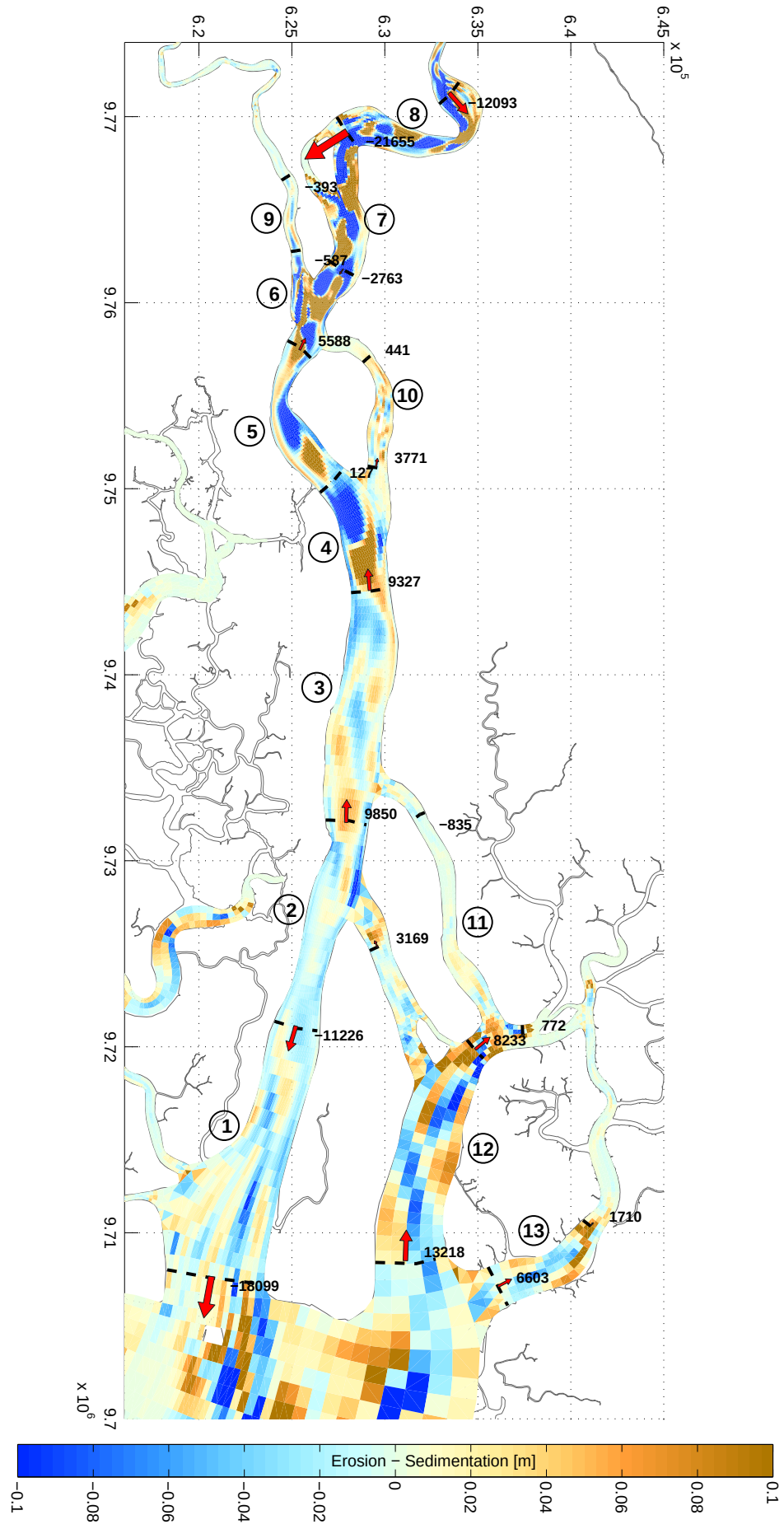

Figure B.15: GRE04. Sedimentation and erosion patterns, and volume exchange of sediment between macro cells during the **wet** season

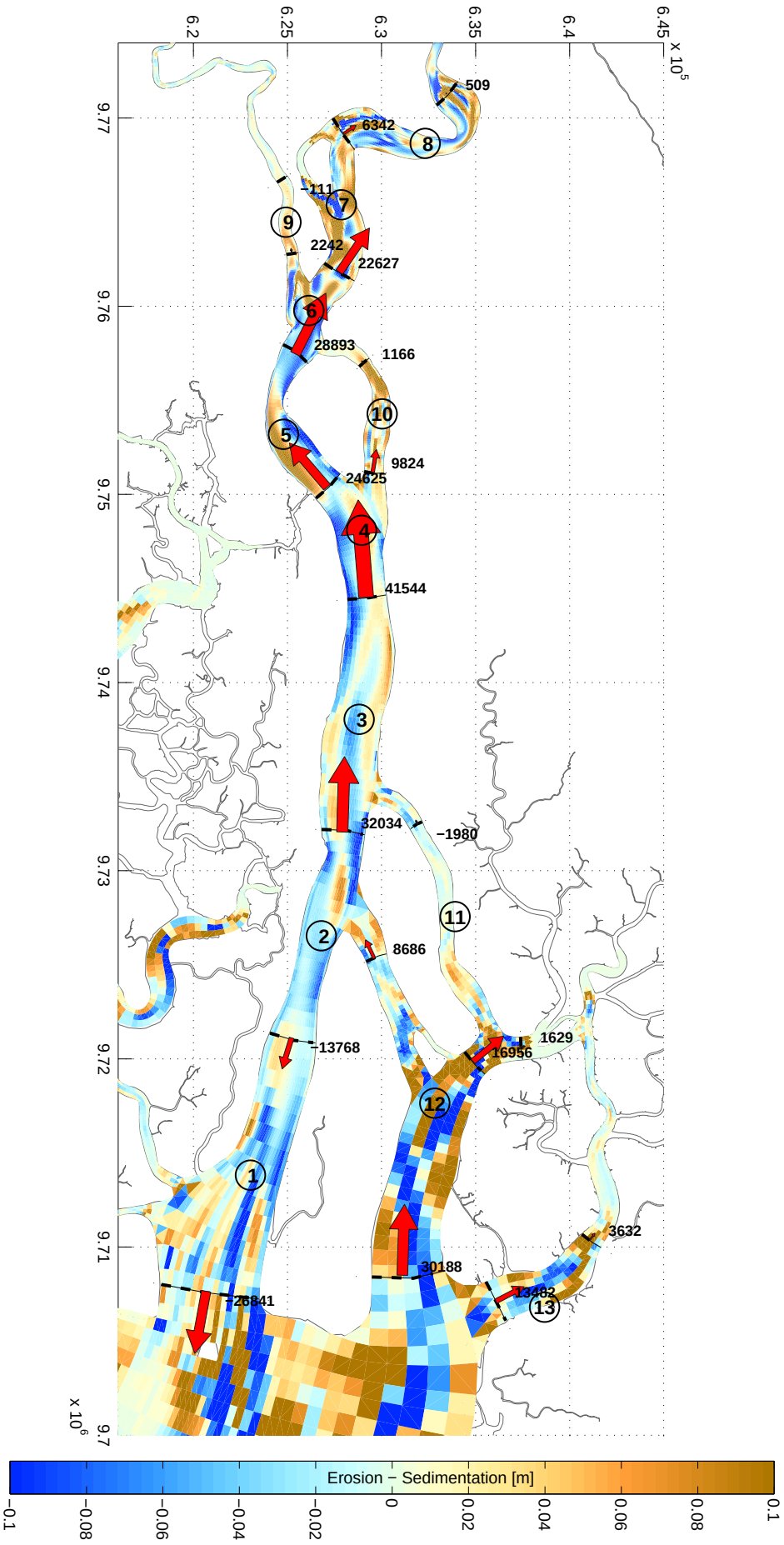

Figure B.16: GRE04. Sedimentation and erosion patterns, and volume exchange of sediment between macro cells in a **yearly** basis

B.5. GRE05

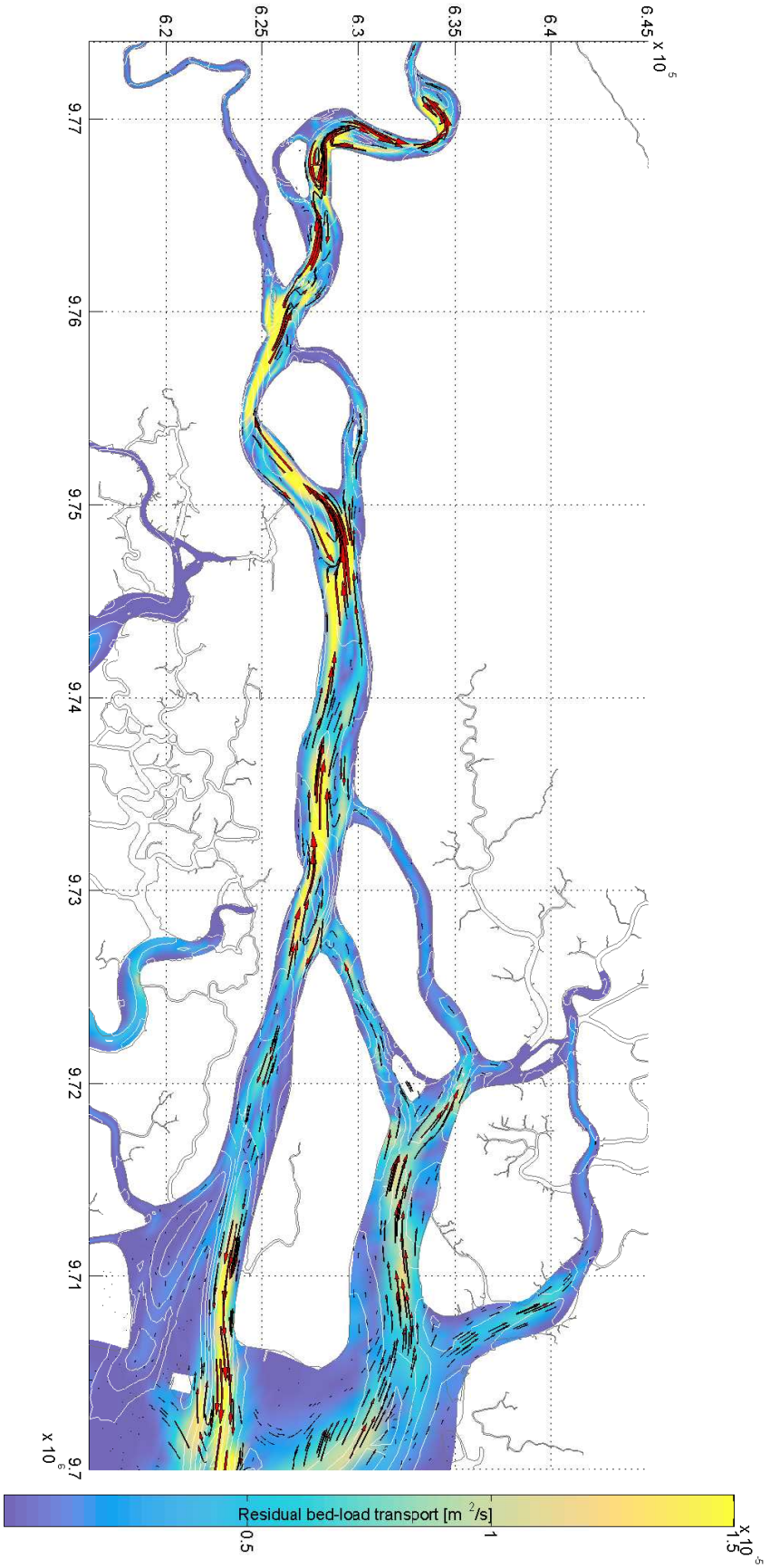

Figure B.17: GRE05. Magnitude and direction of the annual residual sediment transport

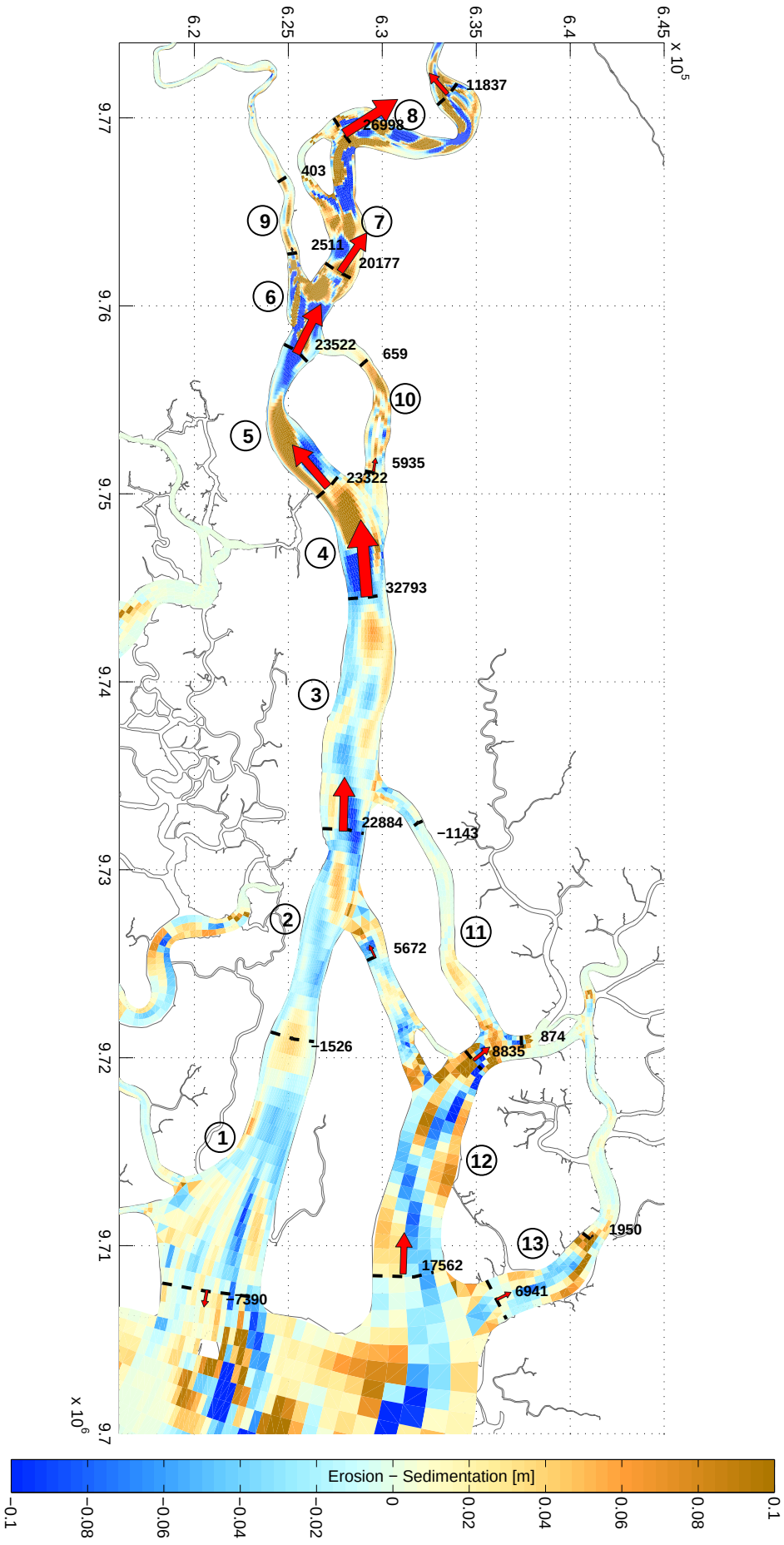

Figure B.18: GRE05. Sedimentation and erosion patterns, and volume exchange of sediment between macro cells during the **dry** season

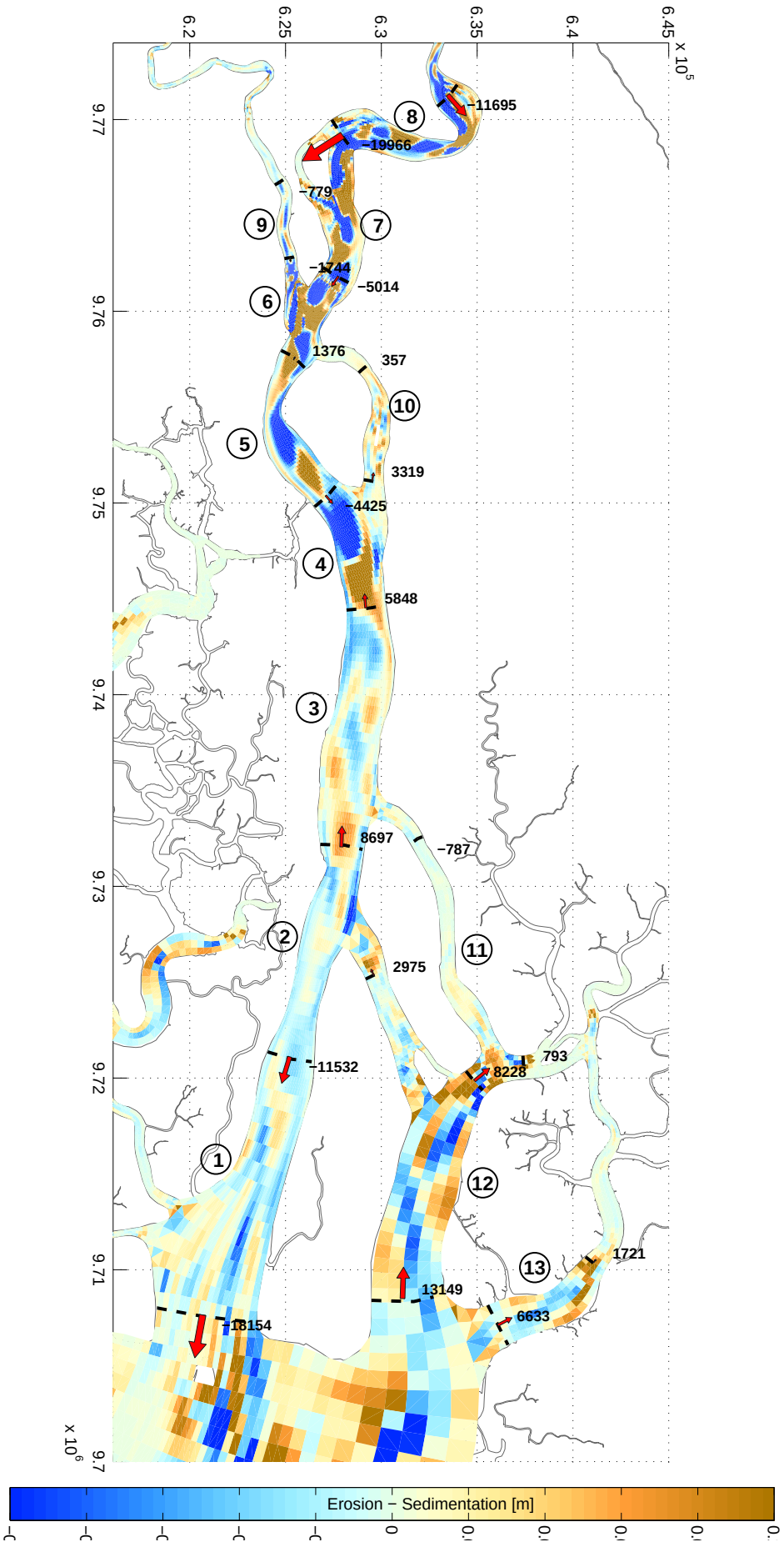

Figure B.19: GRE05. Sedimentation and erosion patterns, and volume exchange of sediment between macro cells during the **wet** season

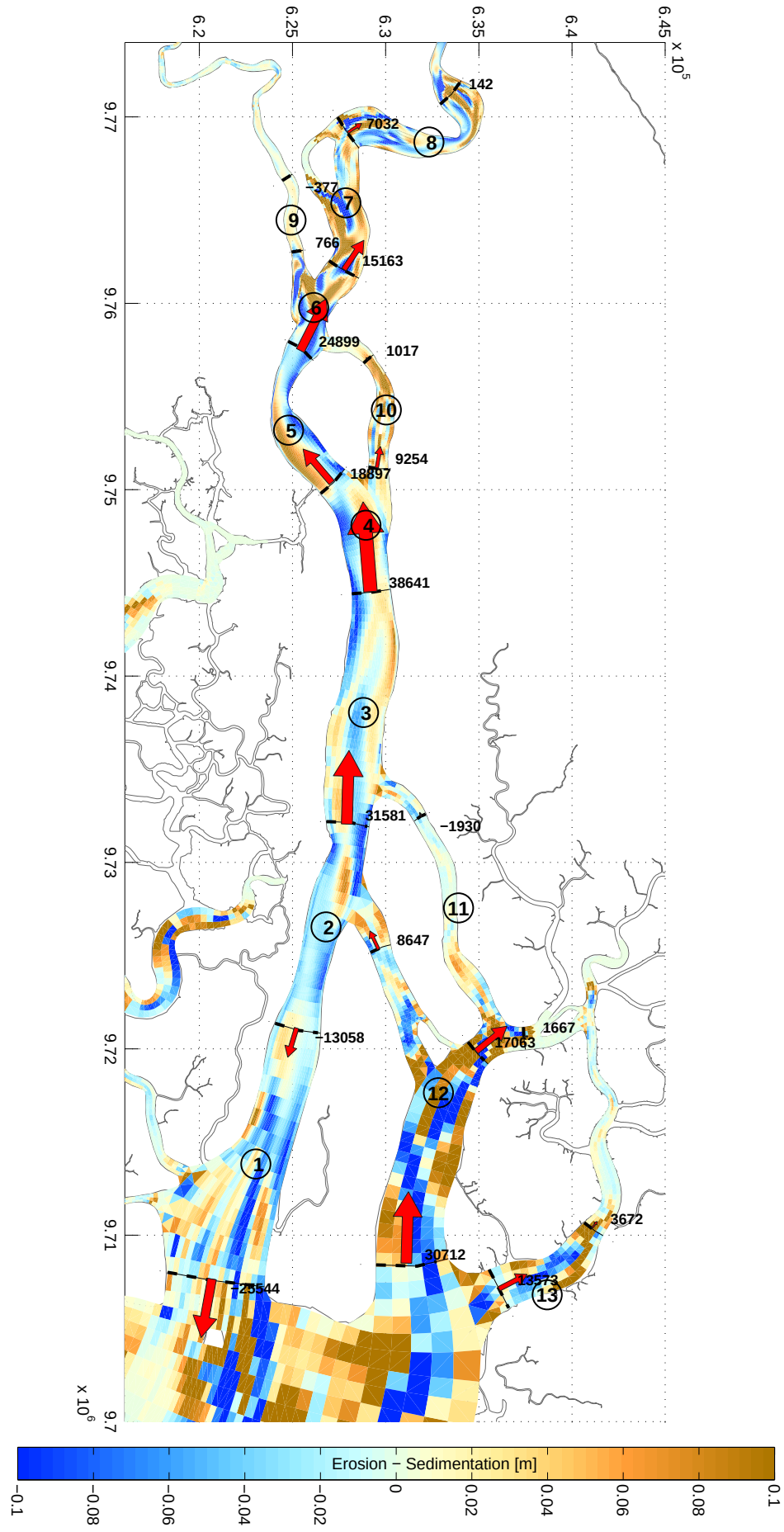

Figure B.20: GRE05. Sedimentation and erosion patterns, and volume exchange of sediment between macro cells in a **yearly** basis

B.6. GRE06

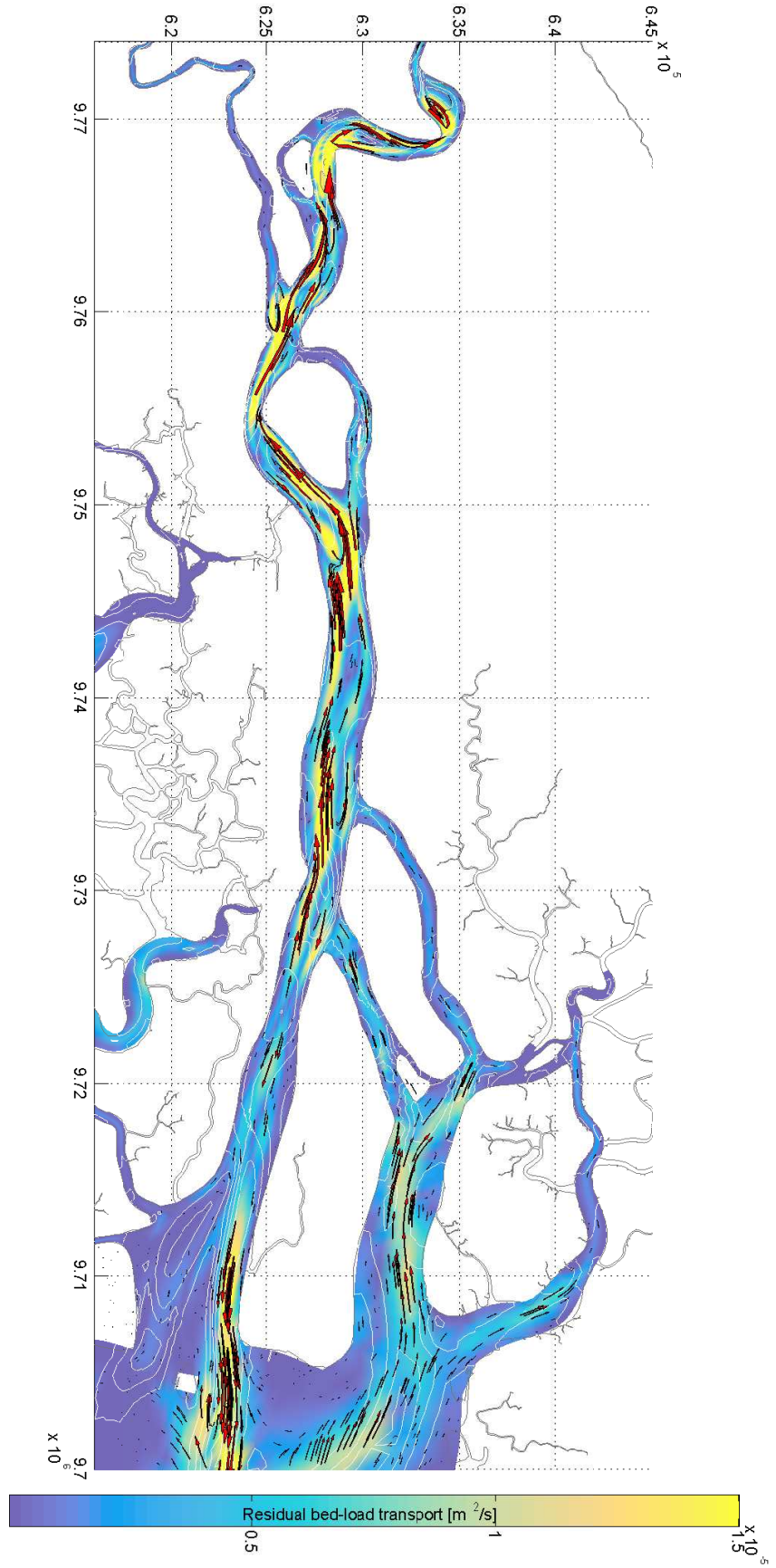

Figure B.21: GRE06. Magnitude and direction of the annual residual sediment transport

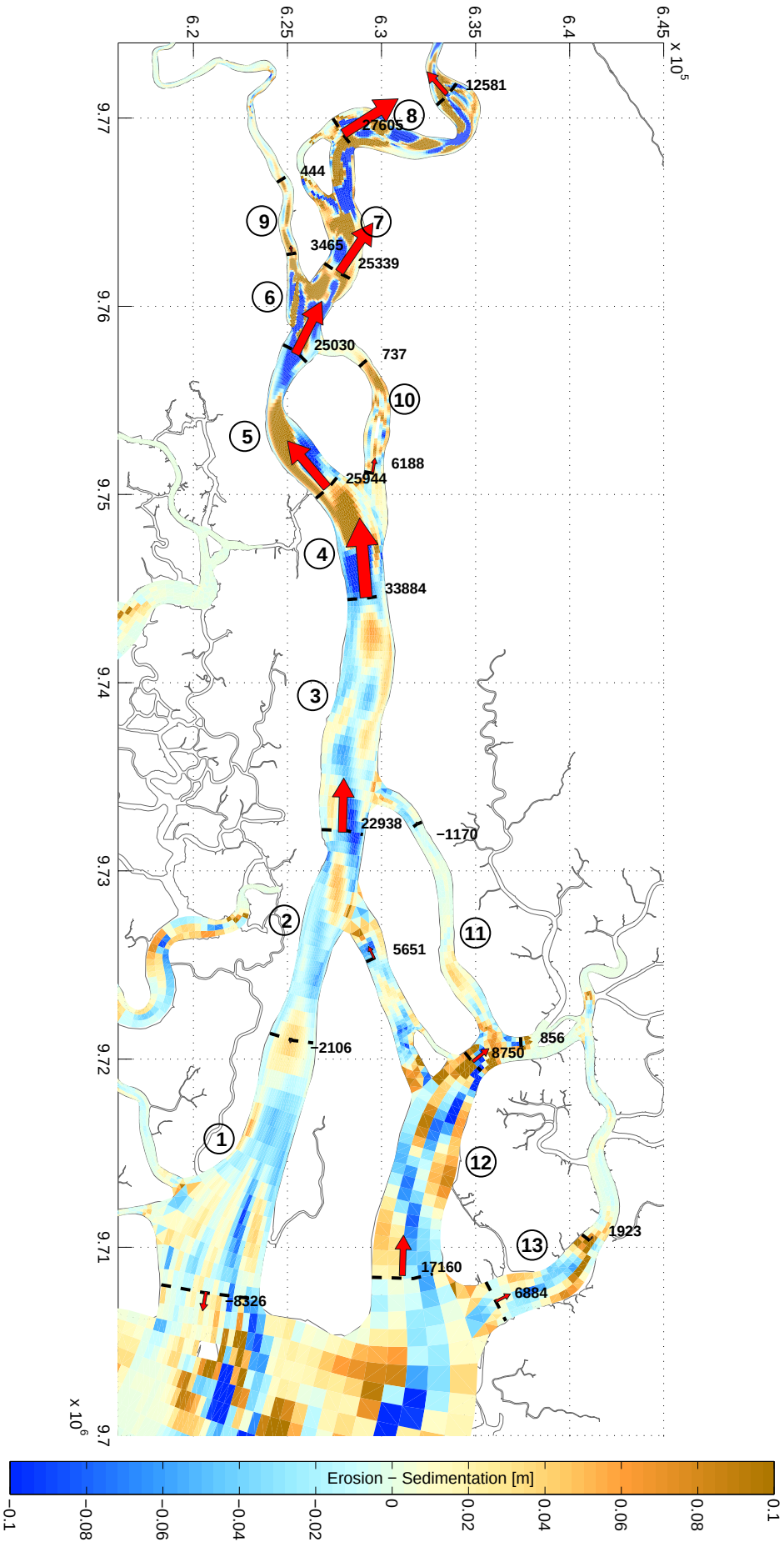

Figure B.22: GRE06. Sedimentation and erosion patterns, and volume exchange of sediment between macro cells during the **dry** season

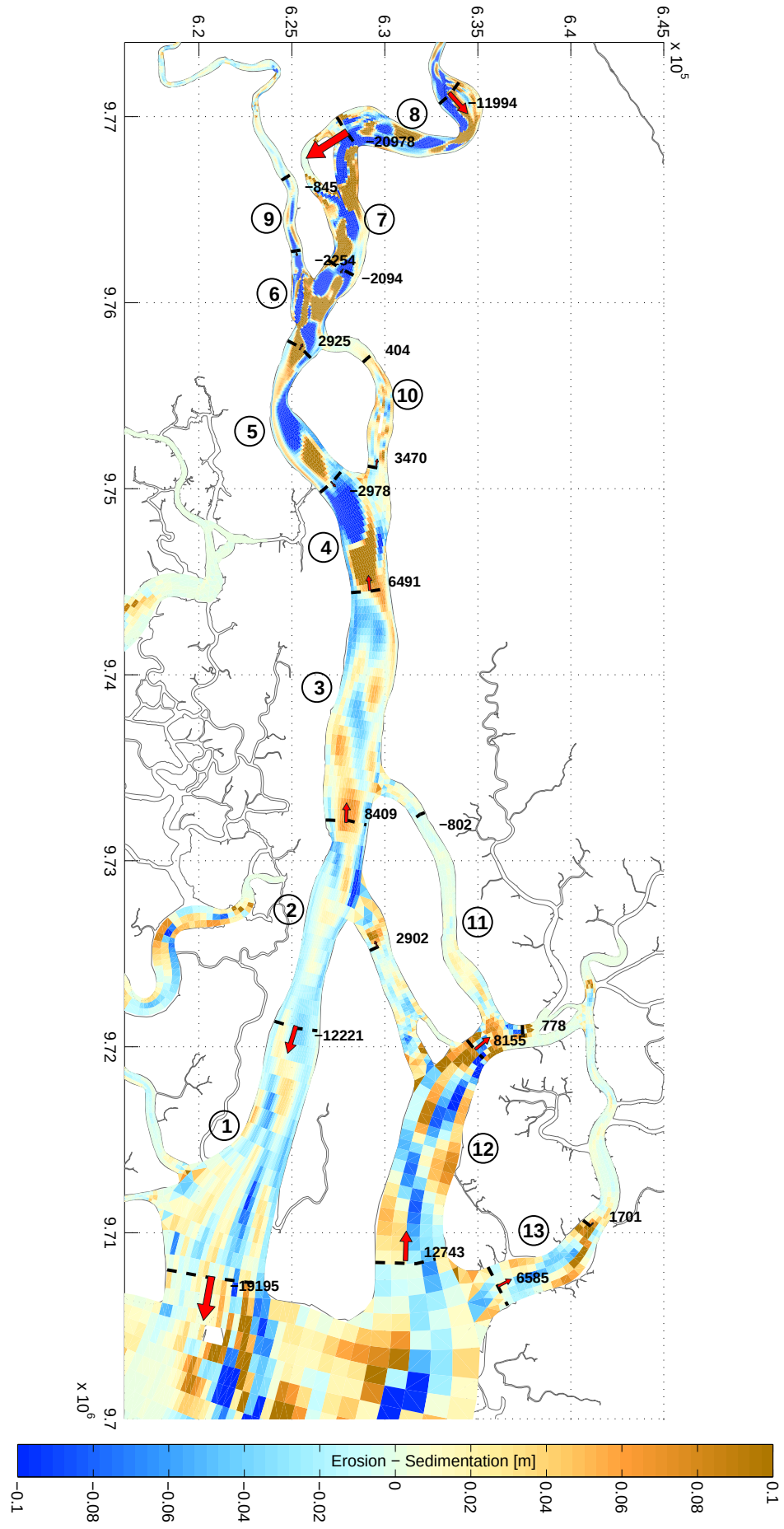

Figure B.23: GRE06. Sedimentation and erosion patterns, and volume exchange of sediment between macro cells during the **wet** season

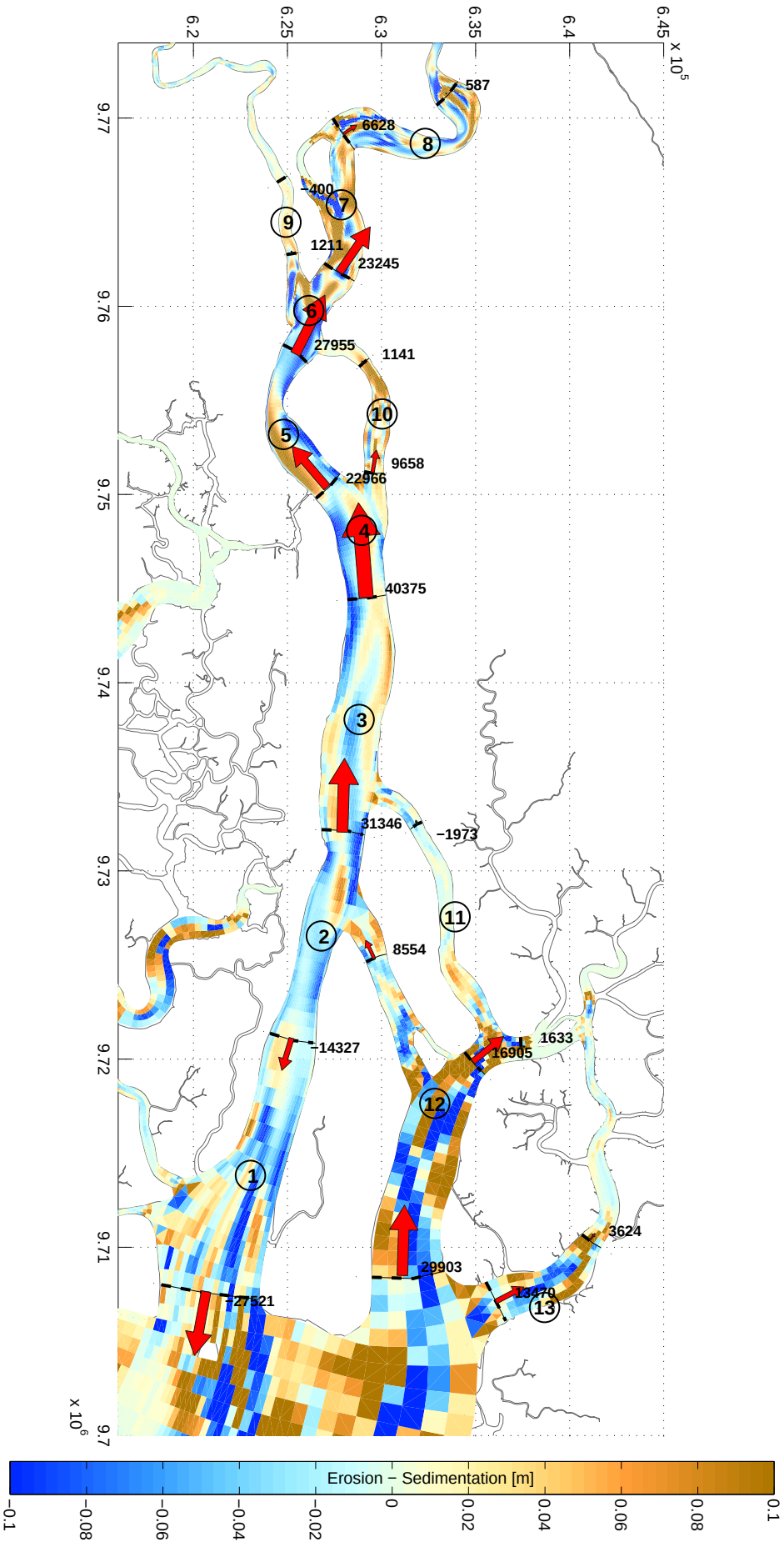

Figure B.24: GRE06. Sedimentation and erosion patterns, and volume exchange of sediment between macro cells in a **yearly** basis

C

TESTS FOR VALIDATION OF THE DELFT3D-FM MORPHOLOGY MODULE

The flow motion simulation capabilities of Delft3D Flow Flexible Mesh has been already validated, for two-dimensional flow situations, through the implementation of several validation models presented by Deltares (2015b). The coupling with the morphology module is still under development. As a part of this research, the tasks of testing and diagnosing problems related to the morphology module were considered as a secondary objective.

Most of the reported issues had to do with adapting the code from the previous structured version of to the current unstructured version of the software. A detailed description of the reported issues is in a sense redundant since the communication with the staff was direct, i.e., there was not an established procedure or format for reporting the issues. Instead a summary of the main identified problems is presented as follows:

- Correcting the angle of the secondary flow and adding it to the output file.
- Adding the effect of spiral-flow to the sediment transport.
- Modifying the calculation of the dispersion stresses to avoid overshooting in dry to wet situations.
- Coupling and connecting the morphology boundary condition file to account for sediment transport, and bed level composition.

The identified issues were of especial interest for the Deltares developer team, whom based on the reports would update the code and implement solutions.

This testing and diagnosing served to implement features in the morphology module that mainly revolved around 2 different topics, i.e., implementation of secondary flow and the coupling with bed shear stress, and sediment transport over fixed layers.

The Deltares developer team has implemented specific test bench cases for each of these topics to validate the functionality of Delft3D-FM. The validation approach is to set up the same model for Delft3D and Delft3D-FM and compare the results for each case. A brief summary of these validation cases is presented below to demonstrate the functionality and applicability of the model.

C.1. IMPLEMENTATION OF SECONDARY FLOW AND THE COUPLING WITH BED SHEAR STRESS

The model set up is reproduced after the experiences with a physical model by Kalkwijk and Booij (1986).

C.1.1. DESCRIPTION

The objective is to assess the performance of Delft3D-FM in computing the bed shear stress and the bedlaod transport induced by the secondary flow in a curved bend channel according to Figure C.1. A 0.50 m^3/s discharge and 0.70 m water level are imposed as boundary conditions. The channel longitudinal bottom slope is set to 0.00 and the Chezy friction coefficient is assumed as 60 $m^{1/2}/s$. For morphology simulations,the sediment is characterized by a medium grain diameter of 0.20 mm, the Engelund-Hansen transport predictor is chosen and the Koch-Folkstra bed slope effect formulation is used.

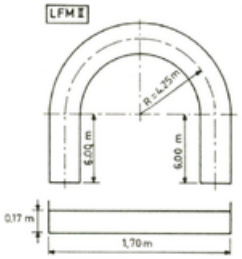

Figure C.1: Dimensions for the curved bend models

C.1.2. RESULTS

From the results of Figure C.2 it can be seen that Delft3D-FM produces similar patterns, for both the bed shear stress and spiral flow intensity, as Delf3D.

Regarding the secondary flow intensity, the differences are minor and in the order of 1%. In case of the bed shear stress the differences are slightly more evident, especially in the bend area where the Delft3D-FM patterns are somewhat more diffuse. Nevertheless there is a good agreement between the structured and unstructured versions of the software.

For further validation, the model is applied to simulate the sediment transport and bed level update. A profile is taken along the center line of the channel and shown in Figure C.3. There is a large agreement between the profiles, again the main differences appear at the bend area. However the differences are minor and only in specific locations.

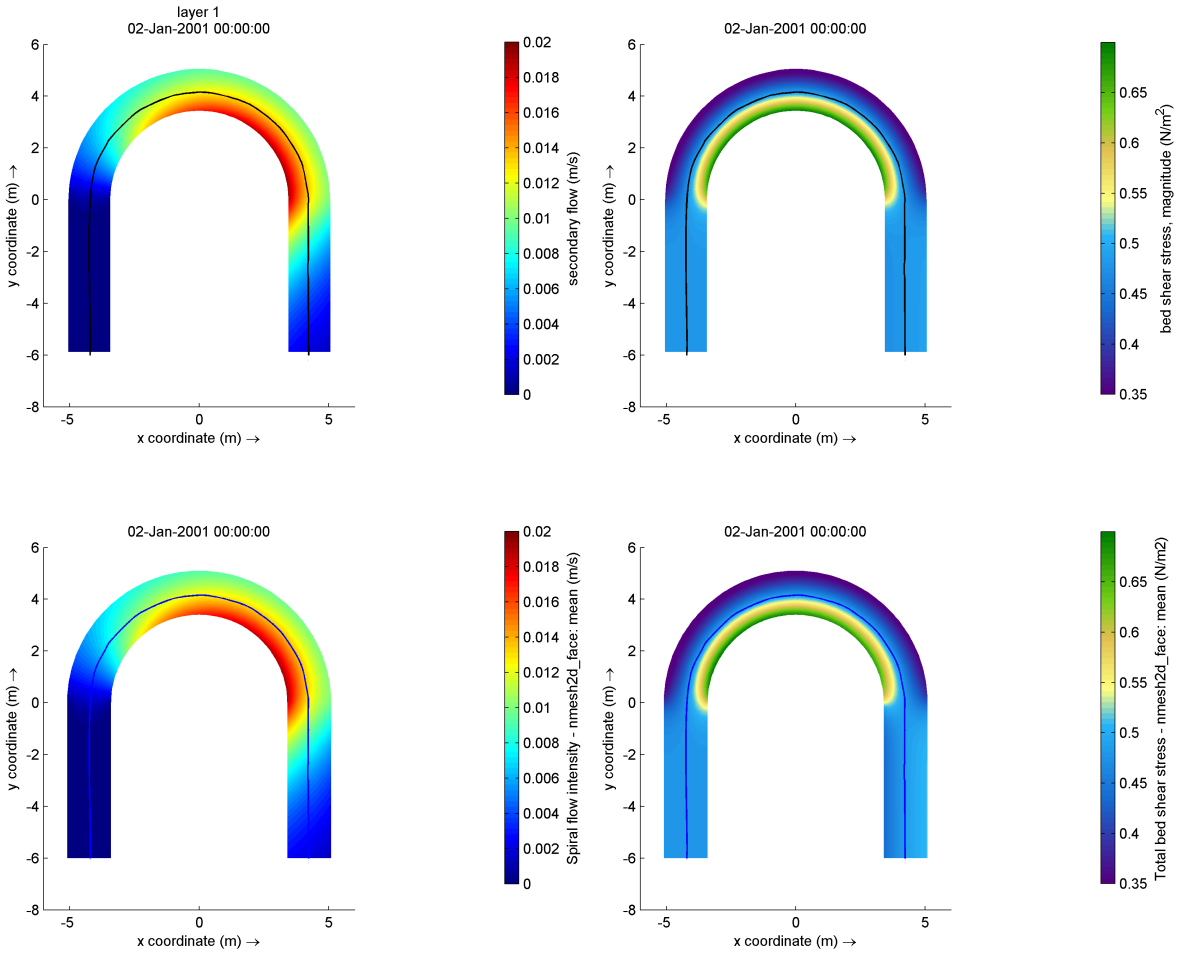

Figure C.2: Secondary flow intensity and bed shear stress magnitude. Results Delft3D (upper plots), Delft3D-FM (bottom plots)

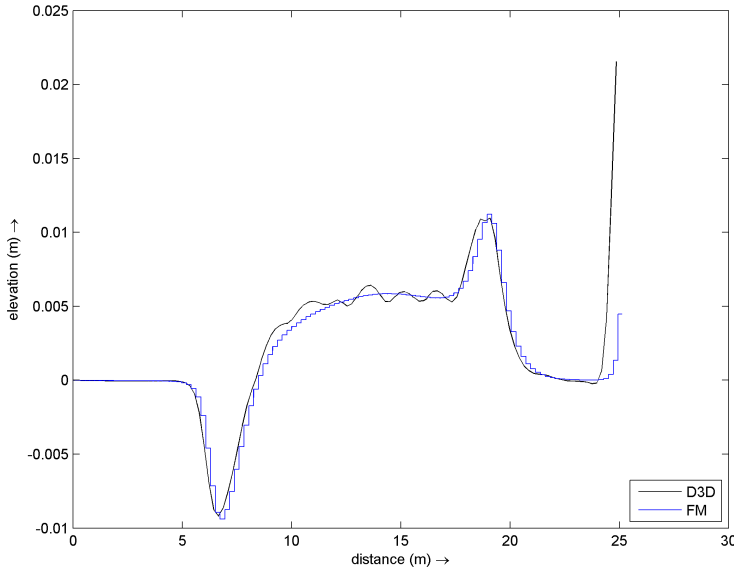

Figure C.3: Bed level along the center line of the channel

C.2. SEDIMENT TRANSPORT OVER A FIXED LAYER

The test case is based on the experiments carried out by Struiksma (1999), in which the propagation of a bed perturbation over non-erodible layer under constant boundary conditions is simulated.

C.2.1. DESCRIPTION

The model consists of a one dimensional flume in which initially water flows across a steep-sided trench cut in the bed. The flume is 11.50 m long and 0.20 m wide with a longitudinal slope of 0.002. The bed material is prescribed as alluvial sediment characterized by a medium diameter of 0.45 mm. In the middle of the flume a non-erodible 3.0 m long sill is also prescribed in such a way that initially an uniform erodible layer of 0.15 m covers the sill. The trench in the other hand, is 0.04 m deep and 2 m long and is located near the upstream boundary. The sediment transport is computed using the Engelund-Hansen formulation.

As for the previous case, the model is setup in Delft3D and Delft3D-FM, the aim is to compare the performance of the latter in relation to the previous version of the software. Some of the most relevant parameters and boundary conditions are summarized in Table C.1.

Table C.1: Model parameters and boundary conditions

Quantity	*Unit*	*Value*
Discharge	[l/s]	9.200
Sediment load at upstream boundary	[l/s]	7.000
Mean water depth	[m]	0.100
Chezy friction coefficient	[$m^{1/2}$/s]	31.400
Water level at downstrem boundary	[m]	0.338

C.2.2. RESULTS

The bed perturbation propagates and disappears once it reaches the non-erodible layer, which is exposed for a moment as the perturbation travels downstream. Once the perturbation passes the non-erodible layer it reappers but with smaller dimensions. Figure C.4 displays the propagation sequence in a 1 hour interval. The bed level profiles have been computed with Delft3D and Delft3D-FM. The agreement between the models is remarkable, the differences are almost imperceptible.

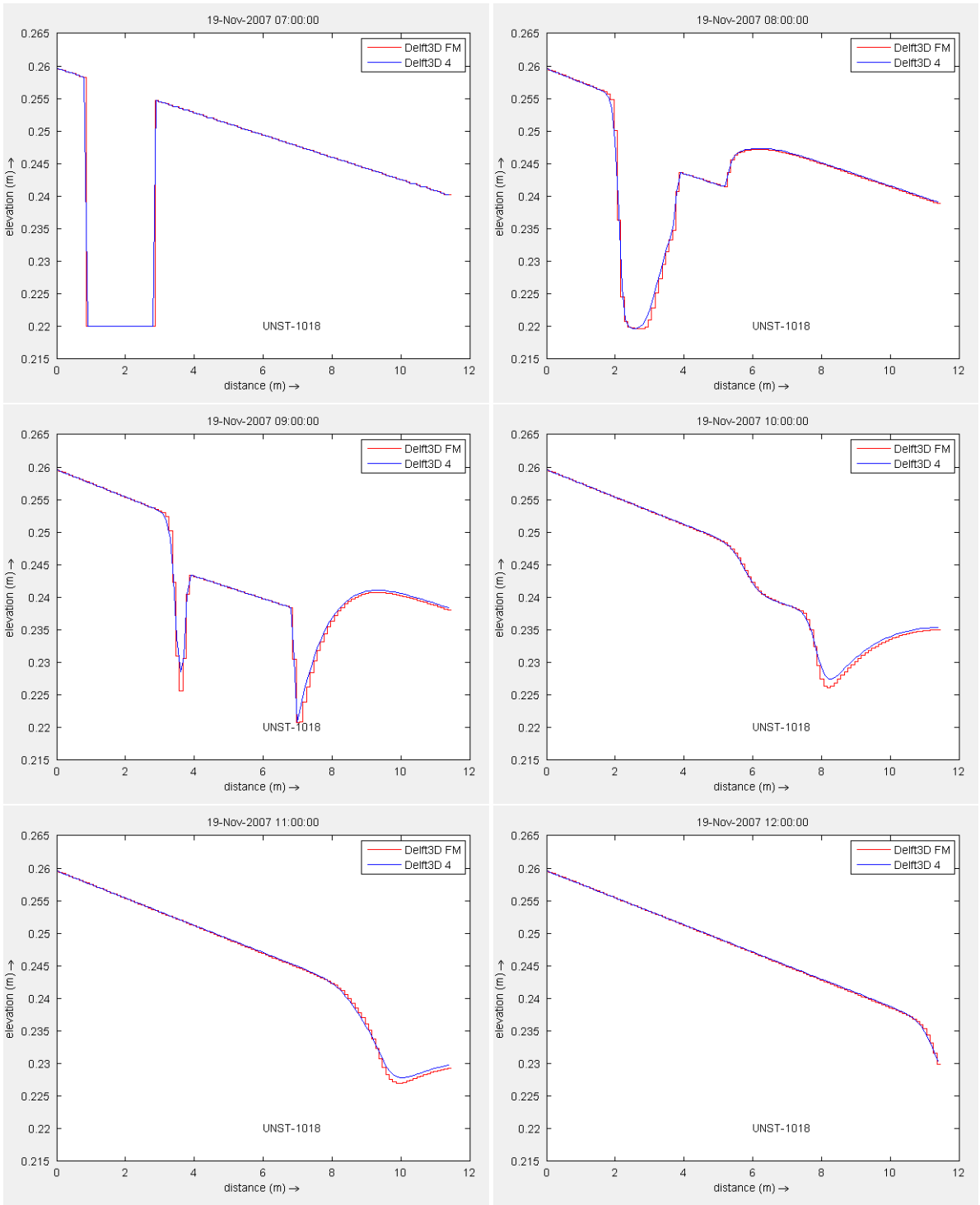

Figure C.4: Sequence of bed level longitudinal profiles